University of Minnesota
St. Anthony Falls Hydraulic Laboratory
Mississippi River at 3rd Ave. S. E.

Project Report No. 278

THEORY OF RIVER MEANDERS

by

Helgi Johannesson and Gary Parker

Prepared for

LEGISLATIVE COMMISSION ON MINNESOTA RESOURCES
State of Minnesota

November 1988
Minneapolis, Minnesota

ABSTRACT

A mathematical model is developed for the calculation of flow field and bed topography in curved channels with an erodible bed. A small perturbation approach is used to linearize the governing equations.

The downstream convective acceleration of the secondary flow is shown to give rise to a phase lag between secondary flow and channel centerline curvature, and also to suppress the magnitude of the secondary flow. The model further accounts for the convective transport of primary flow momentum by the secondary flow. This oft-neglected influence of the secondary flow is shown to be an important cause of the redistribution of the primary flow velocity.

The governing equations retain the full coupling between the flow field, the bedload transport, and the bed topography. This coupling is shown to increase significantly the lateral bed slope in the upstream part of a channel bend, even beyond the value for fully developed bend flow which is approached in the downstream part of a channel bend. This coupling is also shown to give rise to resonant behavior for certain combinations of input variables; the common origin of the two phenomena is explained. The predicted flow field and bed topography compare very well with both laboratory and field data.

Further, assuming the banks to be erodible, the model is used to predict wavelengths of river meanders. The results compare favorably with both laboratory and field data.

This report has also been presented by Helgi Johannesson as a Ph.D. thesis to the University of Minnesota.

TABLE OF CONTENTS

LIST OF FIGURES

LIST OF TABLES

LIST OF VARIABLES

A	coefficient of transverse bed slope, as defined by Eq. 4.13
A_s	coefficient defined by Eq.4.21
a	$\sqrt{r/(2\chi_1)}$
a_1, a_2, a_3, a_4	coefficients in Eqs. 5.17a,b
$\tilde{a}_c, \tilde{a}_F, \bar{a}_F$	coefficients defined by Eqs. 5.45c, 5.53c, and 5.53e, respectively
b	half-with of the channel
$\tilde{b}_c, \tilde{b}_F, \bar{b}_F$	coefficients defined by Eqs. 5.45d, 5.53d, and 5.53f, respectively
C	dimensionless centerline curvature = $b\tilde{C}$
$\tilde{C}$	centerline curvature
C_f	dimensionless Chezy friction factor = gHI/U^2
c	wavespeed of alternate bars defined by Eq. 6.9b
$\tilde{c}_c$	coefficient defined by Eq. 5.45e
c_d	damping coefficient defined by Eq. 5.55a
D_{50}	median size of bed material
D_1, D_2	coefficients defined by Eqs. 5.46c,d
$\tilde{d}_c$	coefficient defined by Eq. 5.45f
F	Froude number = $U/\sqrt{gH}$
f_*	calibration coefficient in Eq. 2.14 equal to 1.19
$G(\zeta)$	function of ζ defined by Eq. 5.13
$G_0(\zeta)$	function of ζ defined by Eq. 4.9
$G_s(\zeta)$	function of ζ defined by Eq. 5.23
g	acceleration of gravity
H	reach averaged value of $\tilde{h}$
$H(\zeta)$	function of ζ defined by Eq. 5.13, not to be confused with the reach averged depth H

h	dimensionless channel depth = $\tilde{h}/H$
$\tilde{h}$	channel depth
h_1	perturbation of h
h_{1C}, h_{1F}	defined by Eq. 5.38
I	average channel water-surface slope
I_*	(b/H)I
J_1, J_2	coefficients defined by Eqs. 5.53g,h
k	dimensionless meander wavenumber = $b\tilde{k}$
$\tilde{k}$	meander wavenumber
k_{res}	resonant wavenumber defined by Eq. 5.55b
k_*	bed roughness
M, M_1	dimensionless coefficients in the equation of sediment continuity, defined in Appendix A.
n	dimensionless cross-stream coordinate = $\tilde{n}/b$
$\tilde{n}$	cross-stream coordinate
n_{u1F}, $n_{\eta 1F}$	first moments of the lateral distributions of u_{1F} and η_{1F}, respectively, defined by Eqs. 5.47a,b)
P, P_1	dimensionless coefficients in the equation of downstream momentum balance, defined in Appendix A
p	sediment porosity
Q	water discharge
Q_0	ratio between the scale of sediment discharge and the flow rate, defined by Eq. 2.28d
q_s, q_n	dimensionless volumetric bedload transport per unit width in the (s, n) direction
$\tilde{q}_s$, $\tilde{q}_n$	volumetric bedload transport per unit width in the (s,n) direction
q_{s0}	reach averaged value of q_s

q_{s1}, q_{n1}	perturbations of q_s and q_n
R	submerged specific gravity of the sediment
r	k/ε
$\tilde{r}$	radius of curvature of the channel centerline
$\tilde{r}_m$	minimum magnitude of $\tilde{r}$
r_*	$2 + 2.5 \ln (\tilde{h}/k_*)$
s	dimensionless downstream coordinate = $\tilde{s}/b$
$\tilde{s}$	downstream coordinate
T	dimensionless velocity shape function
U	reach averaged value of $\tilde{u}$
u	dimensionless vertically averaged downstream velocity
$\tilde{u}$	downstream velocity
$\bar{u}$	vertically averaged downstream velocity
u_1	perturbation of u
u_{1b}	value of u_1 at n = 1
u_{1C}, u_{1F}	defined by Eq. 5.38
$\tilde{u}_b$	downstream velocity at the bed
$\tilde{u}_*$	shear velocity
v	$\hat{v}/\varepsilon$
$\tilde{v}$	transverse velocity
$\bar{v}$	vertically averaged transverse velocity
$\hat{v}$	dimensionless vertically averaged transverse velocity
v_1	perturbation of v
v_{1C}, v_{1F}	defined by Eq. 5.38
$\tilde{x}$, $\tilde{y}$, $\tilde{z}$	Cartesian coordinates, $\tilde{z}$ being directed upward from the bed
Y_1, Y_2	defined by Eqs. 8.19a,b
α	coefficient = 0.077 (Eq. 2.16), no to be confused with α given by Eq. 6.9a

α	exponential growth rate of alternate bars given by Eq. 6.9a
α_0	exponential growth rate of meander bends given by Eq. 9.12a
α_*	ratio of lift coefficient to drag coefficient = 0.85
β	coefficient defined by Eq. 2.14
Γ	$\beta/(\gamma^2 \varepsilon)$
γ	b/H
γ_c	critical value of γ, below which alternate bars are not present
δ	coefficient defined by Eq. 8.2c
ε	$(b/H)C_f$
ζ	$\tilde{z}/\tilde{h}$
η	dimensionless bed elevation
$\tilde{\eta}$	bed elevation
$\tilde{\eta}_r$	reference elevation for the bed
η_1	perturbation of η
η_{1C}, η_{1F}	defined by Eq. 5.38
θ	angle between the centerline down-channel direction and the $\tilde{x}$-axis
θ_0	angle amplitude of channel centerline
$\tilde{\lambda}$	meander wavelength, measured along the river channel
$\tilde{\lambda}_c$	meander wavlength, measured along the river valley
μ	dynamic coefficient of Coulomb friction = 0.43
υ	dimensionless secondary flow velocity = $\tilde{\upsilon}/U$
$\tilde{\upsilon}$	secondary flow velocity
υ_1	perturbation of υ
υ_t	eddy viscosity
ξ	dimensionless water-surface elevation
$\tilde{\xi}$	water-surface elevation
$\tilde{\xi}_r$	reference elevation for the water-surface

ξ_1	perturbation of ξ
ρ	density of water
σ	dimensionless centerline curvature
σ_g	geometric standard deviation of the bed material = $\sqrt{D_{84} / D_{16}}$
σ_s	dimensionless secondary current cell strength
$\sigma_{WL}, \sigma_{SL}, \sigma_{BL}$	phase lags of the water-surface, the secondary flow, and the bed topography, respectively
τ_s	dimensionless bed shear stress in the down-channel direction
$\tilde{\tau}_s$	bed shear stress in the down-channel direction
τ^*	Shields stress defined by Eq. 2.11
τ^*_C	critcal Shields stress
τ^*_G	grain Shields stress given by Eqs. 2.11a,b
ϕ	ks
χ	$r_* \alpha = \chi_1 - 1/3$
χ_1	$\alpha/\sqrt{C_f}$
χ_{20}	coefficient defined by Eq. 4.7
χ_2, χ_3	coefficients in Eq. 5.14
χ_W	coefficient defined by Eq. 5.20
ψ_0	$b/\tilde{r}_m$
ω_0	circular frequancy of meander bends given by Eq. 9.12b

ACKNOWLEDGEMENTS

This research was funded by the United States Science Foundation, through grants No. MSM-8311721-02 and INT-8412678, and the Legislative Commission on Minnesota Resources.

The figures were drafted by Aaron Gimbel and Karl Wikstrom did the photographic work.

1. INTRODUCTION

1.1 General Description

Natural alluvial river channels can be divided into three categories. They are either straight, meandering, or braided. The fluvial processes encountered in natural meandering rivers have long intrigued engineers. Not only does the geometric shape of river bends give rise to a complicated three-dimensional flow field, but equally importantly, the flow field reshapes the bends through the process of bank erosion. An example of a typical mature river with developed meanders is the Klaralven River of Sweden shown in Fig. 1.1. The work presented herein deals with the possibility of calculating the flow field and bed topography of river meanders. A simple bank erosion relation which allows for simulation of the lateral river migration is then assumed . The model is used to calculate the most unstable wavelength of river meanders. The results for all of the above (flow field, bed topography, and wavelength) are compared with both laboratory and field data.

There are several reasons why the ability to calculate the flow field and bed topography in an existing river channel, and then being able to predict the future location of that channel, may be of importance. For example, for site selection of a bridge or a intake structure, it is invaluable to know the present and the future impact of the river on those structures. Secondly, when protecting existing structures from a migrating river, by bank protection or other methods, it is necessary to quantify the response of the river to different engineering solutions. Thirdly, a migrating river may be eroding into valuable farmland, and having some means of estimating the rate at which this is happening is of considerable interest.

Since the original work of Hansen (1967) and Callander (1969), instability of the alternate bar type in straight channels has long been identified as the cause of fluvial meandering. This instability, which is responsible for the apparent lack of natural straight rivers, has been observed in laboratory studies (e.g. Anderson et al. (1976)) and in meandering rivers that have been artificially straightened i.e. the Walla Walla River shown in Fig. 1.2.

The work of Hansen (1967) and Callander (1969) has been improved and extended by Adachi (1967), Hayashi (1970), Sukegawa (1970), Engelund and Skovgaard (1973), Parker (1975,1976), Ponce and Mahmood (1976), Hayashi and Ozaki (1976), and Fredsoe (1978). All of the above are, however, unsatisfactory to the extent that bank deformation is not allowed. By relaxing the restraint of fixed sidewalls, Ikeda, Parker, and Sawai (1981) investigated the stability of channels with sinuous erodible banks and found conditions for the lateral bend amplitude to grow. Therein, it is assumed that the bank erosion rate is proportional to the near-bank primary flow velocity excess, i.e. the difference between the near-bank primary flow velocity and the mean channel velocity. Two instability mechanisms have therefore been identified:

1) The bar instability mechanism found by Hansen (1967) and Callander (1969). The alternate bars in a straight channel so formed migrate downstream.

2) The bend instability mechanism found by Ikeda et al. (1981). The location of point bars on the inside of each bend is determined by the channel curvature.

Ikeda et al. (1981) showed that, in the case of alluvial meanders, the two mechanisms operate at similar characteristic wavelengths. This suggests that alternate bars develop into true bends such that each bend contains one alternate bar.

Using the theory of Ikeda et al. (1981), Parker (1982) and Beck et al. (1983a,b) developed a computer program for the simulation of lateral migration of meandering rivers. This model has been used by Parker (1982) to analyze the Minnesota River in Minnesota,

Fig. 1.1. The Klaralven River of Sweden, a typical mature river with developed, confined meanders. (Photo courtesy A. Sundborg)

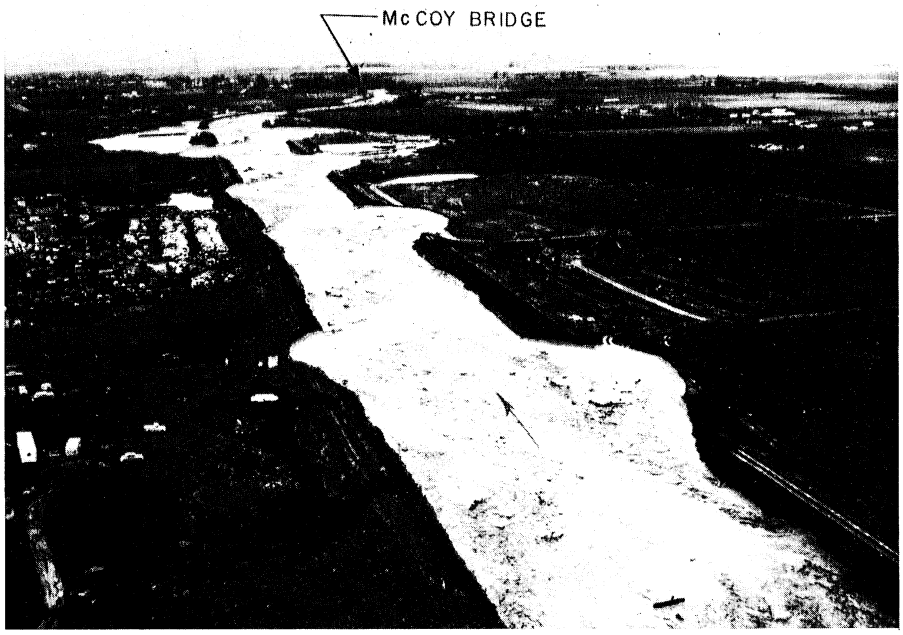

Fig. 1.2. A straightened reach of the Walla Walla River near McCoy bridge, Washington, U.S.A. Note that the straight channel is unstable, and the river is eroding the banks, creating again a meandering channel. (Photo courtesy P. Klingeman, Oregon State Univ.)

by Beck et al. (1983a,b) to analyze the Pembina River in Alberta, Canada, and the Genesee River in New York, and more recently by Johannesson (1985) to analyze four river reaches in Minnesota. Based on all of the above applications Johannesson (1985) concluded:

1) The consistent result of the model not being able to simulate the observed bend migration patterns, without artificially increasing bed friction, indicates that the modeling theory needs to be improved.

2) The recommended approach is to compare the computed flow field and bed topography to field data or experimental results available in the literature. If satisfactory agreement is obtained, the emphasis should be shifted toward the bank erosion model. However, if the agreement between the calculated and the measured flow field and bed topography is not satisfactory, these components of the model must be improved before the bank erosion model is changed, since there is no easy way to test the bank erosion model.

The above conclusions summarize both the motivation for the research presented, herein, and outline the approach which is followed.

Since the original work of Engelund (1974) and Ikeda et al. (1981), much progress has been made in furthering the understanding of the complicated flow field and the resulting bed topography that arise in curved channels. The model of Ikeda et al. (1981) was corrected by Tamai and Ikeuchi (1984), Johannesson (1985), and Blondeaux and Seminara (1985) to account for the metric coefficients that arise in a curvilinear coordinate system. Although the correction was seen to be modest, it had a very interesting physical implication. The model predicts that, for the classical case of subcritical, developed bend flow in a channel of constant curvature, flow over a flat non-erodible bed always realizes a higher downstream velocity near the inside bank than near the outside bank. This is in strong contradiction to the experimental results of Kikkawa et al. (1976), which clearly indicate that in this case the highest velocity is near the outside bank. Several researchers (Leschziner and Rodi, 1979; Kalkwijk and De Vriend, 1980; De Vriend, 1981; and De Vriend and Geldof, 1983) have emphasized that an important cause of primary flow velocity redistribution in meandering rivers is the convective transport of primary flow momentum by the secondary flow. This mechanism, however, was neglected by Engelund (1974) and Ikeda et al. (1981) and more recently by Smith and McLean (1984), Blondeaux and Seminara (1985), Struiksma et al. (1985), and Odgaard (1986a,b). Herein, the flow field model of Ikeda et al. (1981) is rederived, taking into account the above-mentioned convective transport of primary flow momentum by the secondary flow. This is seen to be precisely the mechanism needed to resolve the contradiction between the theoretical results of Ikeda et al. (1981), Tamai and Ikeuchi (1984), Johannesson (1985), and Blondeaux and Seminara (1985), and the experimental results of Kikkawa et al. (1976). The resulting flow model further accounts for the phase lag between the secondary flow strength and the channel curvature. The flow models of Gottlieb (1976), Kitanidis and Kennedy (1984), and Ikeda and Nishimura (1986) also include this effect, which was neglected by Engelund (1974), Smith and McLean (1984), and Blondeaux and Seminara (1985).

Recently, Blondeaux and Seminara (1985) and Struiksma et al. (1985) have emphasized the importance of the coupling between the flow field and the sediment transport when calculating the bed topography. Struiksma et al. (1985) observed that a significant part of the lateral bed slope in bends can be due to an "overshoot" effect induced by the redistribution of water and sediment in the first part of the bend. Both their experimental and theoretical findings indicate that the lateral bed slope at, or just downstream of, the entrance to a bend can be substantially higher than the slope obtained if the flow is assumed to be fully adapted to the bend curvature, as may be the case farther downstream. This phenomenon is called "overdeepening" herein. Overdeepening cannot be simulated using the model of Ikeda et al. (1981), since therein the transverse bed slope

is assumed to be a function only of local channel curvature, rather than being calculated under the restriction imposed by the continuity equation of sediment transport.

Herein, the bed topography is calculated through a relation describing the transverse force balance on a sediment particle moving along an inclined bed. The continuity equation of bedload transport is also satisfied, so that the coupling between the flow field, sediment transport, and bed topography is retained. It is shown that the overdeepening of Struiksma et al. (1985) and the resonance detected by Blondeaux and Seminara (1985) are closely related phenomena, both arising from the same above-mentioned coupling. The predicted flow field and bed topography is compared with both laboratory and field data.

Finally, using the bank erosion model of Ikeda et al. (1981), the new model is used to calculate the most unstable wavelength of river meanders. The results compare favorably with both laboratory and field data, and are shown to be significantly better than those of Ikeda et al. (1981).

1.2 Overview of Available Flow Field and Bed Topography Models

A summary of the available models, for calculating the flow field and the bed topography in sinuous channels, is given in Table 1.1, together with some of the underlying assumptions. All the models, except the one of Gottlieb (1976), consider only the central region of the channel, assume hydrostatic pressure and neglect the vertical velocity component (Table 1.1). This is generally a very good assumption, as briefly discussed in Chapter 2. Six equations are then needed to solve for the following six unknowns: The downstream and the cross-stream components of velocity and sediment transport, the water surface, and the bed topography.

As illustrated in Table 1.1 the first complete model is that of Engelund (1974). This model is the foundation on which all the remaining ones have been built. Its main drawback is that the interaction between the flow field and the sediment transport, when calculating the bed topography, is not properly accounted for. A simplified expression, based on the solution for fully developed bend flow, is assumed for the transverse bed slope, which becomes only a function of local channel centerline curvature. This allows for calculation of the flow field. The bed topography is then corrected in order to satisfy sediment continuity. However, interaction between the bed topography and the flow field is excluded at this point, since the flow field is not updated to account for the new bed.

The model of Gottlieb (1976) does not suffer from the same drawback as the approach of Engelund (1974). Although this work has not received much attention since it was published in 1976, this is the first model to correctly account for the interaction of the flow field and the sediment transport when calculating the bed topography. The models of Engelund (1974) and Gottlieb (1976) are linear models. Inherent in both of them is the assumption that the channel half-width is small compared to the minimum radius of curvature of the channel centerline. Gottlieb (1976), however, further assumed that the minimum radius of curvature is larger or equal to the meander wavelength. This restricts the application of his model severely. It applies only to very low amplitude meanders or to the area around the inflexion points for medium to high amplitude meanders (called "transition" areas therein). For example, it can not be used to calculate fully developed bend flow in a constant curvature channel. Gottlieb (1976) proposed that a model of uniform validity could be obtained by matching his solution (valid around the inflexion points) with the solution of Engelund (1974) (valid around the apex areas), following the procedure given by Van Dyke (1964). This seems to be a rather obscure approach since the solution of Engelund (1974) is uniformly valid.

Ikeda et al. (1981) derived more formally the model of Engelund (1974). Their approach is that of small perturbation in which the small parameter is the channel half-width over the minimum radius of curvature of the channel centerline. As done by Engelund (1974) they assumed the transverse bed slope to be a function only of local channel

Table 1.1 - Available Models for Flow Field and Bed Topography

	Downstream momentum eq.	Cross-stream momentum eq.	Vertical momentum eq.	Continuity eq. for water	Continuity eq. for sediment	Downstream sediment transport relation	Cross-stream sediment transport relation
Engelund (1974)	X	X	X*	X	X	X	X
Gottlieb (1976)	X	X	X	X	X	X	X
Ikeda et al. (1981)	X	X	X*	X			X
Smith & Mc Lean (1984)	X	X	X*	X			
Blondeaux & Seminara (1985)	X	X	X*	X	X	X	X
Struiksma et al. (1985)	X	X	X*	X	X	X	X
Odgaard (1986a,b)	X	X	X*	X			X
Beck (1988)	X	X	X*	X			X
Nelson (1988)	X	X	X*	X	X	X	X
Proposed model	X	X	X*	X	X	X	X

* Pressure assumed to be hydrostatic.

centerline curvature. However, since the continuity equation of sediment is totally neglected in the model of Ikeda et al. (1981), Table 1.1, they did not even once update the bed elevation as done by Engelund (1974).

Smith and McLean (1984) avoided addressing the calculation of the bed elevation by assuming it to be given a priori (Table 1.1). They, however, included the most important of several nonlinear terms, not retained in the linear models, in their flow field model.

As mentioned earlier, the models of Blondeaux and Seminara (1985) and Struiksma et al. (1985) correctly account for the interaction between the flow field and the sediment transport when calculating the bed topography. The model of Blondeaux and Seminara (1985) is a linear model which allows for an analytical solution for some simple channel geometries, whereas the model of Struiksma et al. (1985) is a nonlinear model from which a solution is obtained numerically.

The model of Odgaard (1986a,b) is based on essentially the same equations as that of Ikeda et al. (1981) (Table 1.1). Odgaard (1986a) simplified the governing equations without following any formal procedure. His final result is in many ways similar to the result of Ikeda et al. (1981). The major difference is in the transverse momentum equation, in which Odgaard retained the influence of the depth-averaged transverse velocity on the helical flow. He then assumed the transverse bed slope to be determined by the strength of the helical flow, and obtained an equation for the transverse bed slope that can encompass the overdeepening of Struiksma et al. (1985). The fact, however, remains that the physical process driving the overdeepening arises from the depth-averaged transverse flow in the model of Odgaard (1986a,b), whereas it arises from the continuity equation of sediment transport in the model of Struiksma et al. (1985). Note that the equation of sediment continuity is absent from the model of Odgaard (1986a,b) (Table 1.1). One reason why the model of Odgaard (1986a,b) is able to simulate overdeepening (Odgaard and Bergs, 1988), using essentially what seems to be the wrong physical process, is that therein the stabilizing influence of the depth-averaged transverse velocity on the lateral bed slope is not included in the particle force balance relation. Only the influence of the helical flow velocity is retained.

The model of Beck (1988) is essentially the same as that of Ikeda et al. (1981) (Table 1.1), except that the transverse bed slope is no longer a function only of local centerline curvature. Beck (1988) assumed a semi-empirical relation, when calculating the bed topography, rather than attempting to satisfy sediment continuity.

Nelson (1988) used the flow field model of Smith and McLean (1984) to simulate the measurements of Dietrich and Smith (1983), taken in two consecutive bends in Muddy Creek. The measured bed topography was used as input; the calculated flow field matched the measurements very well. Nelson (1988) then incorporated into the model the additional relations needed to calculate the bed topography, Table 1.1. With a somewhat oversimplified cross-stream sediment transport relation, the model predicted the experimental bed topography measurements of Hooke (1974) rather well. No attempt was, however, made to simulate the measured bed topography in Muddy Creek.

Listed last in Table 1.1 is the proposed model, which corresponds to a complete rederivation of the linear theory of Ikeda et al. (1981). The continuity equation of sediment transport and the downstream sediment transport relation is added to the model of Ikeda et al. (1981) (Table 1.1). The coupling between the flow field, sediment transport, and bed topography is therefore retained. It is shown that the overdeepening of Struiksma et al. (1985) and the resonance detected by Blondeaux and Seminara (1985) are closely related phenomena, both arising from the same above-mentioned coupling. The results are compared with both laboratory and field data, and it is concluded that the overdeepening can be very satisfactorily simulated with a linear model.

1.3 Overview of Available Bank Erosion Models

A summary of available models for simulating the bank erosion process and the lateral migration rates of meandering rivers is given in Table 1.2, together with some of the underlying assumptions.

The first model quoted therein for estimating bank erosion rates is that of Hickin and Nanson (1975) (Table 1.2). They suggested the existence of a relationship between the outward normal migration rate and the ratio of channel half-width, b, to channel centerline radius of curvature, $\tilde{r}$. Their data, determined from scroll bars (Hickin, 1974), indicates that normal outward migration rate increases as $b/\tilde{r}$ increases, up to a limiting value of $b/\tilde{r}$ of about 1/6. For tighter bends, the migration rate declines. This empirical relation has since been improved upon by Nanson and Hickin (1983).

The model proposed by Hickin and Nanson (1975) and Nanson and Hickin (1983) is empirical in nature, since the dimensionless curvature, $b/\tilde{r}$, cannot by itself generate bank erosion. Hickin (1978) suggested, based on field observations, that the underlying physical process driving bank erosion is the shear stress, exerted on the bank by the primary flow. This leads to the following conclusion: If the downchannel component of the primary flow is higher at the left river bank than the right bank, the left bank will erode and deposition will occur at the right bank. The lateral variation in the primary flow velocity is, however, driven by the channel curvature. This explains the relation between the physical process causing bank erosion (Hickin, 1978) and the proposed empirical relation of Hickin and Nanson (1975) and Nanson and Hickin (1983).

The algebraic relation between channel migration rate and dimensionless channel curvature as proposed by Hickin and Nanson (1975) and Nanson and Hickin (1983), cannot be true everywhere along the channel, as discussed by Parker (1983), since it cannot reproduce the commonly observed downvalley migration of river meanders. Ikeda et al. (1981) resolved this problem by calculating the lateral distribution of the depth-averaged primary flow velocity along the channel. As done by Hickin (1978) they then assumed the river migration to be proportional to the difference between the near-bank primary flow velocity and the mean channel velocity. The model of Ikeda et al. (1981) predicts that, in the downstream part of a long bend of approximately constant curvature, where the flow approaches fully developed bend flow, the bank erosion rate increases linearly with the dimensionless curvature, $b/\tilde{r}$. This was shown by Parker (1983) to agree with the empirical relation of Hickin and Nanson (1975) and Nanson and Hickin (1983) for values of $b/\tilde{r} < 1/6$. For values of $b/\tilde{r} > 1/6$ the agreement becomes progressively worse. This is to be expected, since the model of Ikeda et al. (1981) is a linear model, valid only for $b/\tilde{r} << 1$.

Beck (1988) tried to improve the river meander model of Ikeda et al. (1981) by using the bank erosion model of Roher (1983) (Table 1.2). Roher (1983) suggested that if the actual sediment transport at the bank is less than the transport capacity of the flow, local scour may occur and steepen the bank until it fails, leading to bank retreat. As shown in Table 1.1, the sediment continuity equation and the downstream sediment transport relation are absent from the flow field and bed topography model of Beck (1988). He, however, used the downstream sediment transport relation and a force balance relation on a sediment particle, together with the previously determined flow field and bed topography, to calculate the downstream and cross-stream sediment transport. The continuity equation of sediment is then satisfied by calculating the unsteady scour and deposition. Finally, the bank erosion rate is assumed to be proportional to the unsteady bed scour rate at the bank. It should be noted that Roher (1983) calculated the sediment imbalance at the bank very differently than proposed by Beck (1988).

Table 1.2 - Overview of Available Bank Erosion Models

	Bank Erosion Model
Hickin & Nanson (1975) Nanson & Hickin (1983)	Obtained an empirical expression that relates the bank erosion rate to the dimensionless channel centerline curvature, $b/\tilde{r}$.
Ikeda et al. (1981) Blondeaux & Seminara (1985) Odgaard (1987) Crosato (1987) Proposed model	Bank erosion rate is proportional to the near-bank primary flow velocity excess, i.e. the difference between the near-bank primary flow velocity and the mean channel velocity.
Roher (1983) Beck (1988)	Bank erosion rate is proportional to sediment imbalance at the bank.
Kitanidis & Kennedy (1984)	Bank erosion rate is proportional to the strength of the secondary flow.

The problem with the approach of Beck (1988) is the failure to realize that the time scale of river migration is usually much larger than that of bed deformation (at least for sand-bed streams. The steady version of the continuity equation of sediment transport should therefore be satisfied as the flow field and the bed topography is calculated (Blondeaux and Seminara, 1985, Struiksma et al., 1985). This leads to no sediment imbalance at the bank, or anywhere else as that matters, and no bank erosion if the bank erosion model of Beck (1988) is used.

Over the last few years, the bank erosion model of Ikeda et al. (1981) has gradually become accepted as a very reasonable choice. It has been extensively used by the river mechanics group at the St. Anthony Falls Hydraulic Laboratory (Parker, 1982; Beck et al. 1983a,b; Johannesson, 1985) and more recently at the University of Genova, Italy (Blondeaux and Seminara, 1985), at the Iowa Institute of Hydraulic Research (Odgaard, 1987), and at the Delft Hydraulics Laboratory, Netherlands (Crosato, 1987) (Table 1.2). It can, however, by no means be concluded that this is the one and only, or even the dominant, process driving bank erosion in meandering rivers. For example, it has been suggested by Kitanidis and Kennedy (1984), Table 1.2, that the secondary flow may be the dominant mechanism responsible for the initiation and development of meanders. They described the physical process by the following quotation from Zimmermann and Kennedy (1978, p. 34):

> Near the bed, where the concentration of transported sediment is higher, the secondary current moves sediment inward across the channel and deposits some of it near the inside of the bend, while the concave bank is subjected to the erosive attack of the sediment-deficient fluid from the upper levels of the stream and the bed near the outside bank is scoured. It is this pattern of scour and deposition produced by the secondary flow that leads to the increase in channel sinuosity and that produces the transverse bed slope that is one of the dominant characteristics of alluvial channel meanders. Accordingly, any analytical model of flow in river bends must include a mathematical description of the secondary flow and its effect on the local direction and rate of sediment transport.

In addition, Lapointe and Carson (1986) concluded based on their field measurements that outward erosion of channel bends starts further upstream than predicted by the bank erosion model of Ikeda et al. (1981). They emphasized the importance of including the hydraulic processes allowing evacuation of entrained bank materials from the bank region. They further postulated that in early transitional flow zones, at bend entrances, outer bank erosion can occur despite low primary flow velocities, because the nascent secondary flow provides favorable sediment removal conditions at the bank toe. On the other hand, in developed flow zones, the intensity of near-bank primary flow velocities may indeed be the main control of the distribution of erosion. This is, they argued, because the secondary flow circulation in these reaches appears capable of evacuating the bank influxes, laterally away from the thalweg.

The reason why it is not possible to conclude which is the right, or the dominant, bank erosion process, is that it is not at all apparent how the different mechanisms can be measured experimentally. This is why the approach followed, herein, is to improve the calculation of the flow field and bed topography before the emphasis is shifted toward the bank erosion model. Where a bank erosion model is needed, the model of Ikeda et al. (1981) is used (Table 1.2).

2. FLOW AND BED TOPOGRAPHY

2.1 Governing Equations

2.1.1 Equations Describing the Flow Field

The curved channel is shown in Fig. 2.1. The channel has an erodible bed. The location of the channel centerline is assumed to be given, and its curvature is by definition equal to

$$\tilde{C}(\tilde{s}) = -\frac{d\theta}{d\tilde{s}} = \frac{1}{\tilde{r}} \tag{2.1}$$

where θ is the angle between the downchannel direction and the $\tilde{x}$-axis, and $\tilde{r}$ is the radius of curvature of the channel centerline. The tilde denotes a dimensional variable.

Let $\tilde{u}$ and $\tilde{v}$ denote fluid velocity in the $\tilde{s}$ and $\tilde{n}$ directions, respectively (Fig. 2.1). The following velocity structure is assumed:

$$\tilde{u} = \bar{u}(\tilde{s},\tilde{n})T(\zeta) \quad ; \quad \tilde{v} = \bar{v}(\tilde{s},\tilde{n})T(\zeta) + \tilde{v}(\tilde{s},\tilde{n},\zeta) \tag{2.2a,b}$$

where $\bar{u}$ and $\bar{v}$ denote the vertically averaged values of $\tilde{u}$ and $\tilde{v}$, $T(\zeta)$ is a dimensionless velocity shape function averaging to unity, $\zeta = \tilde{z}/\tilde{h}$ where $\tilde{z}$ is distance upward normal from the bed, $\tilde{h}$ is upward normal depth, and $\tilde{v}$ is the transverse helical (secondary) flow (e.g. Kalkwijk and De Vriend, 1980; Smith and McLean, 1984). Since $\tilde{v}$ must average in the vertical to $\bar{v}$, it follows that

$$\int_0^1 T(\zeta)d\zeta = 1 \quad ; \quad \int_0^1 \tilde{v}d\zeta = 0 \tag{2.3a,b}$$

The multiple length scales that characterize the flow in a meander bend are: The mean flow depth H, the channel half-width b, the meander wavelength $\tilde{\lambda}$, measured along the channel centerline, and the minimum radius of curvature $\tilde{r}_m$. It is assumed in the following analysis that since $b/\tilde{\lambda} << 1$, the downstream momentum balance can be stated in depth-averaged form, although the same approximation cannot be made when stating the transverse momentum balance.

Under the assumption of steady flow slender enough to satisfy the boundary layer approximations and hydrostatic pressure, the depth-averaged equation of downstream momentum balance can be written as

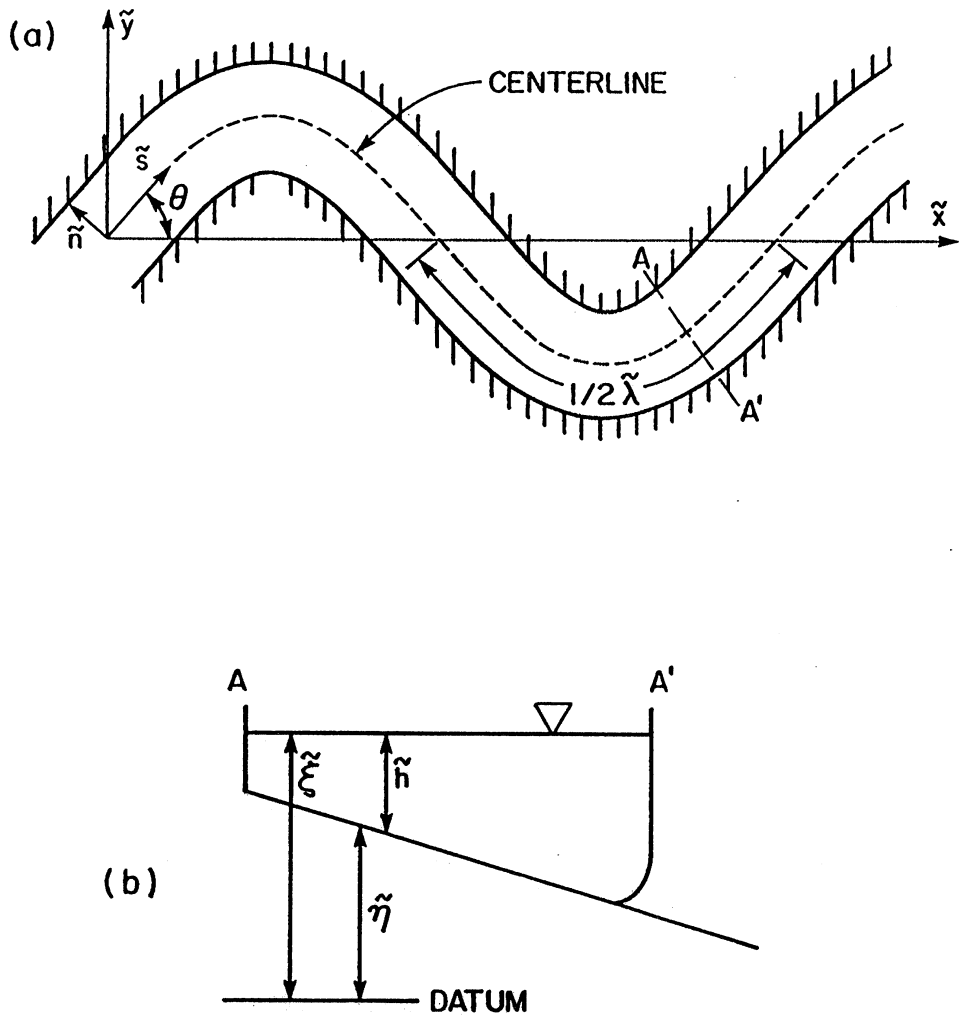

Fig. 2.1. Definition of variables and coordinate system.

$$\overline{T^2}\left[\frac{1}{1+\tilde{n}\tilde{C}}\bar{u}\frac{\partial\bar{u}}{\partial\tilde{s}}+\bar{v}\frac{\partial\bar{u}}{\partial\tilde{n}}+\frac{\tilde{C}}{1+\tilde{n}\tilde{C}}\bar{u}\bar{v}\right]=-g\frac{1}{1+\tilde{n}\tilde{C}}\frac{\partial\tilde{\xi}}{\partial\tilde{s}}-\frac{\tilde{\tau}_s}{\rho\tilde{h}}$$

$$-\frac{1}{\tilde{h}}\left\{\frac{\partial}{\partial\tilde{n}}\left[\bar{u}\tilde{h}\int_0^1 T\tilde{v}d\zeta\right]+\frac{2\tilde{C}}{1+\tilde{n}\tilde{C}}\bar{u}\tilde{h}\int_0^1 T\tilde{v}d\zeta\right\} \quad (2.4)$$

where g is acceleration due to gravity, $\tilde{\xi}$ is the water-surface elevation, $\tilde{\eta}$ is the bed-surface elevation, $\tilde{\tau}_s$ is the bed shear stress component in the $\tilde{s}$ direction, ρ is the density of water, and $\overline{T^2}$ is the momentum correction coefficient which variation from unity is small and will be neglected.

Further assuming a fully turbulent flow and constant eddy viscosity, υ_t, the equation of transverse momentum balance can be written as

$$\frac{1}{1+\tilde{n}\tilde{C}}\bar{u}T\frac{\partial}{\partial\tilde{s}}(\bar{v}T+\tilde{v})+(\bar{v}T+\tilde{v})\frac{\partial}{\partial\tilde{n}}(\bar{v}T+\tilde{v})-\frac{\tilde{C}}{1+\tilde{n}\tilde{C}}\bar{u}^2T^2=-g\frac{\partial\tilde{\xi}}{\partial\tilde{n}}+\upsilon_t\frac{\partial^2}{\partial\tilde{z}^2}(\bar{v}T+\tilde{v}) \quad (2.5)$$

The depth-averaged continuity equation is

$$\frac{\partial\bar{u}\tilde{h}}{\partial\tilde{s}}+\frac{\partial}{\partial\tilde{n}}\left[(1+\tilde{n}\tilde{C})\bar{v}\tilde{h}\right]=0 \quad (2.6)$$

The bed stress in the $\tilde{s}$-direction is evaluated with the use of a friction factor, C_f;

$$\tilde{\tau}_s=\rho C_f\sqrt{\bar{u}^2+\bar{v}^2}\,\bar{u} \quad (2.7)$$

It is important to realize that Eqs. 2.4, 2.5, and 2.6 are valid only in the central portion of the channel at a distance greater than one channel depth from each bank. Close to the banks the assumption that the vertical velocity component is negligible, and the corresponding reduction of the equation of vertical momentum to the hydrostatic condition, are no longer valid. This does not seriously diminish the range of problems to which this model can be applied, since for natural rivers depth over half-width ratio H/b ~ 0.1, making the model typically valid over about 90% of the channel width.

So far the following five unknown variables have been introduced; $\tilde{u}$, $\tilde{v}$, $\tilde{\xi}$, $\tilde{\eta}$, and $\tilde{\tau}_s$. Equations 2.4 to 2.7 are therefore not enough to fully specify this problem. The additional relation needed is the one that determines the bed-surface elevation, $\tilde{\eta}$.

2.1.2 Equations Describing the Bed Topography

The equation of sediment conservation for transport of bedload takes the form

$$(1-p)\frac{\partial \tilde{\eta}}{\partial \tilde{t}} + \frac{1}{1+\tilde{n}\tilde{C}}\left\{ \frac{\partial \tilde{q}_s}{\partial \tilde{s}} + \frac{\partial}{\partial \tilde{n}}\left[(1+\tilde{n}\tilde{C})\,\tilde{q}_n \right] \right\} = 0 \qquad (2.8)$$

where $(\tilde{q}_s, \tilde{q}_n)$ denotes the volumetric sediment transport per unit width in the $(\tilde{s}, \tilde{n})$ direction, and p is bed sediment porosity.

Following the analysis of Engelund (1974), Gottlieb (1976), and Struiksma et al. (1985) the downstream sediment transport relationship is taken to be

$$\tilde{q}_s \sim (\tilde{u})^M \qquad (2.9)$$

where M is a given O(1) constant. If the Engelund-Hansen (1967) sediment transport formula is used M (see derivation in Appendix A) is given as

$$M = 2 + \frac{3}{2}\frac{1}{1 - \tau_C^*/\tau_G^*} \qquad \text{(lower regime dune-covered bed)} \qquad (2.10a)$$

$$M = 5 \qquad \text{(upper regime flat bed)} \qquad (2.10b)$$

where

$$\tau^* = \tilde{\tau}_s/(\rho R g D_{50}) \qquad (2.11)$$

is the downstream Shields stress, τ_C^* denotes critical Shields stress, τ_G^* (grain Shields stress) is that part of τ^* active in the bedload process, R is the submerged specific gravity of the sediment, and D_{50} is the mean particle grain size of the bed material.

The appropriate friction law to use in connection with the Engelund-Hansen (1967) sediment transport formula is

$$(C_f \tau_G^*/\tau^*)^{-1/2} = 6 + 2.5 \ln\left(\frac{1}{2.5}\frac{\tau_G^*}{\tau^*}\frac{\tilde{h}}{D_{50}}\right) \qquad \text{(lower regime dune covered bed)} \qquad (2.12a)$$

$$\tau_G^* = \tau^* \qquad \text{(upper regime flat bed)} \qquad (2.12b)$$

In order to determine the existing flow regime, the approximate procedure of Brownlie (1983) is used. He analyzed a large number of both experimental and field data and found that upper regime flow exists if at least one of the following conditions are satisfied

$$\frac{U}{\sqrt{RgD_{50}}} > 1.74\,(I)^{-1/3} \quad ; \quad I > 0.006 \tag{2.12c,d}$$

Finally, the lateral sediment transport relationship, obtained by equating all the forces acting on a spherical sand grain moving on the bed, takes the form (Kikkawa et al., 1976; Parker, 1984)

$$\frac{\tilde{q}_n}{\tilde{q}_s} = \frac{\bar{v}T(0) + \tilde{v}(0)}{\bar{u}T(0)} - \beta\frac{\partial\tilde{\eta}}{\partial\tilde{n}} \tag{2.13}$$

where

$$\beta = \frac{1 + \alpha_* \mu}{f_* \mu}\sqrt{\frac{\tau_C^*}{\tau_G^*}} \tag{2.14}$$

In the above equation α_* is the ratio of lift coefficient to drag coefficient for a spherical sand particle placed on a rough bed, μ is the dynamic angle of Coulomb friction, and f_* is a coefficient to be determined from data that should equal unity if the theory is perfectly correct. The only difference between Eqs. 2.13 and 2.14 and the corresponding equation derived by Kikkawa et al. (1976) and Parker (1984) is that therein it is assumed that all the shear stress is active in the bed load process rather than just τ_G^*. It will be shown by comparison with data that the use of τ_G^* gives somewhat better results. The values recommended in the literature to be used for α_* and μ vary considerably (e.g. Kikkawa et al. (1976) use $\mu = 0.43$, Wiberg and Smith (1985) use $\mu = 1.73$). Rather than engaging in a fruitless discussion as to which are the appropriate values to use, the suggested values of Kikkawa et al. (1976) are chosen ($\alpha_* = 0.85$, $\mu = 0.43$) and the coefficient f_* is added in order to account for inaccuracies introduced by this choice. The value of f_* will be determined from the data of Zimmermann and Kennedy (1978).

2.2 The Primary Flow for a Straight Channel

The problem is analyzed in terms of an expansion for small curvature. At zeroth order, the primary flow obeys the downstream momentum balance relation for steady, uniform flow in a straight channel. If I is the average down-channel water-surface slope, then,

$$0 = gI + \upsilon_t \frac{d^2\tilde{u}}{d\tilde{z}^2} \tag{2.15}$$

Herein $\tilde{u}$ is obtained using the Engelund (1974) slip-velocity method, according to which

$$\upsilon_t = \alpha \tilde{u}_* \tilde{h} \tag{2.16}$$

where $\alpha = 0.077$ and

$$\tilde{u}_*^2 = \upsilon_t \frac{d\tilde{u}}{d\tilde{z}}\Big|_{\tilde{z}=0} = \frac{\tilde{\tau}_s}{\rho} \tag{2.17}$$

The bed boundary condition is approximated as follows: where $\tilde{u}\,|_{\tilde{z}=0} \equiv \tilde{u}_b$,

$$\frac{\tilde{u}_b}{\tilde{u}_*} = r_* \tag{2.18}$$

where for rough flow, matching with the logarithmic profile yields

$$r_* = 2 + 2.5 \ln\left(\frac{\tilde{h}}{k_*}\right) \tag{2.19}$$

and k_* is the roughness height.

The solution of Eq. 2.15, together with Eq. 2.18 and the condition of vanishing shear stress at the water-surface, is

$$\tilde{u} = \bar{u} T(\zeta) \quad ; \quad T(\zeta) = \frac{\chi + \zeta - \frac{1}{2}\zeta^2}{\chi_1} \tag{2.20a,b}$$

where

$$\chi = r_* \alpha \quad ; \quad \chi_1 = \chi + \frac{1}{3} \tag{2.21a,b}$$

As $\tilde{h}/k_*$ varies from 10 to 200, r_* varies from 7.8 to 15.3 and χ from 0.6 to 1.17, so both χ and χ_1 are order-one.

Several useful auxiliary relations can be established from the above analysis. For example, Eq. 2.18 can be rewritten as

$$T(0) = \chi \dot{T}(0) \tag{2.22}$$

where $\dot{} = d/d\zeta$. If Eq. 2.22 is generalized to the case where the near-bed flow is at an angle to the centerline, reduction with Eq. (2.2a,b) and the condition that the bed shear

stress vector ($\tilde{\tau}_s$, $\tilde{\tau}_n$) should be parallel to the near-bed flow velocity vector yields Eq. 2.22 and the condition

$$\tilde{v}(0) = \chi \dot{\tilde{v}}(0) \tag{2.23}$$

A friction factor C_f for the zeroth-order primary flow can be defined as follows

$$C_f = \frac{\tilde{\tau}_s}{\rho \bar{u}^2} \tag{2.24}$$

The above yield the results

$$C_f \equiv \left(\frac{u_*}{\bar{u}}\right)^2 = \left(\frac{\alpha}{\chi_1}\right)^2 \tag{2.25}$$

$$\tilde{\tau}_s = \rho \upsilon_t \frac{\partial \tilde{u}}{\partial \tilde{z}} = \rho \chi_1 C_f \bar{u}^2 \dot{T} \tag{2.26}$$

2.3 Governing Equations: Dimensionless Form

Let U and H denote reach-averaged values of $\bar{u}$ and $\tilde{h}$. At zeroth order, then,

$$C_f U^2 = gHI \;\; ; \;\; UH = \tilde{q}_w \;\; ; \;\; \tilde{q}_s = \tilde{q}_{s0} \tag{2.27a,b,c}$$

where $\tilde{q}_w$ is water discharge per unit width. Dimensionless variables are defined as follows:

$$s = \frac{\tilde{s}}{b} \;\; ; \;\; n = \frac{\tilde{n}}{b} \;\; ; \;\; u = \frac{\bar{u}}{U} \;\; ; \;\; \hat{v} = \frac{\bar{v}}{U} \;\; ; \;\; \upsilon = \frac{\tilde{v}}{U} \;\; ; \;\; \tau_s = \frac{\tilde{\tau}_s}{\rho U^2} \tag{2.28a}$$

$$\xi = \frac{\tilde{\xi}}{H} \;\; ; \;\; h = \frac{\tilde{h}}{H} \;\; ; \;\; \eta = \frac{\tilde{\eta}}{H} \;\; ; \;\; t = \tilde{t}\,\frac{U}{b} \;\; ; \tag{2.28b}$$

$$C = b\tilde{C} \;\; ; \;\; r = \frac{\tilde{r}}{b} \;\; ; \;\; F = \frac{U}{\sqrt{gH}} \;\; ; \;\; \gamma = \frac{b}{H} \;\; ; \;\; \varepsilon = \gamma C_f \;\; ; \tag{2.28c}$$

$$q_s = \frac{\tilde{q}_s}{\sqrt{RgD_{50}}\,D_{50}} \;\; ; \;\; q_n = \frac{\tilde{q}_n}{\sqrt{RgD_{50}}\,D_{50}} \;\; ; \;\; Q_0 = \frac{\sqrt{RgD_{50}}\,D_{50}}{(1\text{-}p)UH} \tag{2.28d}$$

Eq. 2.1 reduces with the aid of Eq. 2.28 to

$$C = -\frac{d\theta}{ds} = \frac{1}{r} \tag{2.29}$$

The governing equations (Eqs. 2.4, 2.5, 2.6, 2.8, 2.9, and 2.13) reduce with the aid of Eqs. 2.7, 2.16, 2.25, and 2.28 to:

$$\frac{1}{1+nC} u \frac{\partial u}{\partial s} + \hat{v} \frac{\partial u}{\partial n} + \frac{C}{1+nC} u \hat{v} = -\frac{1}{1+nC} F^{-2} \frac{\partial \xi}{\partial s} - \frac{\varepsilon}{h} \sqrt{u^2 + \hat{v}^2}\, u$$
$$- \frac{1}{h} \left\{ \frac{\partial}{\partial n} \left[uh \int_0^1 T \upsilon d\zeta \right] + \frac{2C}{1+nC} uh \int_0^1 T \upsilon d\zeta \right\} \tag{2.30}$$

$$\frac{1}{1+nC} uT \frac{\partial}{\partial s} (\hat{v}T + \upsilon) + (\hat{v}T + \upsilon) \frac{\partial}{\partial n} (\hat{v}T + \upsilon) - \frac{C}{1+nC} u^2 T^2 = -F^{-2} \frac{\partial \xi}{\partial n} + \varepsilon \chi_1 \frac{u}{h} (\hat{v}\ddot{T} + \ddot{\upsilon}) \tag{2.31}$$

$$\frac{\partial uh}{\partial s} + \frac{\partial}{\partial n} [\, (1+nC) \hat{v} h \,] = 0 \tag{2.32}$$

$$\frac{\partial \eta}{\partial t} + \frac{Q_0}{1+nC} \left\{ \frac{\partial q_s}{\partial s} + \frac{\partial}{\partial n} [\, (1+nC)\, q_n \,] \right\} = 0 \tag{2.33}$$

$$q_s = q_{s0}\, (u)^M \tag{2.34}$$

$$\frac{q_n}{q_s} = \frac{\hat{v}}{u} + \frac{\upsilon(0)}{uT(0)} - \frac{\beta}{\gamma} \frac{\partial \eta}{\partial n} \tag{2.35}$$

M, τ_G^*, and β are given as before by Eqs. 2.10, 2.12, and 2.14.

The boundary conditions needed to close the problem are:

1) The requirement of no net flow of water and sediment through the channel walls;

$$\hat{v} = q_n = 0 \quad \text{at } n = \pm 1 \tag{2.36a,b}$$

2) From Eqs. 2.3b, 2.23 and the condition of vanishing shear stress at the water-surface, the boundary conditions on Eq. 2.31 are:

$$\upsilon(0) = \chi\, \dot{\upsilon}(0) \;\; ; \;\; \dot{\upsilon}(1) = 0 \;\; ; \;\; \int_0^1 \upsilon d\zeta = 0 \tag{2.37a,b,c}$$

3. ANALYSIS FOR A SINUOUS CHANNEL

3.1 Introduction

In this chapter, a small perturbation approach is used to linearize the governing equations around the uniform flow solution for a straight channel. A small perturbation parameter, ψ_0, equal to a dimensionless measure of the maximum centerline curvature is defined. A regular perturbation expansion is carried out in this parameter, retaining only terms up to $O(\psi_0)$. This approach has been used successfully by Ikeda et al. (1981) and Blondeaux and Seminara (1983, 1985) to simulate flow field and bed topography in meandering rivers.

3.2 Governing Equations: Linearized Form

The channel centerline is assumed to follow a sinuous shape

$$\tilde{C} = \frac{1}{\tilde{r}} = -\frac{d\theta}{d\tilde{s}} = \frac{1}{\tilde{r}_m}\sigma(\tilde{k}\tilde{s}) \tag{3.1}$$

where $\tilde{r}_m$ is the minimum magnitude of the centerline radius of curvature, σ denotes an order-one dimensionless curvature, $\tilde{k} = 2\pi/\tilde{\lambda}$, and $\tilde{\lambda}$ are characteristic meander wavenumber and wavelength, respectively, both based on centerline arc length.

A dimensionless measure of the maximum centerline curvature is defined as

$$\psi_0 = \frac{b}{\tilde{r}_m} \tag{3.2}$$

Using the above relation, Eq. 3.1 can be rewritten (in dimensionless form) as

$$C = \psi_0\, \sigma(\phi) \tag{3.3}$$

where

$$\phi = k\, s \tag{3.4}$$

denotes phase, and $k = b\,\tilde{k}$. For example, for a sine-generated curve

$$\theta = \theta_0 \cos(ks) \tag{3.5}$$

where θ_0 is the angle amplitude, it follows from Eqs. 3.1, 3.2, and 3.3 that

$$\psi_0 = k\,\theta_0 \;\; ; \;\; \sigma = \sin\phi \tag{3.6a,b}$$

From Eq. 3.4, it follows that

$$\frac{\partial}{\partial s} = k \frac{\partial}{\partial \phi} \tag{3.7}$$

Ikeda et al. (1981) have shown that for typical meander bends, k and ε are of the same order of magnitude (see Fig. 5 therein), so that the rescaled wavenumber

$$r = \frac{k}{\varepsilon} \tag{3.8}$$

is order-one. This is illustrated in Fig. 3.1, where the values of r are plotted versus $\tilde{\lambda}_c$ for 75 field cases, $\tilde{\lambda}_c$ being equal to the meander wavelength measured along the valley (channel sinuosity = $\tilde{\lambda}/\tilde{\lambda}_c$). Although the scatter is notable, 73% of the points plot in the range $0.2 < r < 5$. Since the values of r in Fig. 3.1 are based on $\tilde{\lambda}_c$ rather than $\tilde{\lambda}$, which was not always reported, the resulting values for r are typically $1 \sim 2$ times higher than those based on $\tilde{\lambda}$. The input data used to generate Fig. 3.1 is the field data listed in Table B.1, Appendix B. Reducing Eq. 2.32 with the aid of Eqs. 3.7 and 3.8, it is found that

$$\varepsilon r \frac{\partial uh}{\partial \phi} + \frac{\partial}{\partial n}[(1 + nC)\hat{v}h] = 0 \tag{3.9}$$

By definition, all parameters are order-one except ε and $\hat{v}$; it follows that v is order-one where

$$\hat{v} = \varepsilon v \tag{3.10}$$

Eqs. 2.30 to 2.35 reduce with the aid of Eqs. 2.20b, 3.7, 3.8, and 3.10 to

$$\frac{r}{1+nC} uu' + v \frac{\partial u}{\partial n} + \frac{C}{1+nC} uv = -\frac{r}{1+nC} F^{-2} \xi' - \frac{u}{h} \sqrt{u^2 + \varepsilon^2 v^2}$$

$$- \frac{1}{\varepsilon h}\left[\frac{\partial}{\partial n}\left(uh \int_0^1 T\upsilon d\zeta\right) + \frac{2C}{1+nC} uh \int_0^1 T\upsilon d\zeta\right] \tag{3.11a}$$

$$\frac{1}{1+nC} uT\varepsilon r (\varepsilon vT + \upsilon)' + (\varepsilon vT + \upsilon)\frac{\partial}{\partial n}(\varepsilon vT + \upsilon) - \frac{C}{1+nC} u^2 T^2 = -F^{-2}\frac{\partial \xi}{\partial n} + \varepsilon \frac{u}{h}(-\varepsilon v + \chi_1 \ddot{\upsilon}) \tag{3.11b}$$

$$r(uh)' + \frac{\partial}{\partial n}[(1 + nC)vh] = 0 \tag{3.11c}$$

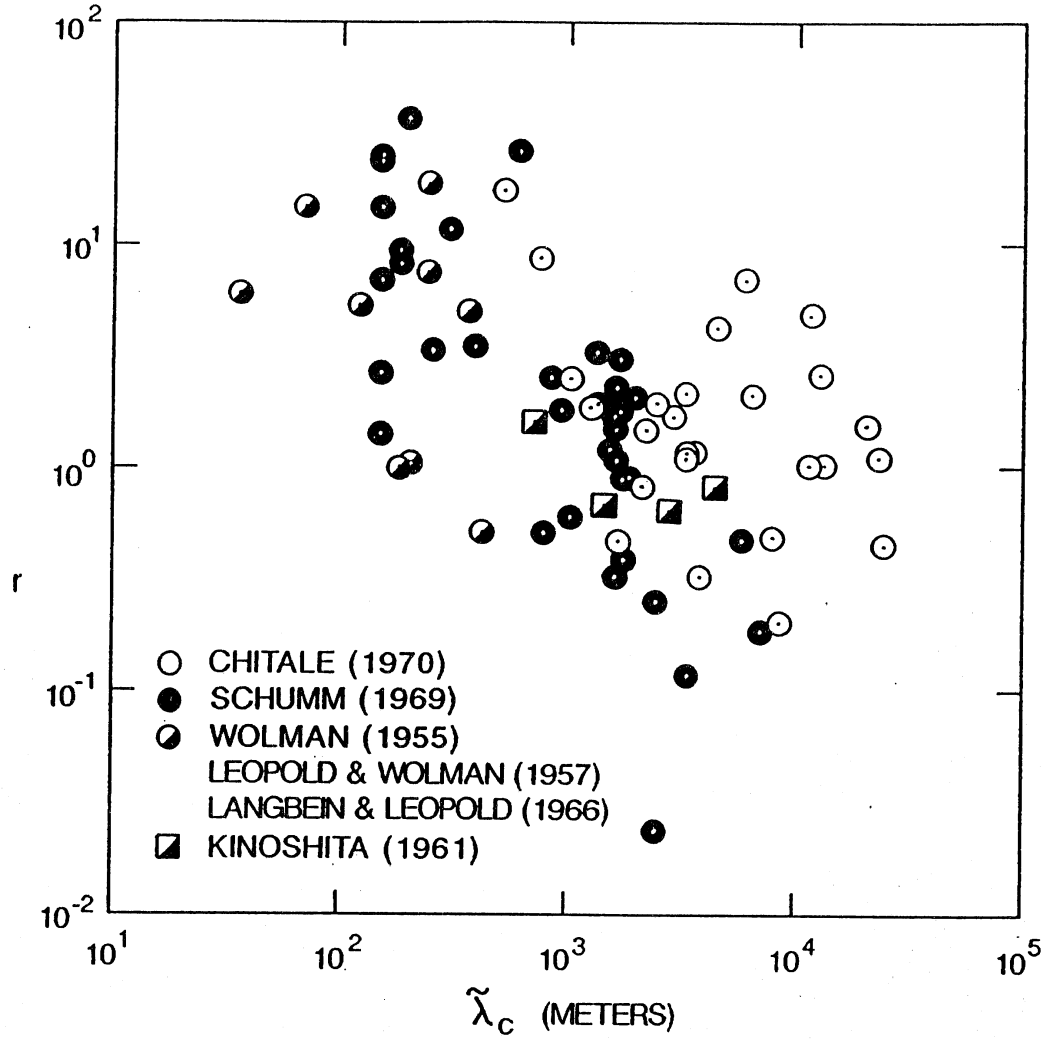

Fig. 3.1. The rescaled wavenumber r versus the wavelength $\tilde{\lambda}_c$ for 75 field cases.

$$\varepsilon r\,(u^M)' + \frac{\partial}{\partial n}[(1+nC)\frac{q_s}{q_{s0}}(\frac{\varepsilon v}{u} + \frac{\chi_1 \dot{\upsilon}(0)}{u} - \frac{\beta}{\gamma}\frac{\partial \eta}{\partial n})] = 0 \qquad (3.11d)$$

where $' = \partial/\partial\phi$, and the unsteady term has been dropped from the continuity equation of sediment transport since the flow and the bed topography is assumed to be fully adapted in time to the channel curvature.

At this point an expansion for small curvature, C, is introduced. Recalling that $C = \psi_0\sigma$, where σ is an order-one function of ϕ, and expanding in ψ_0, it is found that

$$(u, v, \upsilon) = (1, 0, 0) + \psi_0\,(u_1, v_1, \upsilon_1) + \ldots \qquad (3.12a)$$

$$(h, \xi, \eta) = (1, \xi_r - I_*s, \eta_r - I_*s) + \psi_0\,(h_1, \xi_1, \eta_1) + \ldots \quad ; \quad I_* = \frac{b}{H}I \qquad (3.12b,c)$$

$$(q_s, q_n) = q_{s0}\,[(1, 0) + \psi_0\,(q_{s1}, q_{n1}) + \ldots] \qquad (3.12d)$$

where ξ_r and η_r are reference elevations for which $H = \tilde{\xi}_r - \tilde{\eta}_r$. Substituting into Eqs. 3.11a through d, the following result is obtained at zeroth order

$$\varepsilon = F^{-2}I_* \quad ; \quad u = h = 1 \quad ; \quad q_s = q_{s0} \qquad (3.13a,b,c)$$

At $O(\psi_0)$ Eqs. 3.11a through d yield

$$r\,u_1' + 2u_1 = -F^{-2}r\,\xi_1' - n\sigma + \xi_1 - \eta_1 - \frac{1}{\varepsilon}\frac{\partial}{\partial n}\int_0^1 T\upsilon_1 d\zeta \qquad (3.14a)$$

$$\varepsilon Tr\,(\underline{\varepsilon v_1 T} + \upsilon_1)' - T^2\sigma = -F^{-2}\frac{\partial \xi_1}{\partial n} - \underline{\varepsilon^2 v_1} + \varepsilon\chi_1\ddot{\upsilon}_1 \qquad (3.14b)$$

$$r\,u_1' + r\,h_1' + \frac{\partial v_1}{\partial n} = 0 \qquad (3.14c)$$

$$r\,M\,u_1' + \frac{\partial}{\partial n}[\,v_1 + \frac{\chi_1\dot{\upsilon}_1(0)}{\varepsilon} - \Gamma\frac{\partial \eta_1}{\partial n}] = 0 \qquad (3.14d)$$

where $\Gamma = \beta/(\gamma\varepsilon) = \beta/(\gamma^2 C_f)$ is an O(1) coefficient, Table 3.2. In light of Table 3.2, the $O(\varepsilon^2)$ terms (i.e. the underlined terms) are small, and are henceforth dropped in Eq. 3.14b. The input data needed to generate Table 3.2 is given in Table 3.1. Note that for these rivers the observed values for r are typically O(1), with a scatter similar to the data shown in Fig. 3.1.

Table 3.1 - Bankfull Flow Conditions for Several Meandering Sand-Bed Streams

River	Reference	b (m)	$\tilde{\lambda}$ (m)	Q (m^3/s)	H (m)	U (m/s)	I	D_{50} (mm)	σ_g	R
Root	Johannesson (1985)	27.5	1300	430	2.90	2.71	$5.44 \cdot 10^{-4}$	0.50+	----	1.65
Zumbro	Johannesson (1985)	32.5	940	450	3.22	2.15	$6.20 \cdot 10^{-4}$	0.50+	----	1.65
Minnesota*	Johannesson (1985)	52.4	980	560	4.47	1.20	$1.86 \cdot 10^{-4}$	0.45	1.8	1.65
Red Lake	Johannesson (1985)	43.0	1170	330	2.78	1.36	$3.59 \cdot 10^{-4}$	0.50+	----	1.65
Minnesota*	Parker (1982)	46.3	1170	620	4.05	1.66	$0.97 \cdot 10^{-4}$	0.45	1.8	1.65
Pembina	Beck et al. (1983a)	40.5	1940	200	2.50	1.00	$2.60 \cdot 10^{-4}$	0.40	1.2	1.65
Genesee	Beck et al. (1983b)	36.9	1380	275	3.79	0.985	$2.01 \cdot 10^{-4}$	----	----	1.65
Muddy Cr.	Dietrich and Smith (1983)	2.4	50.4	1.1-	0.40	0.573	$14.0 \cdot 10^{-4}$	0.70	2.1	1.65
Fall	Thorne et al. (1985)	4.7	107	4.0	0.75	0.57	$21.5 \cdot 10^{-4}$	1.1	2.1	1.65

* Different reaches

\+ D_{50} not measured but estimated to be 0.5 mm

\- 69% of bankfull discharge

Table 3.2 - Various Parameters for Several Meandering Sand-Bed Streams at Bankfull Flow

River	Reference	$C_f^{-1/2}$	γ	ε	k	r	β	Γ
Root	Johannesson (1985)	21.8	9.5	0.020	0.13	6.5	0.39	2.03
Zumbro	Johannesson (1985)	15.4	10.1	0.043	0.22	5.1	0.34	0.79
Minnesota*	Johannesson (1985)	13.2	11.7	0.067	0.34	5.1	0.90	1.16
Red Lake	Johannesson (1985)	13.7	15.5	0.082	0.23	2.8	0.80	0.63
Minnesota*	Parker (1982)	26.7	11.4	0.016	0.25	15.6	0.67	3.65
Pembina	Beck et al. (1983a)	12.5	16.2	0.103	0.13	1.3	0.93	0.56
Genesee	Beck et al. (1983b)	11.4	9.7	0.075	0.17	2.3	----	----
Muddy Cr.	Dietrich and Smith (1983)	7.73	6.0	0.10	0.30	3.0	1.58	2.62
Fall	Thorne et al. (1985)	4.53	6.3	0.31	0.28	0.90	1.93	1.01

* Different reaches

At $O(\psi_0)$ the boundary conditions given by Eqs. 2.36a,b and 2.37a,b,c reduce to

$$v_1 = q_{n1} = 0 \quad \text{at } n = \pm 1 \tag{3.15a,b}$$

$$\upsilon_1(0) = \chi\dot{\upsilon}_1(0) \;\; ; \;\; \dot{\upsilon}_1(1) = 0 \;\; ; \;\; \int_0^1 \upsilon_1 d\zeta = 0 \tag{3.16a,b,c}$$

Further conditions needed to fully specify the problem are the requirements that the total discharge of water and sediment and the average river slope are unaffected by the perturbed quantities; to wit

$$\int_{-1}^{1}(u_1 + h_1)dn = 0 \;\; ; \;\; \int_{-1}^{1} u_1 dn = 0 \;\; ; \;\; \int_0^{2\pi}\int_{-1}^{1} \xi_1' dn d\phi = 0 \tag{3.17a,b,c}$$

It can be deduced from the governing equations that the form of the solution for ξ_1, η_1, and u_1 is a function of ϕ and n, for which the variation in n is odd, plus a function of ϕ which indicates the variation in the cross-sectionally averaged values of ξ_1, η_1, and u_1 from zero. This fact, together with Eqs. 3.14a and 3.17a,b,c, allows the integral conditions given by Eqs. 3.17a,b,c to be simplified to

$$u_1 = \xi_1 = \eta_1 = 0 \quad \text{at } n = 0 \tag{3.18a,b,c}$$

3.3 Discussion

The above linearized version of the governing equations (Eqs. 3.14a,b,c,d) constitutes a considerable improvement to the model of Ikeda et al. (1981). Therein, the convective transport of primary flow momentum by the secondary flow is not accounted for (the last term on the right hand side of Eq. 3.14a). This term can be of considerable importance, as shown in Chapter 4. Secondly, Ikeda et al. (1981) did not take into account the metric coefficients that arise in a curvilinear coordinate system which introduces the term - $n\sigma$ in Eq. 3.14a (e.g. Tamai and Ikeuchi, 1984; Johannesson, 1985; Blondeaux and Seminara, 1985). As shown in Chapter 4 this term becomes important in the limiting case of a flat bed channel with large aspect ratio, ($\gamma = b/H \rightarrow \infty$). Thirdly, Ikeda et al. (1981) used the depth-averaged form of the transverse momentum equation, which does not allow for the calculation of the secondary flow. As done herein they neglected the underlined terms. They then determined the secondary flow using an expression derived for fully developed bend flow in circular channels. Equation 3.14b, on the other hand, can allow for a more accurate calculation of the secondary flow. Most importantly, it allows for calculation of the phase lag between the channel curvature and the secondary flow strength. This lag tends to be rather small for natural channels, but is quite large for many commonly-quoted experiments (Chapter 5). Finally, Ikeda et al. (1981) assumed the bed topography to be solely driven by the secondary flow. This corresponds to setting M = 0

and neglecting v_1 in Eq. 3.14d. As shown in Chapters 5, 6, 7, and 8 this is the reason the model of Ikeda et al. (1981) can predict neither the resonance phenomenon detected by Blondeaux and Seminara (1985) nor the overdeepening observed and predicted by Struiksma et al. (1985).

The resulting governing equations (Eqs. 3.14a,b,c,d) are very similar to the model of Blondeaux and Seminara (1985), Eq. 32 therein. The most important difference is that Blondeaux and Seminara (1985) did not neglect the underlined terms in Eq. 3.14b. These terms are of importance for alternate bars, which, however, are not the subject of this analysis. Secondly, Blondeaux and Seminara (1985) used the depth-averaged form of the transverse momentum equation, which does not allow for the calculation of the secondary flow. They then determined the secondary flow using an expression derived for fully developed flow in circular channels as done in the model of Ikeda et al. (1981). Thirdly, Blondeaux and Seminara (1985) did not account for the convective transport of primary flow momentum by the secondary flow. Fourthly, Blondeaux and Seminara (1985) expanded the friction factor, which is taken to be constant herein. Finally, Blondeaux and Seminara (1985) included the dependence of the streamwise bedload function on local depth, the influence of which is neglected inherently herein in the power law assumption given by Eq. 2.9. Further discussion is given in Appendix A as regards the final two points.

The relative validity of the various theories is discussed in subsequent chapters where predicted results are compared with data.

4. SOLUTION FOR FULLY DEVELOPED FLOW IN A CONSTANT CURVATURE CHANNEL

4.1 Introduction

Fully developed flow in a constant curvature channel is a classical case that has been analyzed by many researchers (e.g. Rozovskii, 1961; Engelund, 1974; Falcon and Kennedy, 1983).

The main advantage of analyzing this elementary case before developing a solution for an arbitrarily shaped channel is that the model, and its underlying assumptions, can be tested with data for a relatively simple situation before a solution for more complicated channel geometry is attempted. Most importantly, the lateral distribution of the depth-averaged primary flow velocity is approximated to be linear. The well-known "moment method" developed by Aris (1956), commonly used to solve for concentration distributions, is then used to obtain the solution. This makes it possible to take into account the convective transport of primary flow momentum by the secondary flow, as long as the strength of the secondary flow is known at every point. The influence of the secondary flow has been shown to be an important factor affecting the lateral variation in the depth-averaged primary flow velocity (e.g Leschziner and Rodi, 1979; Kalkwijk and De Vriend, 1980; De Vriend, 1981; De Vriend and Geldof, 1983), although it has often been neglected (e.g. Engelund, 1974; Ikeda et al., 1981; Smith and McLean, 1984; Blondeaux and Seminara, 1985; Struiksma et al., 1985; Odgaard, 1986a). The model developed herein is tested with laboratory data; it gives substantially better results than the model of Ikeda et al. (1981).

4.2 Statement of the Problem

In the case of fully developed flow in a channel of constant curvature, $\tilde{C}$, the parameter σ may be set equal to unity without loss of generality, and thus $\psi_0 = C$ (Eqs. 3.2 and 3.3); the streamwise derivatives ($\partial/\partial\phi$) vanish. The water and sediment continuity equations (Eqs. 3.14c,d) then reduce to

$$v_1 = c_1 \tag{4.1a}$$

$$q_{n1} = \varepsilon v_1 + \chi_1 \dot{v}_1(0) - \frac{\beta}{\gamma}\frac{\partial \eta_1}{\partial n} = c_2 \tag{4.1b}$$

where c_1 and c_2 are arbitrary constants. The boundary conditions of no net flow of either water or sediment through the channel walls (Eq. 3.15a,b) may be used to determine the values of the coefficients to be $c_1 = c_2 = 0$. The only solution is the obvious one;

$$v_1 = q_{n1} = 0 \tag{4.2a,b}$$

Eqs. 3.14a,b and d yield

$$2u_1 = -n + \xi_1 - \eta_1 - \frac{1}{\varepsilon}\frac{\partial}{\partial n}\int_0^1 T\upsilon_1 d\zeta \qquad (4.3a)$$

$$-T^2 = -F^{-2}\frac{\partial \xi_1}{\partial n} + \varepsilon\chi_1\ddot{\upsilon}_1 \qquad (4.3b)$$

$$0 = \chi_1\dot{\upsilon}_1(0) - \frac{\beta}{\gamma}\frac{\partial \eta_1}{\partial n} \qquad (4.3c)$$

The boundary conditions are (Eqs. 3.16a,b,c and 3.18a,b,c):

$$\upsilon_1(0) = \chi\dot{\upsilon}_1(0) \;\; ; \;\; \dot{\upsilon}_1(1) = 0 \;\; ; \;\; \int_0^1 \upsilon_1 d\zeta = 0 \qquad (4.4a,b,c)$$

$$u_1 = \xi_1 = \eta_1 = 0 \qquad \text{at } n = 0 \qquad (4.5a,b,c)$$

The problem is now fully specified. Eq. 4.3b together with the boundary conditions given by Eqs. 4.4a,b,c, and 4.5b can be solved to give ξ_1 and υ_1. Using the result for υ_1, Eq. 4.3c can be integrated to give η_1. Direct substitution of ξ_1, υ_1, and η_1 into Eq. 4.3a yields an expression for u_1.

4.3 Solution for the Water-Surface and the Secondary Flow

Eq. 4.3b together with the boundary conditions given by Eqs. 4.4a,b,c, and 4.5b can be integrated directly to give:

$$\xi_1 = F^2\chi_{20}\, n \qquad (4.6)$$

where

$$\chi_{20} = \frac{1}{\chi_1^3}\left(\chi^3 + \chi^2 + \frac{2}{5}\chi + \frac{2}{35}\right) \qquad (4.7)$$

and

$$\varepsilon\chi_1\upsilon_1 = G_0(\zeta) \qquad (4.8)$$

where

$$G_0(\zeta) = \frac{1}{\chi_1^2}\left[\left(\chi^2 + \frac{2}{3}\chi + \frac{2}{15}\right)(\chi + \zeta) - \frac{1}{2}\chi^2\zeta^2 - \frac{1}{3}\chi\zeta^3 - \frac{1}{12}(1-\chi)\zeta^4 + \frac{1}{20}\zeta^5 - \frac{1}{120}\zeta^6 \right]$$

$$- \chi_{20}\left(\chi + \zeta - \frac{1}{2}\zeta^2\right) \qquad (4.9)$$

4.4 Solution for the Bed Topography

The transverse bed slope associated with developed secondary flow is obtained from Eq. 4.3c. From Eqs. 4.8 and 4.9, it is found that

$$\varepsilon\chi_1\dot{\upsilon}_1(0) = -\frac{2}{45\chi_1^3}\left(\chi + \frac{2}{7}\right) \qquad (4.10)$$

in which case $\dot{\upsilon}_1(0) \sim (2/45)/\varepsilon \sim O(1)$ since ε is typically O(0.1), Table 3.2. Substituting this result into Eq. 4.3c, and using the boundary condition given by Eq. 4.5c, it is found that

$$\eta_1 = -A\,n \qquad (4.11)$$

where

$$A = \frac{\gamma}{\varepsilon\beta}\frac{2}{45}\frac{\chi + \frac{2}{7}}{\chi_1^3} \qquad (4.12)$$

is a bed scour factor. Note that by definition from Eq. 4.11, A must vanish for a horizontal non-erodible bed. According to Odgaard (1981), it is typically between 2.5 and 6 for sand-bed rivers. Reducing with Eqs. 2.28c and 2.25, it is found that

$$A = \frac{1}{\alpha^2\beta}\frac{2}{45}\frac{\chi + \frac{2}{7}}{\chi + \frac{1}{3}} \qquad (4.13)$$

For "typical" values $\chi = 1$ and $\beta = 1.5$, for example, a value of A of 4.82 is realized. Equations 4.11 and 4.13 constitute the solution for the bed created by the secondary flow.

4.5 Solution for the Primary Flow

Eq. 4.3a, together with Eqs. 4.6, 4.8, and 4.11, reduce to

$$2u_1 = n\left(F^2\chi_{20} - 1 + A\right) - \frac{1}{\varepsilon^2\chi_1}\frac{\partial}{\partial n}\int_0^1 T\upsilon_1 d\zeta \qquad (4.14)$$

The solution for the secondary flow (Eqs. 4.8, 4.9) does not specify how the secondary flow decays to zero at the banks. Therefore, Eq. 4.14 cannot be solved exactly, since the last term on the right hand side of that equation is not fully defined. However, an approximate solution can be obtained using the well known "moment method" of e.g. Aris (1956). The underlying idea is that, although one cannot exactly solve for the distribution of u_1, it is possible to calculate the moments of the distribution. The solution is then assumed to take some simple characteristic shape that preserves the moments.

As done by Parker (1983), the locus of high velocity, n_u, is defined as the first moment of the lateral distribution of u

$$n_u = \psi_0 n_{u1} = \frac{\int_{-1}^{1} n(1 + \psi_0 u_1)dn}{\int_{-1}^{1} (1 + \psi_0 u_1)dn} = \frac{\psi_0}{2} \int_{-1}^{1} u_1 n dn \qquad (4.15)$$

Multiplying Eq. 4.14 by n and integrating it from n = -1 to 1, the following result is obtained;

$$2 \int_{-1}^{1} n u_1 dn = \int_{-1}^{1} n^2 dn \, (F^2 \chi_{20} - 1 + A) - \frac{1}{\varepsilon^2 \chi_1} \int_{-1}^{1} n \frac{\partial}{\partial n} \int_{0}^{1} TG_0 d\zeta dn \qquad (4.16)$$

Eq. 4.16, together with Eq. 4.15, gives

$$2n_{u1} = \frac{1}{3} (F^2 \chi_{20} - 1 + A) - \frac{1}{2\varepsilon^2 \chi_1} \{ [n \int_{0}^{1} TG_0 d\zeta]_{n=-1}^{n=1} - \int_{-1}^{1} \int_{0}^{1} TG_0 d\zeta dn \} \qquad (4.17)$$

Assuming the secondary to be given by Eqs. 4.8 and 4.9 across the channel width except at the banks (n = ±1) where it suddenly drops to zero, Eq. 4.17 reduces to

$$2n_{u1} = \frac{1}{3} (F^2 \chi_{20} - 1 + A) + \frac{1}{\varepsilon^2 \chi_1} \int_{0}^{1} TG_0 d\zeta \qquad (4.18)$$

An inspection of Eq. 4.14 indicates that in the absence of the redistribution term due to the secondary flow, solutions for u_1 would take the form

$$u_1 = n \, u_{1b}(\phi) \qquad (4.19)$$

where u_{1b} is a normalized near-bank velocity excess. Based on results quoted in De Vriend (1981), this convenient linear form appears to be approximately valid even in the presence of redistribution. According to Eq. 4.15, then n_{u1} is equal to $u_{1b}/3$, so that Eq. 4.18 may also be expressed as

$$u_{1b} = \frac{1}{2}(F^2\chi_{20} - 1 + A + A_s) \tag{4.20}$$

where

$$A_s = \frac{3}{\varepsilon^2\chi_{10}}\int_0^1 TG_0 d\zeta = \frac{2}{315}\frac{1}{\varepsilon^2\chi_1^5}(2\chi^2 + \frac{4}{5}\chi + \frac{1}{15}) \tag{4.21}$$

4.6 Discussion

The solution for the secondary flow and water-surface elevation (Eqs. 4.6 to 4.9) agrees exactly with the result of Engelund (1974), as is to be expected insofar as his approach was followed. This solution is compared with the result of Kikkawa et al. (1976) and Odgaard (1986a) in Fig. 4.1. Figure 4.1a shows that for the case of constant curvature, the dimensionless strength of the secondary flow at the surface $\tilde{v}(1)/(UH\tilde{C})$ is about constant over a wide range of friction factors, as is to be expected (Odgaard, 1986a). More specifically, as $1/\sqrt{C_f}$ varies from 5 to 30, the variation is predicted to be from 6.9 to 8.1 by Kikkawa et al. (1976), from 7.8 to 6.5 by Odgaard (1986a), from 3.4 to 6.0 by the proposed theory (Eq. 4.8), and from 7.1 to 8.5 by Falcon and Kennedy (1983), (see Fig. 2 therein). Whereas, the theory of Kitanidis and Kennedy (1984) predicts the variation to be from 39 to 259. In Fig. 4.1b the predictions for the overall strength of the secondary flow are compared. This approach is more general than a simple comparison of predictions for the velocities at the water-surface. Again, the theory of Kikkawa et al. (1976) gives larger secondary flow velocities than either the theory of Odgaard (1986a) or Eq. 4.8; the latter two give very similar results. The higher velocities velocities predicted by Kikkawa et al. (1976) may be due to the fact that they neglected the transverse bed shear stress. As before, the theory of Kitanidis and Kennedy (1984) gives values which are outside the range of the graph.

The large discrepancy between the results predicted by the theory of Kitanidis and Kennedy (1984) and the other theoretical findings deserves discussion. In both the analysis of Falcon and Kennedy (1983) and Kitanidis and Kennedy (1984) the moment-of-momentum approach is used rather than directly solving the transverse momentum equation (e.g. Engelund, 1974; Kikkawa et al., 1976; Odgaard, 1986a). The reason why the analysis of Kitanidis and Kennedy (1984) gives erroneous results is probably due to the fact that they take the torque about the centroid of the cross-section, thereby equating the small torque induced by the centrifugal acceleration about this point to the torque produced by the boundary shear stress. No net torque about the centroid of the cross-section is generated by the transverse pressure force. This can easily lead to erroneous results, since equating two small terms is always dangerous. Falcon and Kennedy (1983), on the other hand, took the torque about the channel centerline at the bed-surface, and equated the torque induced by the transverse pressure force to the torque generated by the centrifugal acceleration. This allows for determination of the water-surface elevation,

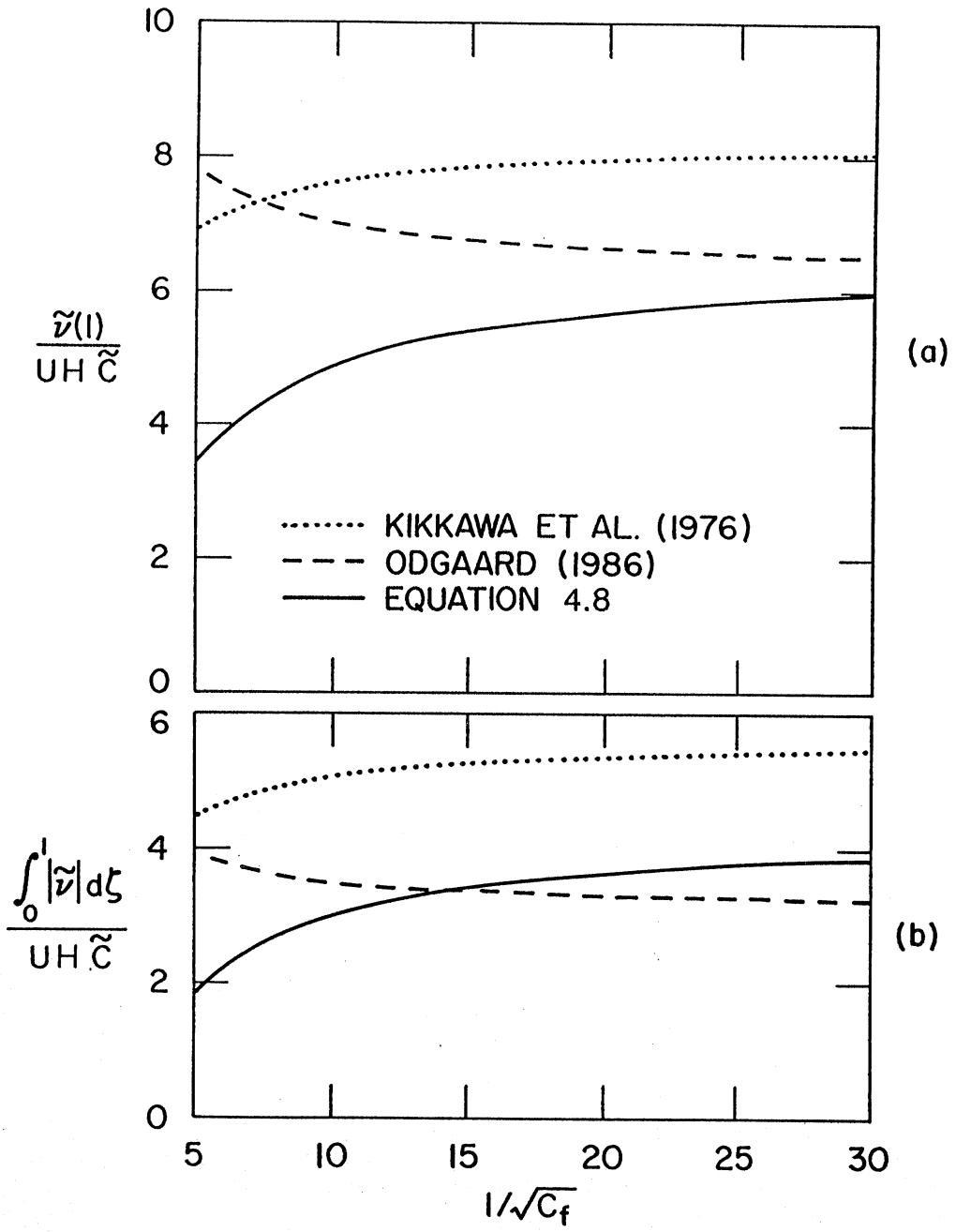

Fig. 4.1. a) Secondary flow velocity at the water-surface, and b) overall strength of the secondary flow, as predicted by various theories, for the case of constant curvature.

which they used as an input in the transverse momentum equation. This approach is much closer to the current analysis than the approach of Kitanidis and Kennedy (1984).

The solution for the lateral distribution of the primary flow, is in many ways different from the corresponding result of Ikeda et al. (1981), (Eq. 10 therein), and deserves some discussion. The most important difference is that Ikeda et al. (1981) neglected the convective transport of primary flow momentum by the secondary flow. This corresponds to setting $A_s = 0$ in Eq. 4.20. However, as shown by Kalkwijk and De Vriend (1980) and De Vriend (1981), this is a most important cause of primary flow velocity redistribution. Values of A_s estimated from Eq. 4.21 for seven meandering streams at bankfull flow are shown in Table 4.1. They are all of order unity, and indeed are within or not far from the range 2.5 - 6 quoted previously for the bed scour factor A. Secondly, Ikeda et al. (1981) did not take into account the metric coefficients that arise in a curvilinear coordinate system, which introduces the term -1 in Eq. 4.20 (e.g. Tamai and Ikeuchi, 1984; Johannesson, 1985; Blondeaux and Seminara, 1985). This term becomes important in the limiting case of a flat bed channel, $A = 0$, with large aspect ratio, (since $A_s \rightarrow 0$ if $\gamma = b/H \rightarrow \infty$). Finally, Ikeda et al. (1981) set $\chi_{20} = 1.0$. This, however is only a minor difference since χ_{20} varies only from 1.41 to 1.01 over the practical range for $1/\sqrt{C_f}$ of 5 to 30. Furthermore, χ_{20} is multiplied by F^2 which is small compared to A and A_s for most sand-bed rivers.

Since one of the most important contributions of the present thesis depends on accurately accounting for the above-mentioned influence of the secondary flow on the lateral distribution of the primary flow velocity, it is worthwhile to compare the result for A_s given by Eq. 4.21 to corresponding results obtained by other researchers. Equation 4.21 was derived using the Engelund (1974) slip-velocity method, which introduces a slip-velocity at the bottom and assumes a constant eddy viscosity (see Chapter 2.2 for further details). Kalkwijk and De Vriend (1980) obtained their results assuming the logarithmic velocity profile for the primary flow, together with a parabolic distribution of the eddy viscosity. The results of both methods are shown in Fig 4.2. The agreement is satisfactory (less than 25% difference) for values of $12 < 1/\sqrt{C_f} < 30$. For values of $1/\sqrt{C_f} < 12$ the percent difference becomes larger; this, however, is of little concern, since for this range of friction factors A_s becomes small (see Fig. 4.2). In the work presented herein, Eq. 4.21 will be used to calculate A_s. However, the results of of Kalkwijk and De Vriend (1980) can just as well be used, resulting in values for A_s that are typically 20% higher. Note, that although it is possible to estimate the values of A_s from the model of Kalkwijk and De Vriend (1980), their numerical model does not apply to rivers with steep banks. They accounted for the dispersive effect of the secondary flow on the primary flow, embodied in the last term on the right hand side of Eq. 4.3a, by requiring the river depth to gradually decrease to zero at the banks. The condition of zero flux of streamwise momentum through the river banks is therefore satisfied. Meandering rivers, however, typically have steep banks. Therefore the model of Kalkwijk and De Vriend (1980) does not apply. On the other hand the "moment method", as introduced herein, allows for an overall estimate of the dispersive effect of the secondary flow and is independent of the river bank shape.

Finally, it should be emphasized that although the moment, as calculated by Eq. 4.18 is exact within the context of a linear theory, the assumption that the transverse variation in the primary flow velocity is linear (Eq. 4.19) breaks down in the limiting case of a channel with a large aspect ratio, i.e. $\gamma = b/H \rightarrow \infty$. This becomes apparent from Eq.

Table 4.1 - Computed Values of A_s for Several Meandering Sand-Bed Streams at Bankfull Flow

River	Reference	$C_f^{-1/2}$	γ	ε	A_s
Root	Johannesson (1985)	21.8	9.5	0.020	5.68
Zumbro	Johannesson (1985)	15.4	10.1	0.043	3.29
Minnesota*	Johannesson (1985)	13.2	11.7	0.067	2.01
Red Lake	Johannesson (1985)	13.7	15.5	0.082	1.20
Minnesota*	Parker (1982)	26.7	11.4	0.016	4.99
Pembina	Beck et al. (1983a)	12.5	16.2	0.103	0.97
Genesee	Beck et al. (1983b)	11.4	9.7	0.075	2.39
Muddy Cr.	Dietrich and Smith (1983)	7.73	6.0	0.10	3.48
Fall	Thorne et al. (1985)	4.53	6.3	0.31	1.05

* Different reaches

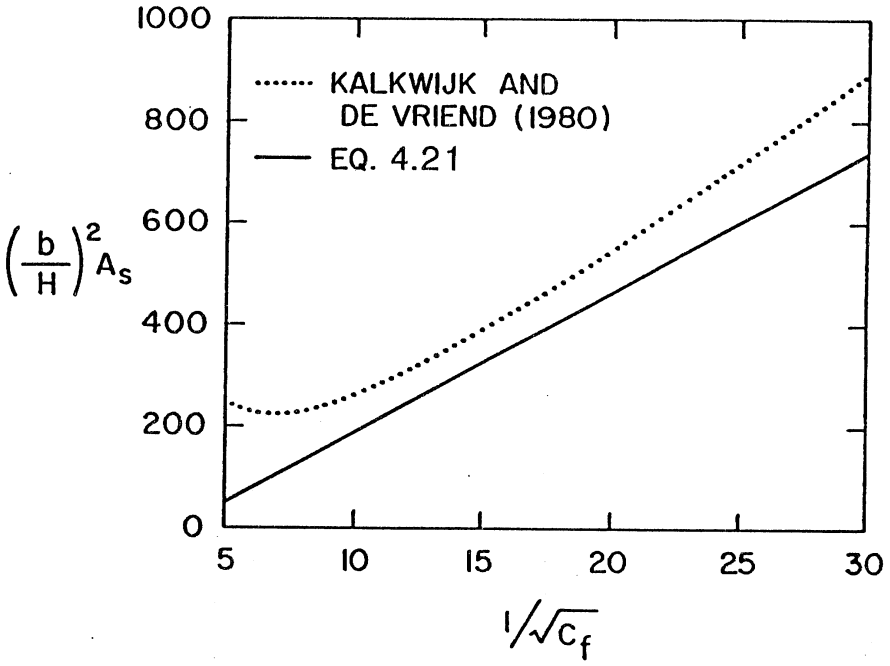

Fig. 4.2. $(b/H)^2 A_s$ as predicted theoretically.

4.14. If the strength of the secondary flow is assumed to be constant across the channel width, except at the banks where it drops to zero, the dispersion term in Eq. 4.14 will be zero except in an infinitely thin layer near the banks where it is infinity. Inherent in the linear profile, used in Eq. 4.19, is the assumption that the influence of this singularity penetrates the flow to the channel centerline. This cannot be true for an extremely wide channel (large γ). Although the results of De Vriend (1981) indicate that the linear form is approximately valid, a more careful examination of his calculation indicates that the transverse variation of the streamwise velocity deviates from linear, showing a surfeit near the outer bank and a deficit near the inner one. This deviation can be expected to increase with increasing γ.

4.7 Comparison with Data

Before comparing the model with data, it is helpful to summarize what data the model needs as input and how the dependent variables are calculated.

Input data:

1) U, H, I, b, $\tilde{C}$.
2) D_{50} and R if the channel has an erodible bed.

Calculation Procedure:

1) C_f (Eq. 2.27a) ; F and ε (Eq. 2.28c) ; $\alpha = 0.077$; χ_1 (Eq. 2.25) ; χ (Eq. 2.21b) ; χ_{20} (Eq. 4.7) ; A_S (Eq. 4.21) ;
2) τ_C^* (Shields Diagram, Vanoni, 1977, Fig. 2.43) ; τ^* (Eq. 2.11) ; τ_G^* (Eq. 2.12) ; β (Eq. 2.14) ; A (Eq. 4.13) ;
3) ξ_1 (Eq. 4.6) ; υ_1 (Eq. 4.8) ; η_1 (Eq. 4.11) ; u_{1b} (Eq. 4.20).

The input data for all the experiments simulated is summarized in Table 4.2, except for the data of Zimmermann and Kennedy (1978) which is summarized in Table 1 therein. Some calculated results are shown in Table 4.3. The flow conditions for all the erodible bed experiments were estimated to be in the lower regime (dune covered bed; Eqs. 2.12c,d).

The (maximum) dimensionless centerline curvature $\psi_0 = b\tilde{C}$, which is assumed to be small in this analysis, varied from 0.182 to 0.333 for the experiments of Zimmermann and Kennedy (1978). It took the respective values of 0.111 and 0.0625 for the experiments of Kikkawa et al. (1976) and Struiksma et al. (1985). This is considered small enough for the analysis to be valid, at least approximately.

The theoretical velocity profiles for the primary and the secondary flow are compared with the experimental findings of Kikkawa et al. (1976) in Fig. 4.3. It is seen that Eq. 2.20b gives very good description of the primary flow, as shown in Fig. 4.3a. The agreement with the secondary flow is satisfactory, though not as good as that obtained with the theoretical relation of Kikkawa et al. (1976), as seen in Fig. 4.3b. Engelund (1974), however reports cases with excellent agreement.

The calculated transverse bed slope parameter A (Eq. 4.13) is plotted in Fig. 4.4 versus the measured one. The data of Zimmermann and Kennedy (1978) was used to determine the value of f_* to be 1.19, (Fig. 4.4a). The scatter is small and much less than if the total shear stress, τ^*, is used instead of τ^*_G in the calculation of β, as recommended by Kikkawa et al. (1976) and Parker (1984), (Fig. 4.5a). The calibrated equation is verified by simulating the measurements of Kikkawa et al. (1976) and Struiksma et al. (1985), (Fig. 4.4b). The results are very good when τ^*_G is used; indeed they are much better than if the total shear stress τ^* is used for the calculation of β, (Fig. 4.5b). The calculated bed profiles for the experiments of Kikkawa et al. (1976), (Exp. M1, M2), and Struiksma et al. (1985), (Exp. T1, T2, T3), are shown in Fig. 4.6 and 4.8a, respectively. The results are good.

The depth-averaged velocities, as predicted by Eq. 4.20, are compared with the experiments of Kikkawa et al. (1976), (Exp. F1, F2, F3), in Fig 4.7. These experiments were carried out in channel with non-erodible flat bed (A = 0). The data clearly shows that the velocities are higher at the outside bank (n = 1) than the inside bank (n = -1) for each of the three experimental runs. The proposed model is able to predict this, and the agreement between the measured and the calculated values is rather good (much better than if the model of Ikeda et al., 1981, is used). However, if the convective transport of primary flow momentum by the secondary flow is neglected, $A_s = 0$, the model will always predict the highest velocity to be at the inside bank, in the case of subcritical flow ($F < 1$) over a transversely horizontal bed.

Finally, the depth-averaged velocities, as predicted by Eq. 4.20, are compared with the measurements of Struiksma et al. (1985), (Exp. T1, T2), in Fig. 4.8b. This is a more complicated case, since the bed was erodible. Again, the model predicts the measurements very satisfactorily. It is apparent that the convective transport of primary flow momentum by the secondary flow plays an important role, and that this is the process missing from the model of Struiksma et al. (1985); see Fig. 11 therein.

The measured transverse variation in the streamwise velocity (Kikkawa et al., 1976; Struiksma et al., 1985) shows a systematic deviation from the linear variation assumed in the theoretical model, (Figs. 4.7 and 4.8). The measured variation is steeper than the predicted linear variation near the banks and gentler in the central region. This is to be expected, as discussed earlier, (Chapter 4.6).

Table 4.2 - Circular Channels: Geometry and Flow Conditions

Run Number	b (m)	$\tilde{r}$ (m)	Q (l/s)	H (m)	U (m/s)	I	D_{50} (mm)	σ_g	R
Kikkawa et al. (1976)									
F1	0.5	4.5	20	0.050	0.400	$2.00 \cdot 10^{-3}$	*flat bed	*flat bed	*flat bed
F2	"	"	25	0.055	0.455	"	"	"	"
F3	"	"	30	0.063	0.476	"	"	"	"
M1	"	"	25	0.055	0.455	"	0.90	$\cong$ 1.0	1.65
M2	"	"	30	0.063	0.476	"	"	"	"
Struiksma et al. (1985)									
T1	0.75	12	47	0.080	0.392	$2.36 \cdot 10^{-3}$	0.45	1.19	1.65
T2	"	"	61	0.100	0.407	$2.03 \cdot 10^{-3}$	"	"	"
T3	"	"	74	0.091	0.542	$4.19 \cdot 10^{-3}$	"	"	"

*flat bed = horizontal in transverse direction

Table 4.3 - Circular Channels: Calculated Results

Run Number	F	C_f	A_s	A meas.	A calc.
Kikkawa et al. (1976)					
F1	0.56	$6.13 \cdot 10^{-3}$	2.63	flat bed	0.00
F2	0.63	$5.22 \cdot 10^{-3}$	3.54	flat bed	0.00
F3	0.61	$5.45 \cdot 10^{-3}$	4.51	flat bed	0.00
M1	0.63	$5.22 \cdot 10^{-3}$	3.54	2.98	3.93
M2	0.61	$5.45 \cdot 10^{-3}$	4.51	4.92	3.90
Struiksma et al. (1985)					
T1	0.44	$12.1 \cdot 10^{-3}$	1.85	3.54	4.61
T2	0.41	$12.0 \cdot 10^{-3}$	2.90	3.85	4.58
T3	0.57	$12.7 \cdot 10^{-3}$	2.30	5.14	6.21

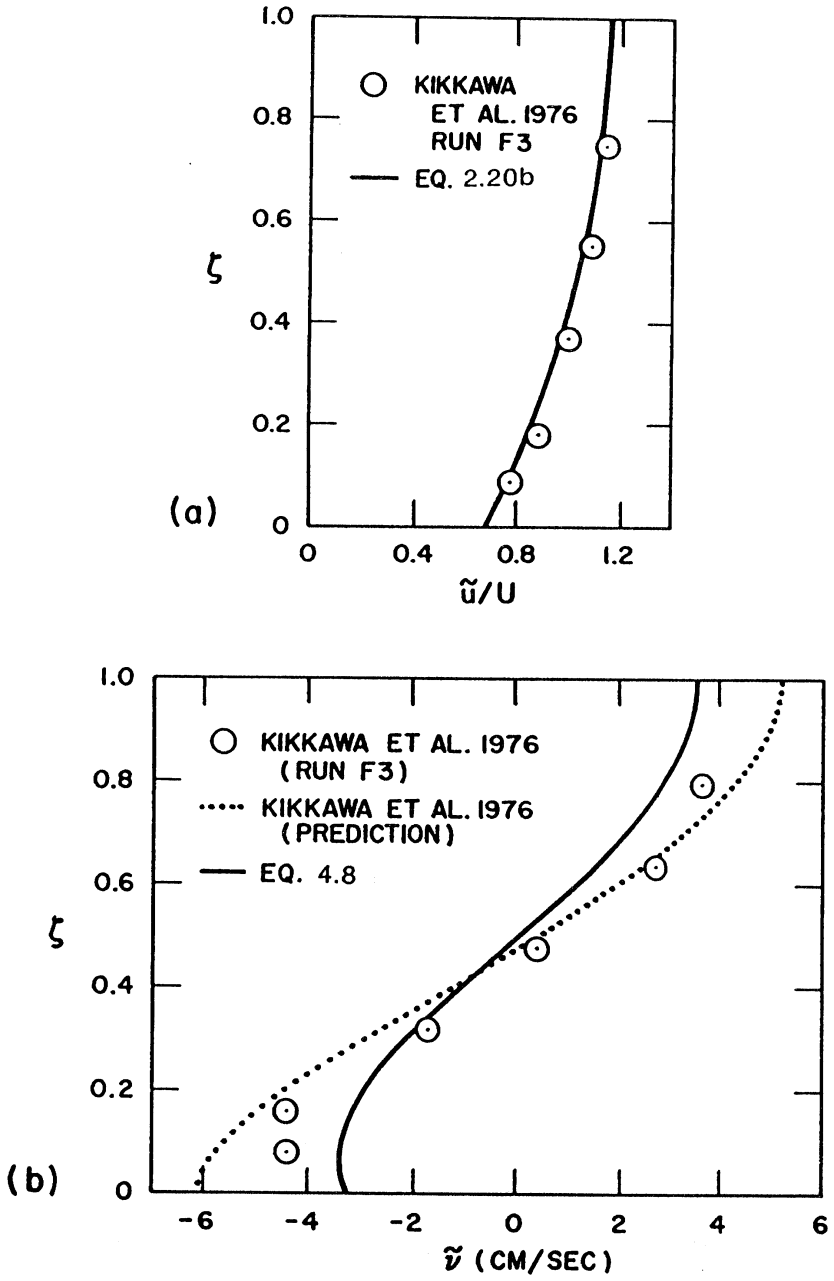

Fig. 4.3. Velocity profiles: a) the primary flow;

b) the secondary flow.

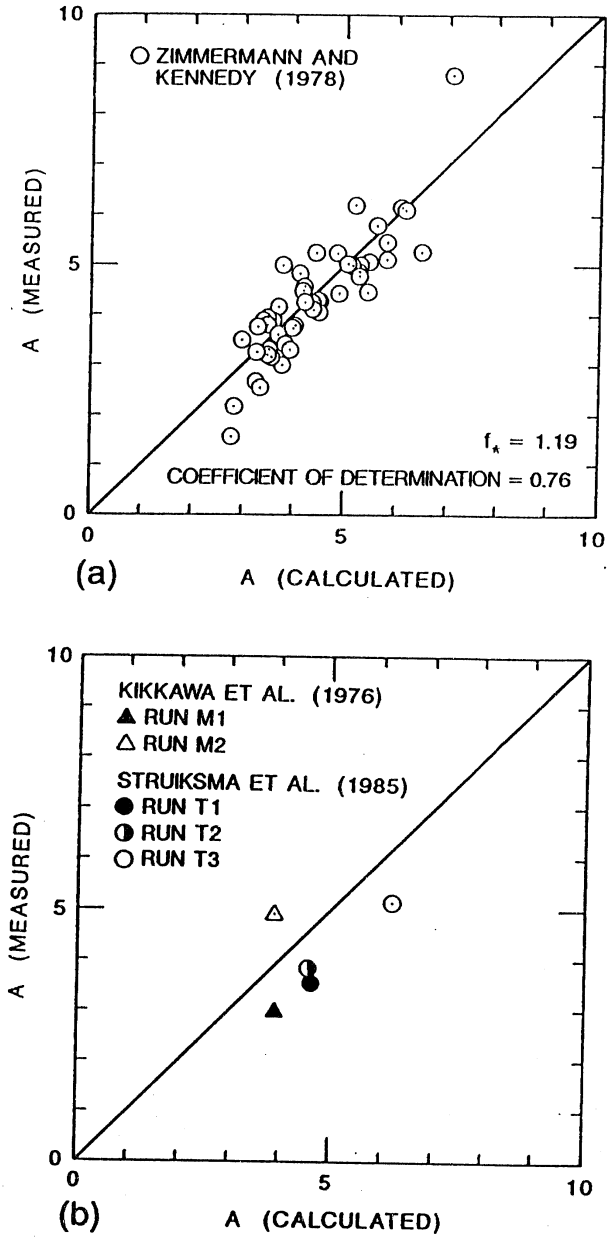

Fig. 4.4. Comparison of transverse bed slope parameter, A, as calculated by Eq. 4.13 and as measured.

a) Calibration of f_*.

b) Validation.

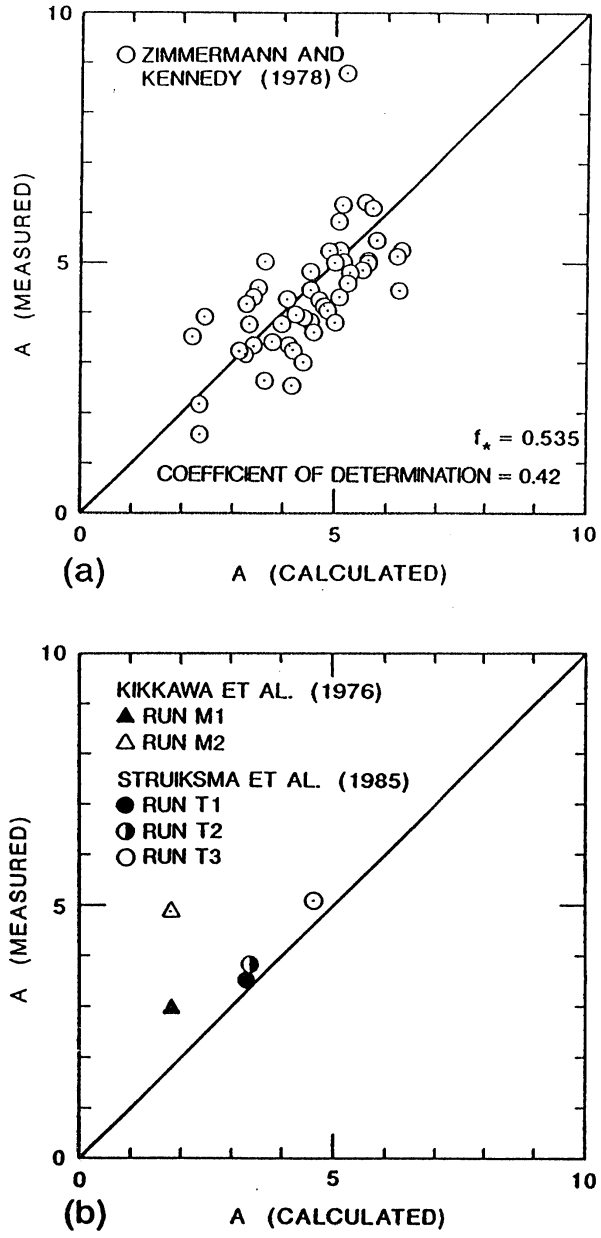

Fig. 4.5. Comparison of transverse bed slope parameter, A, as calculated by Eq. 4.13 (τ^* used instead of τ_G^* in the calculation of β by Eq. 2.14) and as measured.

a) Calibration of f_*.

b) Validation.

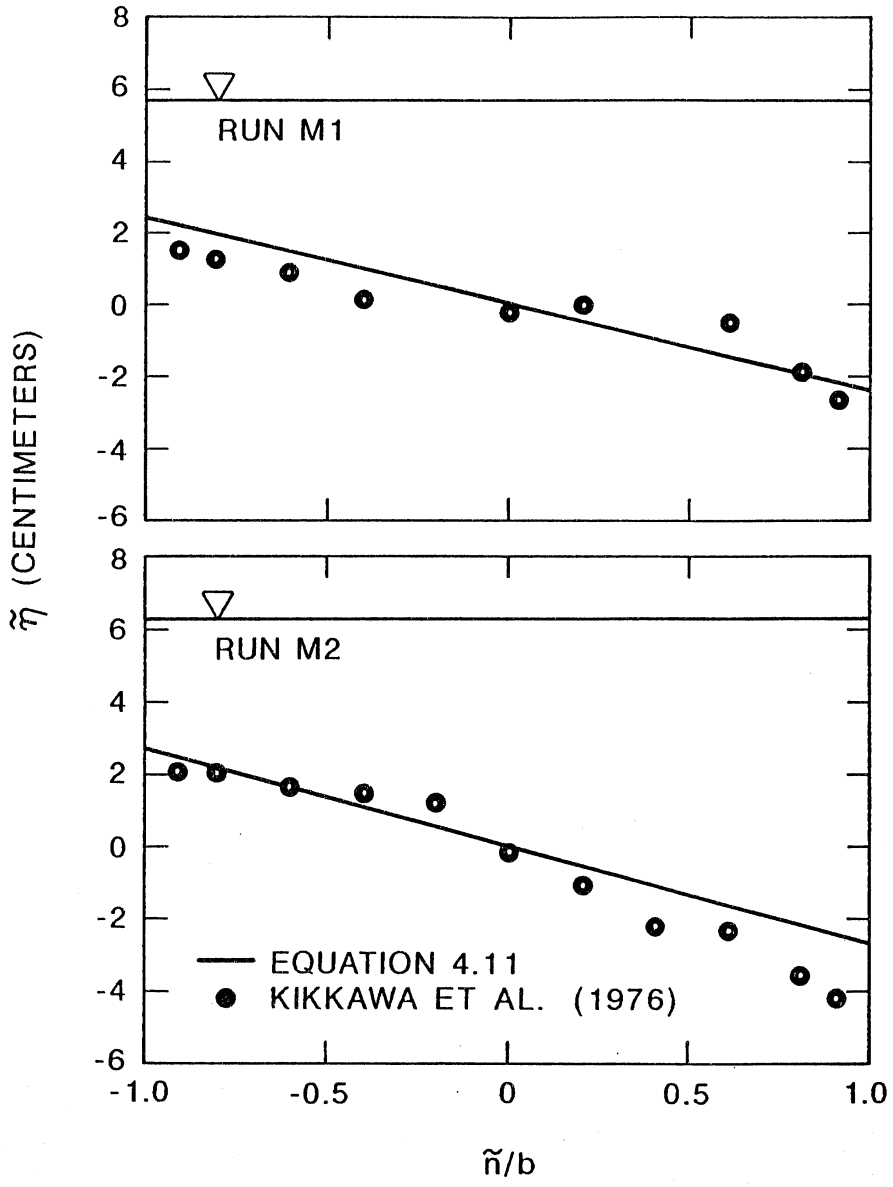

Fig. 4.6. Transverse bed profiles as measured by Kikkawa et al. (1976) and predicted by Eq. 4.11.

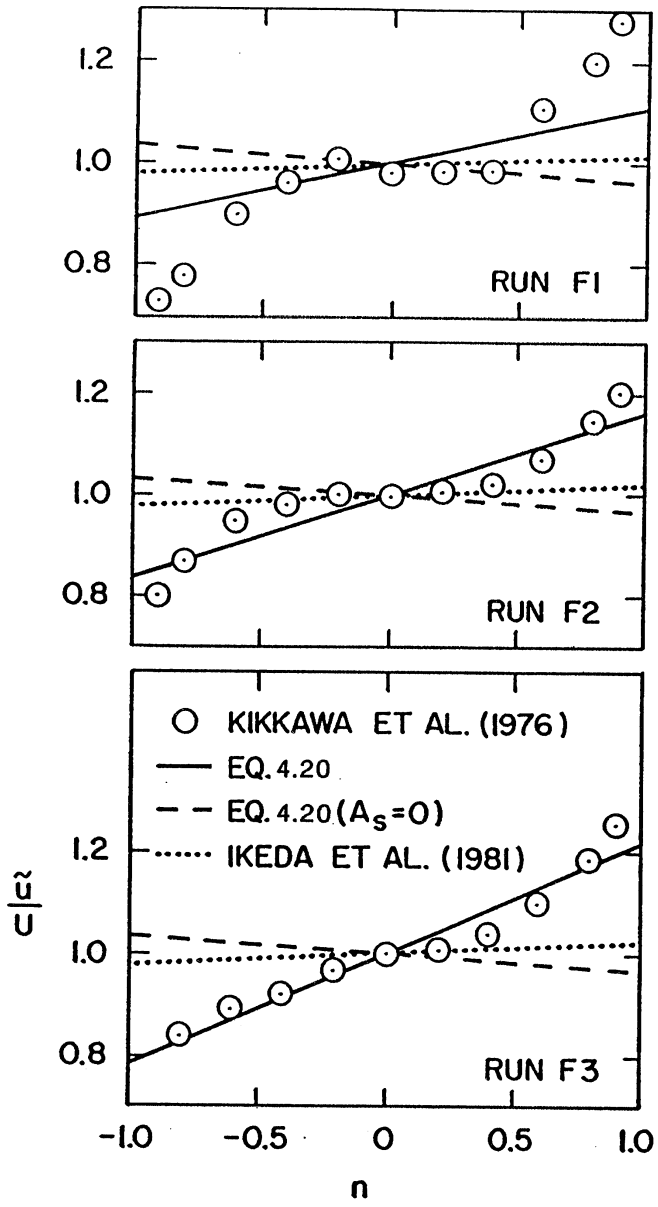

Fig. 4.7. Depth-averaged velocities as measured by Kikkawa et al. (1976) and predicted by various theories.

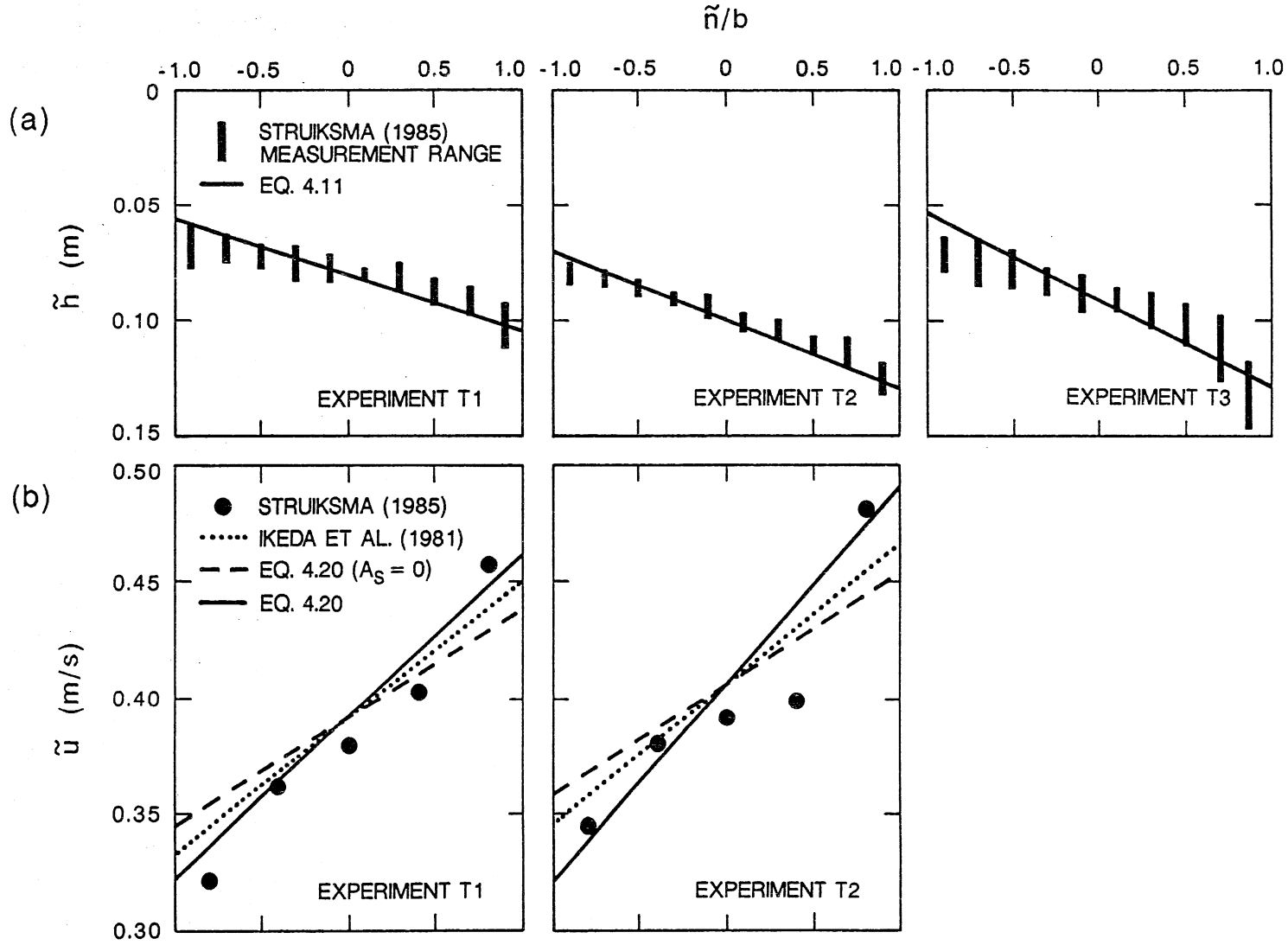

Fig. 4.8. a) Bed topography as measured by Struiksma et al. (1985) between 18 and 28 m from bend entrance and as predicted by Eq. 4.11.

b) Depth-averaged velocities as measured by Struiksma et al. (1985) near bend exit and as predicted by various theories.

4.8 Conclusions

A model for calculation of flow field and bed topography for fully developed flow in constant curvature channels has been developed.

The model predicts satisfactorily the secondary flow and the transverse bed slope. The model of Kitanidis and Kennedy (1984) is shown to highly overpredict the magnitude of the secondary flow.

The model is able to simulate rather well the lateral distribution of the depth-averaged primary flow velocity. It is evident from the analysis that the convective transport of primary flow momentum by the secondary flow is an important cause of the lateral variation in the depth-averaged primary flow velocity. Its effect has often been neglected, e.g. Engelund (1974), Ikeda et al. (1981) Smith and McLean (1984) Blondeaux and Seminara (1985) Struiksma et al. (1985), and Odgaard (1986a). The approximate manner in which this influence of the secondary flow is accounted for, i.e. the "moment method", seems to yield very satisfactory results.

By comparison with data it is shown that the flow field model gives substantially better results than the flow field model of Ikeda et al. (1981) as regards the lateral variation in the depth-averaged primary flow velocity. The new theory, therefore, has the potential to significantly improve the bend migration model Ikeda et al. (1981).

5. SOLUTION FOR A SINE-GENERATED CURVE

5.1 Introduction

As shown by Langbein and Leopold (1966) the geometry of natural meanders often closely resembles a sine-generated curve. For this reason, researchers commonly carry out their experiments in channels having this geometry (e.g. Hooke, 1974; Gottlieb, 1976; Yamaoka and Hasegawa, 1983; Ikeda and Nishimura, 1986). Furthermore, stability theories used to explain the origin of river meandering (e.g. Ikeda et al., 1981; Kitanidis and Kennedy, 1983; Blondeaux and Seminara, 1985), typically assume a sinuous periodic perturbation for the channel centerline. It is therefore appropriate to develop a solution for this case before a solution for more complex channel geometry is attempted.

The additional complication arising in the case of a sinuous channel compared to the simpler situation of a constant curvature channel is due to the variation of curvature, velocity, depth, and sediment transport in the downstream direction. It is shown that the approach taken by Ikeda et al. (1981), according to which the bed topography in a sinuous channel is assumed to be given by the constant curvature solution, is insufficient in general. The importance of the coupling between the flow field and the sediment transport in determining the bed topography is illustrated. This coupling is shown to give rise to resonant behavior for certain combinations of input variables. The theory is compared with the model of Blondeaux and Seminara (1985), who first delineated this resonant behavior. The model is tested with laboratory and field data, and gives substantially better results than the model of Ikeda et al. (1981).

5.2 Statement of the Problem

The channel centerline is assumed to follow the sine-generated curve of Langbein and Leopold (1966), (Fig. 2.1);

$$\theta = \theta_0 \cos \phi \tag{5.1}$$

where θ_0 is the angle amplitude. As illustrated in Chapter 3, this leads to the following expression for the curvature of the channel centerline:

$$C = \psi_0 \sigma \quad ; \quad \psi_0 = k\theta_0 \quad ; \quad \sigma = \sin \phi \tag{5.2a,b,c}$$

Eqs. 3.14a through d yield

$$r\, u_1' + 2u_1 = -F^{-2} r\, \xi_1' - n\sigma + \xi_1 - \eta_1 - \frac{1}{\varepsilon}\frac{\partial}{\partial n}\int_0^1 T v_1 d\zeta \tag{5.3a}$$

$$\varepsilon Tr\, v_1' - T^2\sigma = -F^{-2}\frac{\partial \xi_1}{\partial n} + \varepsilon \chi_1 \ddot{v}_1 \tag{5.3b}$$

$$r\, u_1' + r\, h_1' + \frac{\partial v_1}{\partial n} = 0 \tag{5.3c}$$

$$r\, M\, u_1' + \frac{\partial}{\partial n}\left[v_1 + \frac{\chi_1 \dot{\upsilon}_1(0)}{\varepsilon} - \Gamma \frac{\partial \eta_1}{\partial n} \right] = 0 \tag{5.3d}$$

The boundary conditions are (Eqs. 3.15a,b, 3.16a,b,c, and 3.18a,b,c):

$$v_1 = q_{n1} = 0 \quad \text{at } n = \pm 1 \tag{5.4a,b}$$

$$\upsilon_1(0) = \chi \dot{\upsilon}_1(0) \;\; ; \;\; \dot{\upsilon}_1(1) = 0 \;\; ; \;\; \int_0^1 \upsilon_1 d\zeta = 0 \tag{5.5a,b,c}$$

$$u_1 = \xi_1 = \eta_1 = 0 \quad \text{at } n = 0 \tag{5.6a,b,c}$$

The problem is now solved in the same order as done for the case of constant curvature. Eq. 5.3b, together with the boundary conditions given by Eqs. 5.5a,b,c and 5.6b, can be solved to give ξ_1 and υ_1. Eq. 5.3c is used to eliminate v_1 from Eq. 5.3d. Eqs. 5.3a,d are then solved together to obtain a solution for u_1 and η_1.

5.3 Solution for the Water-Surface and the Secondary Flow

5.3.1 The Ikeda-Nishimura Approximation

Ikeda and Nishimura (1986) utilized a form for $T(\zeta)$ in their calculations that is different from the one employed herein. For the sake of comparability, their calculation is repeated using the techniques of the present analysis.

Noting from Eq. 2.3a that $T(\zeta)$ averages in the vertical to unity, Eq. 5.3b is approximated to

$$\varepsilon r\, \upsilon_1' - T^2 \sigma = -F^{-2} \frac{\partial \xi_1}{\partial n} + \varepsilon \chi_1 \ddot{\upsilon}_1 \tag{5.7}$$

Differentiating once with respect to ζ, it is found that

$$\varepsilon r\, \dot{\upsilon}_1' - (\dot{T}^2)\, \sigma = \varepsilon \chi_1 \dddot{\upsilon}_1 \tag{5.8}$$

The central assumption of Ikeda and Nishimura (1986) is that the secondary flow maintains the same vertical profile as that of developed bend flow, with changes only in magnitude and phase. To wit, it is assumed that

$$\varepsilon\chi_1 \upsilon_1 = \chi_* G_0(\zeta) \sin(\phi - \sigma_{SL}) \tag{5.9}$$

where the parameter χ_* controls the magnitude, and σ_{SL} denotes the phase lag of the secondary current, and G_0 is given by Eq. 4.9.

Since G_0 was determined so as to satisfy the boundary conditions, Eqs. 4.4a,b,c, υ_1 as given by Eq. 5.9 must also satisfy them. Substituting Eq. 5.9 into Eq. 5.8 and solving for χ_* and σ_{SL}, it is found that

$$\tan\sigma_{SL} = -\frac{r}{\chi_1}\frac{\dot{G}_0}{\ddot{G}_0} \quad ; \quad \chi_* = \frac{(\dot{T}^2)}{\frac{r}{\chi_1}\dot{G}_0 \sin\sigma_{SL} - \ddot{G}_0 \cos\sigma_{SL}} \tag{5.10a,b}$$

It is apparent from Eqs. 5.10a,b that since G_0 varies in the vertical, σ_{SL} and χ_* should vary similarly. Both, however, are assumed to be constants in Eq. 5.9. In order to overcome this difficulty, $\dot{G}_0$, $\ddot{G}_0$, $(\dot{T}^2)$ are further approximated by their vertical averages in Eqs. 5.10a,b. After some tedious algebra, this yields

$$\tan\sigma_{SL} = \frac{r}{\chi_1^2}\frac{\frac{1}{12}\chi^2 + \frac{11}{360}\chi + \frac{1}{504}}{\chi + \frac{1}{4}} \tag{5.11}$$

$$\chi_* = \cos\sigma_{SL} \tag{5.12}$$

It is thus seen from Eqs. 5.11 and 5.12 that the effect of the inertial term is to cause the secondary flow to lag behind channel curvature, and to cause the magnitude of the secondary current to be damped.

5.3.2 General Solution

In order to investigate the error introduced by the similarity assumption introduced by Eq. 5.9, an exact solution to Eqs. 5.7, 5.5a,b,c, and 5.6b is obtained as follows:

$$\varepsilon\chi_1 \upsilon_1 = G(\zeta)\sin\phi + H(\zeta)\cos\phi \tag{5.13}$$

$$\xi_1 = F^2 n\,(\chi_2 \sin\phi + \chi_3 \cos\phi) \tag{5.14}$$

where

$$G = G_p + G_h \quad ; \quad H = H_p + H_h \tag{5.15a,b}$$

The subscripts "p" and "h" refer to the particular and homogeneous parts of the solutions. The function $H(\zeta)$, as defined in Eq. 5.13, has nothing to do with the average channel depth, H, although the same symbol is used. It is found that

$$G_p = \frac{\chi_1}{r}\left[\frac{6}{r}T - \frac{2}{r\chi_1}(2\chi + 1) - \chi_3\right] \tag{5.16a}$$

$$H_p = \frac{\chi_1}{r}\left[\chi_2 - T^2 + \frac{6}{r^2}\right] \tag{5.16b}$$

and

$$G_h = e^{a\zeta}\left[a_1\cos(a\zeta) + a_2\sin(a\zeta)\right] + e^{-a\zeta}\left[a_3\cos(a\zeta) + a_4\sin(a\zeta)\right] \tag{5.17a}$$

$$H_h = e^{a\zeta}\left[-a_2\cos(a\zeta) + a_1\sin(a\zeta)\right] + e^{-a\zeta}\left[a_4\cos(a\zeta) - a_3\sin(a\zeta)\right] \tag{5.17b}$$

where

$$a = \sqrt{\frac{r}{2\chi_1}} \tag{5.18}$$

The unknown coefficients a_1, a_2, a_3, a_4, χ_2, and χ_3 are found by applying the boundary conditions given by Eqs. 5.5a,b,c. The resulting equations are given in Appendix C.

Equation 5.14 can also be written in the form

$$\xi_1 = F^2 n \chi_W \sin(\phi - \sigma_{WL}) \tag{5.19}$$

where

$$\chi_W = \sqrt{\chi_2^2 + \chi_3^2} \tag{5.20}$$

governs the amplitude of the water-surface disturbance, and

$$\tan\sigma_{WL} = -\frac{\chi_3}{\chi_2} \tag{5.21}$$

denotes the phase lag between the water-surface and the centerline curvature. Neither the amplitude effect nor the lag effect is described by the Ikeda-Nishimura treatment.

It is seen explicitly from Eq. 5.13 that the phase shift between the secondary flow and centerline curvature is a function of distance ζ above the bed. The near-bed secondary flow velocity, being of interest since it influences bed topography, is described by the relation

$$\varepsilon\chi_1 \upsilon_1(0) = G(0) \sin\phi + H(0) \cos\phi = G_S(0) \sin(\phi - \sigma_{SL}) \tag{5.22}$$

where

$$G_S(0) = -\sqrt{G^2(0) + H^2(0)} \tag{5.23}$$

governs the amplitude of the near-bed secondary flow velocity, and

$$\tan\sigma_{SL} = -\frac{H(0)}{G(0)} \tag{5.24}$$

denotes the phase lag between the near-bed secondary flow velocity and the channel curvature.

5.3.3 Discussion

The various relations obtained herein can be expressed as functions of rescaled wavenumber r and friction factor C_f, in accordance with Eqs. 3.8 and 2.25. The effect of inertia on the water-surface is studied in Fig. 5.1, in which the phase lag σ_{WL} and the amplitude ratio χ_W/χ_{20} (ratio of the water-surface amplitude with convective acceleration to its value without) predicted by Eqs. 5.21, 5.20, and 4.7 are plotted. The influence of inertia, or convective acceleration, on the water-surface is seen to be very small. The phase lag σ_{SL} and the amplitude ratio $G_S(0)/G_0(0)$ associated with the effect of inertia on the near-bed secondary flow is shown in Fig. 5.2. It is seen that the inclusion of convective acceleration has a considerable influence on the secondary flow for certain combinations of C_f and r.

The values of σ_{SL} and $G_S(0)/G_0(0)$ predicted by the modified version of the Ikeda-Nishimura theory are given by Eqs. 5.11 and 5.12. The original forms predicted by them, using a logarithmic rather than slip velocity treatment, can be expressed as

$$\tan\sigma_{SL} = r\,(1.11\sqrt{C_f} - 1.42C_f) \tag{5.25}$$

$$\chi_* = \frac{G_S(0)}{G_0(0)} = \cos\sigma_{SL} \tag{5.26}$$

In Fig. 5.3, the values of σ_{SL} and $G_S(0)/G_0(0)$ predicted by Eqs. 5.24 and 5.23 of the present theory are compared with the values predicted by the original and modified Ikeda-Nishimura theory, for the value of r of 1.5 typical of natural streams. The agreement is seen to be quite good for $C_f^{-1/2} > 10$. The original Ikeda-Nishimura theory shows some deviation for friction coefficients larger than this, since therein the influence of the transverse shear stress is not accounted for. Similar results are obtained for other values of r.

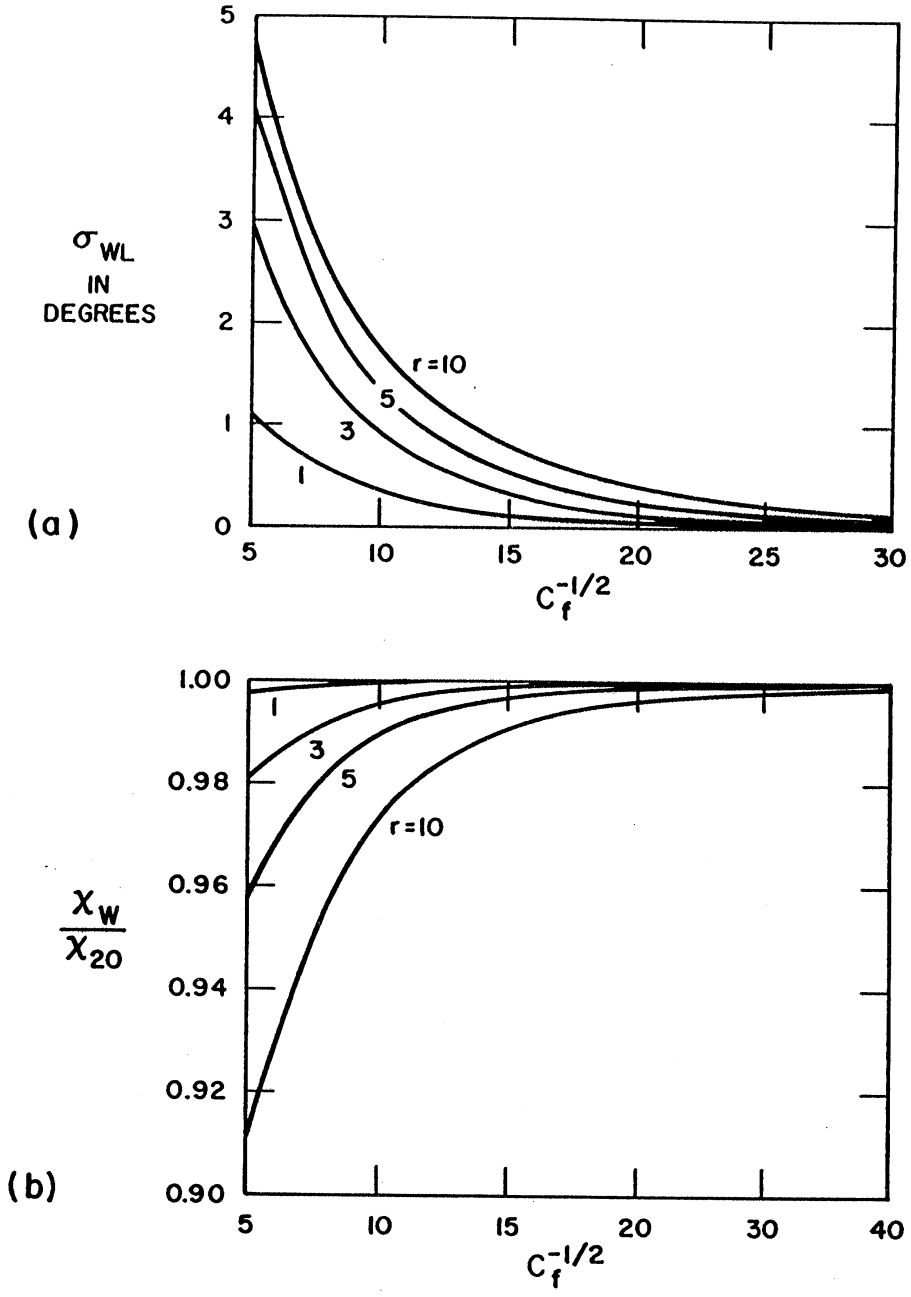

Fig. 5.1. a) The phase lag σ_{WL}, and b) the amplitude ratio χ_W/χ_{20}, for the water-surface, from Eqs. 5.21 and 5.20, respectively.

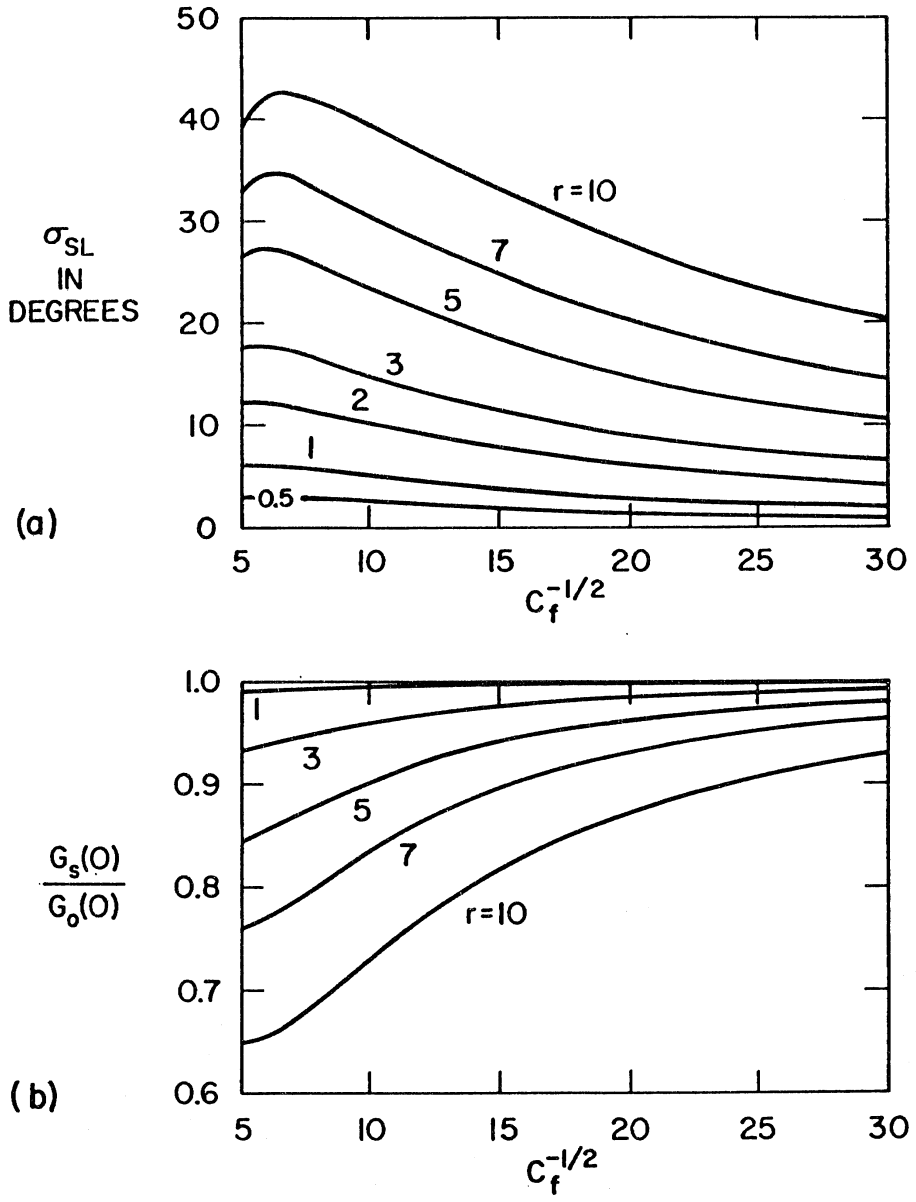

Fig. 5.2. a) The phase lag σ_{SL}, and b) the amplitude ratio $G_S(0)/G_0(0)$ for the secondary flow, from Eqs. 5.24 and 5.23, respectively.

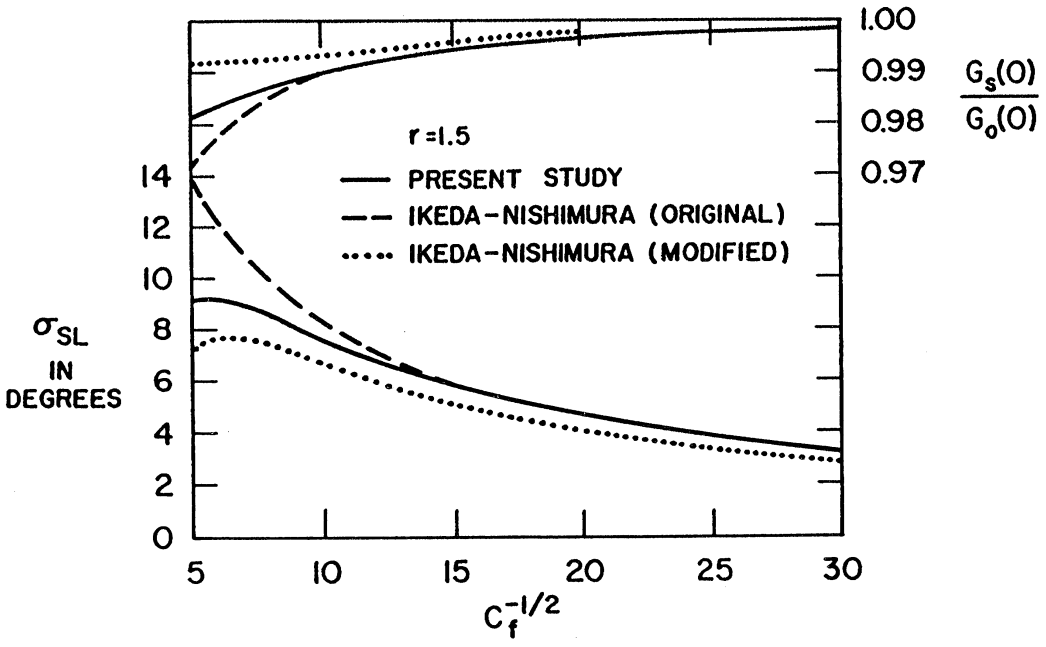

Fig. 5.3. The phase lag σ_{SL} and amplitude ratio $G_S(0)/G_0(0)$ for r = 1.5, as predicted by various theories.

It is interesting to compare the results of the present analysis to the relation for σ_{SL} obtained by Kitanidis and Kennedy (1984). Their result is

$$\tan \sigma_{SL} = 2.22\, r \tag{5.27}$$

which gives, for example, $\sigma_{SL} = 73^{\circ}$ for r = 1.5. As seen from Fig. 5.3, this value is an order of magnitude higher than the values obtained with the present treatment.

The reason for the good performance of the Ikeda-Nishimura theory, in spite of a rather bold assumption, is studied in Fig 5.4, in which G, H, and G_0, obtained from Eqs. 5.15a,b, and 4.9, respectively, are plotted against ζ for r = 5 and $C_f^{-1/2} = 10$. All three functions are seen to take similar shapes. Comparing Eqs. 5.9, 5.12, and 5.13, it is seen that the central assumption of Ikeda and Nishimura implies that

$$G(\zeta) \cong \cos^2\sigma_{SL}\, G_0(\zeta) \quad ; \quad H(\zeta) \cong -\cos \sigma_{SL} \sin \sigma_{SL}\, G_0(\zeta) \tag{5.28a,b}$$

or from Eq. 5.24,

$$\frac{H(\zeta)}{H(0)} \cong \frac{G(\zeta)}{G(0)} \tag{5.29}$$

i.e., an approximate similarity relation must hold between the two functions. This approximate similarity is verified in Fig. 5.4.

One aspect of the original Ikeda-Nishimura (1986) treatment deserves discussion. They reduce Eq. 5.7 to a vorticity balance, and in doing so make the following approximation in the term representing the centrifugal acceleration:

$$\sigma \frac{dT^2}{d\zeta} = 2\sigma T \frac{dT}{d\zeta} \cong 2\sigma \frac{dT}{d\zeta} \tag{5.30}$$

This partial neglect of the vertical structure of the centrifugal acceleration was not made in the present analysis. A consequence of the approximation is that the solution of Ikeda and Nishimura (1986) in the limit of constant curvature no longer agrees with their previously-obtained solution (without said approximation) for constant curvature. This necessitated, in their analysis, the use of a value of υ_t for the case of sinuous channels that is 49% larger than the value employed for channels of constant curvature. In the modified Ikeda-Nishimura treatment presented herein, Eq. 5.30 was not used.

5.3.4 Comparison with Data

The experimental flow conditions of Yen (1965), Gottlieb (1976), and Ikeda et al. (1985) are summarized in Table 5.1. The experiments of Gottlieb (1976) and Ikeda et al. (1985) were performed in a channel following a sine-generated curve, with the respective values of ψ_0 being 0.0206 and 0.279. The channel of Yen (1965) was constructed of 90° constant curvature bends connected by straight reaches. Therein ψ_0 varied from 0.120 to 0.134.

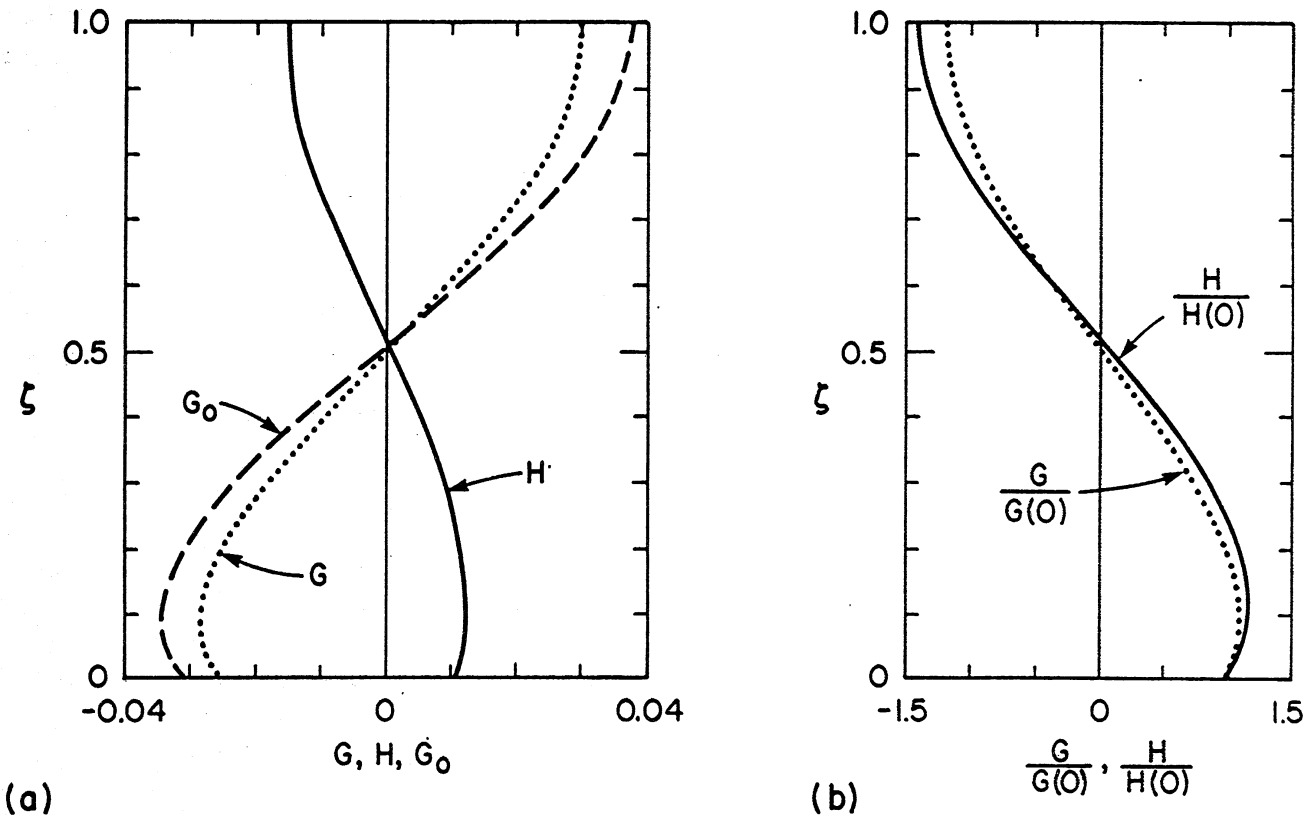

Fig. 5.4. a) Plots of $G(\zeta)$, $H(\zeta)$, and $G_0(\zeta)$ for $1/\sqrt{C_f} = 10$ and $r = 5$;

b) Plots of $G(\zeta)/G(0)$ and $H(\zeta)/H(0)$ for the same case.

Approximating all the channels as sine-generated curves, the measured values of the shift, σ_{SL}, of the secondary flow are compared with those predicted by the modified and the original Ikeda and Nishimura theories (Eqs. 5.11 and 5.25), and the theory of Kitanidis and Kennedy (1984), (Eq. 5.27). The results are summarized in Table 5.2. The modified and the original Ikeda and Nishimura theories are seen to give very similar results which are in general agreement with the measurements, both for large and small phase shifts. The theory of Kitanidis and Kennedy is seen to overpredict the phase shift considerably. This point is emphasized herein, since Kitanidis and Kennedy (1984) assumed local bank erosion rate to be a function of the strength of the secondary flow.

The experiments of Gottlieb (1976) Runs 1 and 2 merit further discussion. These are fixed bed runs for which measurements of the secondary flow were reported at the bend apexes only. Thus, it is not possible to estimate the phase shift. Gottlieb (1976), however, also shows results generated by his numerical model (see Fig. 4.4 therein), from which the phase shift can be extracted ($\sigma_{SL} = 63^{o}$). This agrees very well with the results obtained by the modified and original Ikeda and Nishimura theories; see Table 5.2.

It is of importance to note that the measured phase shifts in the above-mentioned experiments are large, i.e. $\sigma_{SL} \sim 34^{o} - 56^{o}$. The shifts predicted by Eq. 5.11 for typical natural meander bends are rather small (e.g. for the rivers in Table 5.3, $\sigma_{SL} \sim 4^{o} - 29^{o}$). The reason for this difference is that the values for r, which are typically O(1) for natural meander bends (see Fig. 3.1), but vary from 8.4 - 27.6 for the experiments. This phase shift must therefore be accounted for in the simulation of many experiments, although it can be neglected without making a large error for most natural meandering rivers (e.g. Smith and McLean, 1984).

5.3.5 Conclusions

A theoretical model for the calculation of water-surface and secondary flow in mildly sinuous channels is developed. The analysis is based upon, but is more rigorous than, that of Ikeda and Nishimura (1986). Downstream convective acceleration of the secondary flow is shown to give rise to a phase lag between the secondary flow and channel centerline curvature, and also to suppress the magnitude of the secondary flow. The results of the present analysis vindicate the approximate procedure of Ikeda and Nishimura (1986). The analysis of Kitanidis and Kennedy (1984) appears to considerably overpredict the shift of the secondary flow.

The analysis indicates that although the predicted lag must be accounted for in the simulation of the flow field and the bed topography in many experiments, it can be neglected without making a large error for most natural meandering rivers.

5.4 Solution for the Bed Topography and the Primary Flow

5.4.1 Formulation

Since the "Modified Ikeda-Nishimura" treatment of the secondary flow (Eqs. 5.9, 5.11, and 5.12) gives very good results, (see Fig. 5.3), it will be used instead of the "General Solution" which is substantially more complicated. The water-surface is correspondingly taken to be

$$\xi_1 = F^2 \chi_{20} \, n \sin \phi \tag{5.31}$$

Table 5.1 - Flow Conditions

Run Number	$\tilde{\lambda}$ (m)	b (m)	ψ_0	H (m)	U (m/s)	I
Yen (1965)						
1	35.3	1.02	0.120	0.102	0.817	$1.44 \cdot 10^{-3}$
2	35.3	1.06	0.125	0.142	0.957	$1.44 \cdot 10^{-3}$
3	35.3	1.07	0.126	0.145	0.692	$0.72 \cdot 10^{-3}$
4	35.3	1.08	0.126	0.145	0.427	$0.29 \cdot 10^{-3}$
5	35.3	1.14	0.134	0.206	0.527	$0.29 \cdot 10^{-3}$
Air duct	8.84	0.285	0.134	0.0514		
Gottlieb (1976)						
1	12.0	0.5	0.0206	0.229	0.328	$0.30 \cdot 10^{-3}$
2	12.0	0.5	0.0206	0.137	0.474	$0.62 \cdot 10^{-3}$
Ikeda et al. (1985)						
Air duct	3.09	0.15	0.240	0.025	5.3	

Table 5.2 - Calculated Results

Run Number	γ	$C_f^{-1/2}$	ε	r	σ_{SL} (Meas.)	σ_{SL} Eq. 5.11	σ_{SL} Eq. 5.25	σ_{SL} Eq. 5.27
Yen (1965)								
1	10.0	21.5	0.0216	8.41	34	20.1	22.2	86.9
2	7.5	21.4	0.0163	11.5	36	26.8	29.3	87.8
3	7.4	21.6	0.0158	12.1	36	27.7	30.3	87.9
4	7.4	21.0	0.0169	11.4	36	26.9	29.5	87.7
5	5.5	21.8	0.0117	17.4	56	36.9	39.9	88.5
Air duct	5.5	22.2*	0.0113	17.9	56	37.3	40.2	88.6
Gottlieb (1976)								
1	2.18	12.6	0.0137	19.1		51.6	56.5	88.6
2	3.65	16.4	0.0135	19.3		46.4	50.3	88.7
Num. Exp.	5.0	27.2	0.00674	44.5	63	57.7	59.9	89.4
Ikeda et al. (1985)								
Air duct	6.0	17.8*	0.0190	16.1	40 ~ 45	39.4	43.0	88.4

* Estimated by Yen (1965) and Ikeda et al. (1985), (Eq. 2.27a not used since I is not given).

Table 5.3 - Computed Values of σ_{SL} for Several Meandering Sand-Bed Streams at Bankfull Flow

River	Reference	$C_f^{-1/2}$	γ	ε	k	r	σ_{SL} Eq. 5.11
Root	Johannesson (1985)	21.8	9.5	0.020	0.13	6.5	16
Zumbro	Johannesson (1985)	15.4	10.1	0.043	0.22	5.1	16
Minnesota*	Johannesson (1985)	13.2	11.7	0.067	0.34	5.1	18
Red Lake	Johannesson (1985)	13.7	15.5	0.082	0.23	2.8	10
Minnesota*	Parker (1982)	26.7	11.4	0.016	0.25	15.6	29
Pembina	Beck et al. (1983a)	12.5	16.2	0.103	0.13	1.3	5
Genesee	Beck et al. (1983b)	11.4	9.7	0.075	0.17	2.3	9
Muddy Cr.	Dietrich and Smith (1983)	7.73	6.0	0.10	0.30	3.0	14
Fall	Thorne et al. (1985)	4.53	6.3	0.31	0.28	0.90	4

* Different reaches

Eqs. 5.3a through d, together with Eqs. 5.9, 5.11, 5.12, and 5.31, then reduce to

$$r u_1' + 2u_1 = n[-r \chi_{20} \cos \phi + (F^2 \chi_{20} - 1) \sin \phi]$$

$$- \eta_1 - \cos \sigma_{SL} \sin(\phi - \sigma_{SL}) \frac{1}{\varepsilon^2 \chi_1} \frac{\partial}{\partial n} \int_0^1 TG_0 d\zeta \tag{5.32}$$

$$r u_1' + r h_1' + \frac{\partial v_1}{\partial n} = 0 \tag{5.33}$$

$$rM u_1' + \frac{\partial}{\partial n}[v_1 + \frac{\chi_1 \dot{\upsilon}_1(0)}{\varepsilon} - \Gamma \frac{\partial \eta_1}{\partial n}] = 0 \tag{5.34}$$

The solution for the bed profile η_1 is now decomposed as

$$\eta_1 = \eta_{1C} + \eta_{1F} \tag{5.35}$$

where η_{1C} satisfies that portion of Eq. 5.34 that represents the direct effect of the secondary flow on the bed, i.e.

$$\frac{\partial}{\partial n}(\chi_1 \dot{\upsilon}_1(0) - \frac{\beta}{\gamma} \frac{\partial \eta_{1C}}{\partial n}) = 0 \tag{5.36}$$

Between Eqs. 5.9 and 5.36, it is found that

$$\eta_{1C} = - A n \cos \sigma_{SL} \sin(\phi - \sigma_{SL}) \tag{5.37}$$

where A is the bed scour factor given by Eq. 4.13.

We likewise decompose as follows

$$u_1 = u_{1C} + u_{1F} \;\; ; \;\; h_1 = h_{1C} + h_{1F} \;\; ; \;\; v_1 = v_{1C} + v_{1F} \tag{5.38}$$

where u_{1C}, h_{1C}, and v_{1C} are terms generated directly by the curvature-induced bed topography, and η_{1F}, u_{1F}, h_{1F}, and v_{1F} are extra terms needed to to satisfy sediment continuity. The subscripts "C" and "F" are selected so as to indicate the response of the system that is characterized by local curvature forcing (e.g. point bars), and the component characterized by the response of the free system (e.g. alternate bars) to this forcing. Substituting into Eq. 5.32, 5.33, and 5.34 and making use of Eqs. 5.31 and 5.37 the problem is decomposed to:

C - Problem

$$h_{1C} = \xi_1 - \eta_{1C} = n\,[\,F^2\chi_{20}\sin\phi + A\cos\sigma_{SL}\sin(\phi - \sigma_{SL})\,] \tag{5.39a}$$

$$r\,u_{1C}' + 2u_{1C} = n\,[\,-r\,\chi_{20}\cos\phi + (F^2\chi_{20} - 1)\sin\phi\,]$$

$$+\cos\sigma_{SL}\sin(\phi - \sigma_{SL})\,[\,A\,n - \frac{1}{\varepsilon^2\chi_1}\frac{\partial}{\partial n}\int_0^1 TG_0\,d\zeta\,] \tag{5.39b}$$

$$\frac{\partial v_{1C}}{\partial n} = -\,r\,(h_{1C} + u_{1C})' \tag{5.39c}$$

The boundary conditions on v_{1C} (Eq. 5.4a) and u_{1C} (Eq. 5.6a) are:

$$v_{1C}\,|_{n=\pm1} = 0 \;\;;\;\; u_{1C}\,|_{n=0} = 0 \tag{5.40a,b}$$

F - Problem

$$r\,u_{1F}' + 2u_{1F} = -\,\eta_{1F} \tag{5.41a}$$

$$\frac{\partial v_{1F}}{\partial n} = -\,r\,(u_{1F} - \eta_{1F})' \tag{5.41b}$$

$$r\,M\,u_{1F}' + \frac{\partial v_{1F}}{\partial n} - \Gamma\frac{\partial^2\eta_{1F}}{\partial n^2} = -\,rM\,u_{1C}' - \frac{\partial v_{1C}}{\partial n} \tag{5.41c}$$

The above three relations can be reduced to

$$r\,u_{1F}' + 2u_{1F} = -\,\eta_{1F} \tag{5.42a}$$

$$r\,(M\text{-}1)\,u_{1F}' + r\,\eta_{1F}' - \Gamma\frac{\partial^2\eta_{1F}}{\partial n^2} = -\,r\,(M\text{-}1)\,u_{1C}' + r\,h_{1C}' \tag{5.42b}$$

The boundary conditions on v_{1F} (Eq. 5.4a), and η_{1F} (Eqs. 5.4b, 5.3d, and 5.6c), and u_{1F} (Eq. 5.6a) are:

$$v_{1E}\,|_{n=\pm1} = 0 \;\;;\;\; \frac{\partial\eta_{1E}}{\partial n}\,|_{n=\pm1} = 0 \tag{5.43a,b}$$

$$\eta_{1F} = u_{1F} = 0 \quad \text{at } n = 0 \tag{5.43c,d}$$

Once the solution for the C - Problem is obtained, the F -Problem (Eqs. 5.42a,b together with the boundary conditions given by Eqs. 5.43a,b,c,d) becomes fully defined.

5.4.2 Solution of the C - Problem

Using again the "moment method", as was done in for the constant curvature case, Eq. 5.39b is reduced to

$$r\, u'_{1Cb} + 2u_{1Cb} = [\, -r\, \chi_{20} \cos\phi + (F^2\chi_{20} - 1) \sin\phi + (A + A_s) \cos\sigma_{SL} \sin(\phi - \sigma_{SL})\,] \tag{5.44}$$

where u_{1Cb} is the value of u_{1C} at n = 1. The solution of the C - Problem (Eqs. 5.44 and 5.39c) is

$$u_{1Cb} = \tilde{a}_c \cos\phi + \tilde{b}_c \sin\phi \tag{5.45a}$$

$$v_{1C} = \frac{1}{2}(1 - n^2)\, [\, \tilde{c}_c \cos\phi - \tilde{d}_c \sin\phi\,] \tag{5.45b}$$

where

$$\tilde{a}_c = -\frac{1}{r^2 + 4} \left\{ r\, [\, \chi_{20}\, (F^2 + 2) - 1 + (A + A_s) \cos^2\sigma_{SL}\,] + (A + A_s) \sin 2\sigma_{SL} \right\} \tag{5.45c}$$

$$\tilde{b}_c = \frac{1}{r^2 + 4} \left\{ 2\, [\chi_{20}\, F^2 - 1 + (A + A_s) \cos^2\sigma_{SL}\,] - r\, [\, r\, \chi_{20} + \frac{1}{2}(A + A_s) \sin 2\sigma_{SL}\,] \right\} \tag{5.45d}$$

$$\tilde{c}_c = r\, (\, \tilde{b}_c + F^2\chi_{20} + A \cos^2\sigma_{SL}\,) \tag{5.45e}$$

$$\tilde{d}_c = r\, (\, \tilde{a}_c - \frac{1}{2} A \sin 2\sigma_{SL}\,) \tag{5.45f}$$

5.4.3 Solution of the F - Problem

Having solved the C - Problem, the F - Problem can be stated as follows

$$r\, u'_{1F} + 2u_{1F} = -\, \eta_{1F} \tag{5.46a}$$

$$r\, (M\text{-}1)\, u'_{1F} + r\, \eta'_{1F} - \Gamma \frac{\partial^2\eta_{1F}}{\partial n^2} = n\, (\, D_1 \cos\phi + D_2 \sin\phi\,) \tag{5.46b}$$

where

$$D_1 = \tilde{c}_c - rM\,\tilde{b}_c \tag{5.46c}$$

$$D_2 = rM\,\tilde{a}_c - \tilde{d}_c \tag{5.46d}$$

The boundary conditions are given, as before, by Eqs. 5.43a,b,c,d.

Having so successfully used the "moment method" on the C - Problem, and knowing that the transverse bed profile in an actual river is often well described by a linear profile, the "moment method" is also used to simplify the F - Problem.

The first moments of the lateral distribution of u_{1F} and η_{1F} are, (see Eq. 4.15):

$$n_{u1F} = \frac{1}{2}\int_0^1 u_{1F} n\,dn \quad ; \quad n_{\eta 1F} = \frac{1}{2}\int_0^1 \eta_{1F} n\,dn \tag{5.47a,b}$$

Multiplying Eqs. 5.46a,b by n and integrating from n = -1 to n = 1, the following result is obtained

$$r\int_{-1}^{1} n u'_{1F}\,dn + 2\int_{-1}^{1} n u_{1F}\,dn = -\int_{-1}^{1} n\eta_{1F}\,dn \tag{5.48a}$$

$$r\,(M\text{-}1)\int_{-1}^{1} n u'_{1F}\,dn + r\int_{-1}^{1} n\eta'_{1F}\,dn - \Gamma\int_{-1}^{1} n\frac{\partial^2 \eta_{1F}}{\partial n^2}\,dn = \int_{-1}^{1} n^2\,dn\,(D_1\cos\phi + D_2\sin\phi) \tag{5.48b}$$

Eqs. 5.48a,b together with Eqs. 5.47a,b, give

$$r\,n'_{u1F} + 2n_{u1F} = -n_{\eta 1F} \tag{5.49a}$$

$$r\,(M\text{-}1)\,n'_{u1F} + r\,n'_{\eta 1F} - \frac{1}{2}\Gamma\left\{\left[n\frac{\partial \eta_{1F}}{\partial n}\right]_{n=-1}^{n=1} - \eta_{1F}\big|_{n=1} + \eta_{1F}\big|_{n=-1}\right\} = \frac{1}{3}(D_1\cos\phi + D_2\sin\phi) \tag{5.49b}$$

The lowest order term in the Fourier series for η_{1F} is

$$\eta_{1F} = \eta_{1Fb}\sin\left(\frac{\pi}{2}n\right) \tag{5.50a}$$

where $\eta_{1Fb} = \eta_{1F}$ at n = 1. This together with Eq. 5.47b gives

$$n_{\eta 1F} = (\frac{2}{\pi})^2 \eta_{1Fb} \tag{5.50b}$$

Eq. 5.49b, together with Eqs. 5.43b and 5.50a,b, reduce to

$$r\,(M\text{-}1)\,n'_{u1F} + r\,n'_{\eta 1F} + (\frac{\pi}{2})^2 \Gamma\, n_{\eta 1F} = \frac{1}{3}(D_1 \cos\phi + D_2 \sin\phi) \tag{5.51}$$

Although the solution to the F - Problem (if Fourier expansion is used) yields the result that the lowest mode variation in the transverse direction goes as sin(π/2 n) instead of n itself (note that the difference is modest), a linear solution, that preserves the first moments n_{u1F} and $n_{\eta 1F}$, is obtained by replacing n_{u1F} and $n_{\eta 1F}$, respectively, by $u_{1Fb}/3$ and $\eta_{1Fb}/3$ in Eqs. 5.49a and 5.51. This gives

$$r\,u'_{1Fb} + 2u_{1Fb} = -\eta_{1Fb} \tag{5.52a}$$

$$r\,(M\text{-}1)\,u'_{1Fb} + r\,\eta'_{1Fb} + (\frac{\pi}{2})^2 \Gamma\, \eta_{1Fb} = D_1 \cos\phi + D_2 \sin\phi \tag{5.52b}$$

The solution to Eqs. 5.52a,b can be written as

$$u_{1Fb} = \tilde{a}_F \cos\phi + \tilde{b}_F \sin\phi \tag{5.53a}$$

$$\eta_{1Fb} = \bar{a}_F \cos\phi + \bar{b}_F \sin\phi \tag{5.53b}$$

where

$$\tilde{a}_F = \frac{J_1 D_1 + r\,J_2 D_2}{J_1^2 + r^2\,J_2^2} \tag{5.53c}$$

$$\tilde{b}_F = \frac{-r\,J_2 D_1 + J_1 D_2}{J_1^2 + r^2\,J_2^2} \tag{5.53d}$$

$$\bar{a}_F = -2\,\tilde{a}_F - r\,\tilde{b}_F \tag{5.53e}$$

$$\bar{b}_F = r\,\tilde{a}_F - 2\,\tilde{b}_F \tag{5.53f}$$

$$J_1 = r^2 - 2(\frac{\pi}{2})^2 \Gamma \tag{5.53g}$$

$$J_2 = (\frac{\pi}{2})^2 \Gamma - M + 3 \qquad (5.53h)$$

5.5 Discussion

In Chapter 4.6, the difference between the present model and the model of Ikeda et al. (1981) was discussed for the case of constant curvature. That discussion also applies to sinuous channels, except that now the difference is greater. First, Ikeda et al. (1981) assumed the strength of the secondary flow to be in phase with curvature. This corresponds to setting $\sigma_{SL} = 0$ and $\chi_* = 1$, and is not necessarily a reasonable approximation if the transport of primary flow momentum by the secondary flow is to be modeled accurately. Secondly, Ikeda et al. (1981) did not take into account the influence of the redistribution of the sediment, which corresponds to setting $M = 0$ in the calculation of the F - Problem. Thirdly, Ikeda et al. (1981) did not include the influence of the depth-averaged component of the transverse velocity, v, in the force balance relation for the sediment particle, i.e. Eq. 2.35. This, together with setting $M = 0$, corresponds to completely neglecting the contribution of the F - Problem.

An interesting feature of the solution to Eqs. 5.52a,b deserves some discussion. For certain combinations of input variables, the solution to the F - Problem shows resonant behavior. The solution, of course, fails to be valid in the neighborhood of this resonance. The model of Blondeaux and Seminara (1985) also shows the same behavior. The condition for the occurrence of the resonance can be determined from Eqs. 5.52a,b. Using Eq. 5.52a to eliminate η_{1Fb} from Eq. 5.52b, one gets

$$u''_{1Fb} + \frac{1}{r}[3 - M + (\frac{\pi}{2})^2 \Gamma]\, u'_{1Fb} + 2(\frac{\pi}{2})^2 \frac{\Gamma}{r^2} u_{1Fb} = -\frac{1}{r^2}(D_1 \cos\phi + D_2 \sin\phi) \qquad (5.54)$$

Resonance occurs if both of the following conditions are satisfied: The coefficient of damping must vanish, i.e.

$$c_d = \frac{1}{2}\frac{1}{r}[3 - M + (\frac{\pi}{2})^2 \Gamma] = 0 \qquad (5.55a)$$

and the wavenumber of the undamped homogeneous equation, k_{res}, must equal the wavenumber of the forcing function, k, to wit

$$k_{res}^2 = 2(\frac{\pi}{2})^2 \Gamma \varepsilon^2 = k^2 \qquad (5.55b)$$

Equation 5.55a,b is satisfied if J_1 and J_2, as defined by Eqs. 5.53g,h, both approach zero. As seen from Eqs. 5.53c,d, this obviously leads to resonance.

In Fig. 5.5, the results for the amplitude of the component of u_1 in phase with curvature, i.e. $\tilde{b}_C + \tilde{b}_F$, predicted by the present model are compared with the results of Blondeaux and Seminara (1985), as reported in Fig. 2 therein. The input variables have been selected so as to agree with those used by Blondeaux and Seminara (1985). That is,

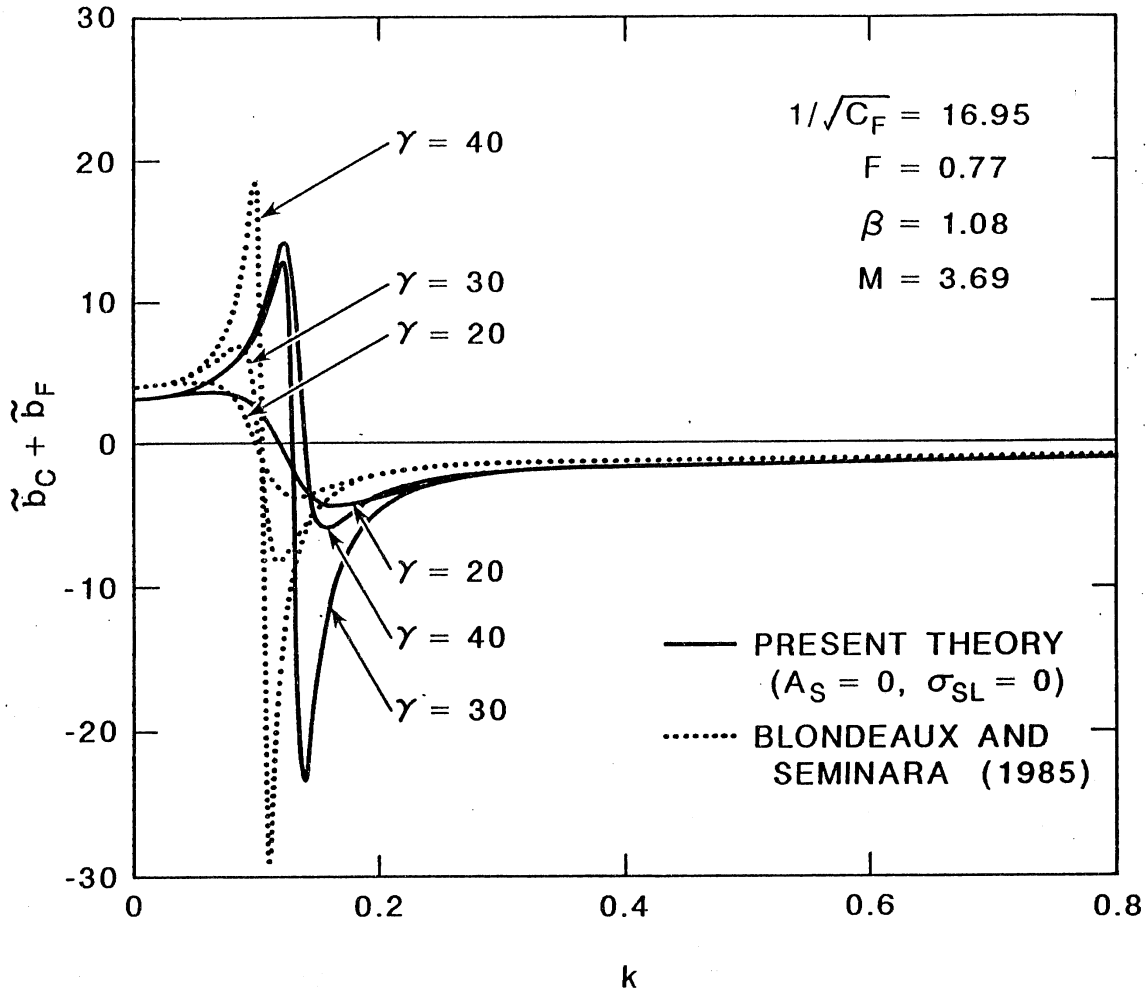

Fig. 5.5. Comparison between the present theory and the theory of Blondeaux and Seminara (1985) for the amplitude of the component of u_1 in phase with curvature.

$\tau^* = 0.25$, $D_{50}/H = 0.005$, and $F = 0.77$. Assuming an upper regime flat bed, Eq. 2.12a gives $1/\sqrt{C_f} = 16.95$. Using the sediment transport formula of Meyer-Peter-Müller (Table A.3 in Appendix A) gives $M = 3.69$ if $\tau_C^* = 0.047$. Also note that β is taken to be 1.08 as predicted by Blondeaux and Seminara (1985) whereas if Eq. 2.14 is used $\beta = 1.16$). Further, A_s, χ_*, and σ_{SL} have been taken to be zero, one, and zero, respectively, to make the comparison as precise as possible. The agreement is seen to be excellent. The present theory predicts resonance conditions to be $\gamma = 33.3$ and $k_{res} = 0.136$, from Eqs. 5.55a,b, whereas the theory of Blondeaux and Seminara (1985) predicts the conditions to be approximately $\gamma = 40$ and $k_{res} = 0.15$. The overall structure of the two solutions is also seen to be very similar. In fact the agreement between the two theories can be made very precise; see Parker and Johannesson (1989).

The physical mechanism behind the resonance is explained in Chapter 6. It is, however, important to realize at this point that the resonance phenomenon is solely a contribution of the F - Problem. The model of Ikeda et al. (1981) cannot therefore predict resonance. Therein, the coupling between the flow field and the sediment transport is not retained when calculating the bed topography, which is assumed to be a function only of the local channel curvature.

5.6 Comparison with Data

Before comparing the model with data, it is helpful to summarize what data the model needs as input, and how the dependent variables are calculated.

Input Data:

1) U, H, I, b, θ_0, $\tilde{\lambda}$.
2) D_{50} and R if the channel has an erodible bed.

Calculation Procedure:

1) C_f (Eq. 2.27a) ; F and ε (Eq. 2.28c) ; $\alpha = 0.077$; χ_1 (Eq. 2.25) ; χ (Eq. 2.21b) ; χ_{20} (Eq. 4.7) ; A_s (Eq. 4.21) ;
2) τ_C^* (Shields Diagram, Vanoni, 1977, Fig. 2.43) ; τ^* (Eq. 2.11) ; τ_G^* (Eq. 2.12) ; M (Eq. 2.10) ; β (Eq. 2.14) ; A (Eq. 4.13) ;
3) ξ_1 (Eq. 5.31) ; σ_{SL} (Eq. 5.11) ; η_{1C} (Eq. 5.37) ; u_{1Cb} (Eq. 5.45a) ; η_{1Fb} (Eq. 5.53b) ; u_{1Fb} (Eq. 5.53a).

The input data for all the experiments and the one field study simulated are summarized in Tables 5.4 and 5.5. Some calculated results are shown in Table 5.6. The flow conditions for all the data sets were estimated (Eqs. 2.12c,d) to be in the lower regime

(dune covered bed) except for Exp. M1 and M3 of Yamaoka and Hasegawa (1983), for which Eq. 2.12d predicts upper regime flow (flat bed). Exp. M1 was the only one which had supercritical flow (F > 1).

The perturbation parameter ψ_0, assumed to be small in this analysis, varied from 0.0206 to 0.363 (Table 5.4). This is considered small enough for the analysis to be at least approximately valid.

The measured and predicted shifts $\sigma_{BL} = \text{ATAN}\,[(0.5A \sin 2\sigma_{SL} + \bar{a}_F)/(A \cos^2\sigma_{SL} - \bar{b}_F)]$ in the bed topography with respect to the channel curvature are shown in Fig. 5.6a. The agreement is seen to be good except for all four of the experiments of Gottlieb (1976). It is especially gratifying to see that the model is able to predict that the shift for Exp. 10 of Hooke (1974) is negative. This indicates that the deepest scour happens upstream of the bend apex for this experiment, which indeed is the case. It is important to realize that without the contribution of the F - Problem the model would always predict a positive shift. One plausible reason why the model does not reproduce the measured results of Gottlieb (1976) becomes apparent after studying Fig. 5.7, (Fig. 6.5 in Gottlieb (1976)). It is seen that high amplitude dunes were present in the experiments. Although, the model partly accounts for dunes (in the calculation of M and A), it seems rather hopeless to apply the model to a situation where the dune amplitude is larger than the maximum transverse variation in the bed, as was the case for Gottlieb's (1976) experiments.

The reason why M is taken to be 5 in Exp. 3S of Gottlieb (1976) is that τ^*_G, as predicted by Eq. 2.12 is less than τ^*_C. This indicates that the bed was flat and immobile, which cannot be true, since τ^* was found experimentally to be more than twice τ^*_C. The most reasonable thing to do is then to set τ^*_G equal or slightly above τ^*_C. Eq. 2.10a then gives the value $M \rightarrow \infty$, which violates the implicit perturbation assumption that $(M\, u_1\, \psi_0) << 1$. To avoid this difficulty, M is arbitrarily taken to be equal to a typical value of about 5, which corresponds to selecting $\tau^*_G = 2\, \tau^*_C$.

The measured and predicted amplitude $A_\eta = [(A \cos^2\sigma_{SL} - \bar{b}_F)^2 + (0.5A \sin 2\sigma_{SL} + \bar{a}_F)^2]^{1/2}$ of the transverse variation in the bed topography are shown in Fig. 5.6b. The results are satisfactory. The scatter is considerably greater than that obtained for the constant curvature case, (Fig. 4.4a,b). This is not surprising, since the model for a sinuous channel is considerably more complicated. From Fig. 5.6b it is apparent that for the two data sets where the sediment grain size distribution was highly non-uniform (the geometric standard deviation of the bed material $\sigma_g > 1.6$), better results are obtained by setting M = 0.0 rather than using the value based on the mean particle grain size, D_{50}. This is not totally unexpected, since the model does not take into account sorting of bedload in channel bends. By forcing M to be zero, a component of the model that is very sensitive to sorting of the bedload is thrown out of it, which may easily be more appropriate than retaining it, for the case of non-uniform bedload. This ad hoc correction, however, deserves a more formal justification than is given herein.

Finally, a more detailed comparison is done with the data set from Muddy Creek. The measurements were taken when the flowrate was 1.1 m^3/s, which is 69% of bankfull discharge. A plan view of the Muddy Creek study reach is shown in Fig. 5.8. In Fig. 5.9, centerline water-surface elevation, channel width, and centerline depth are shown as a function of location along the channel centerline. The water-surface slope and centerline depth are seen to be fairly constant, (Fig. 5.9), as assumed in the theoretical model at $O(\psi_0)$. The channel width, however, varies from 4.2 meters at Section 10 to 6.0 meters at Section 19. In the theoretical model the width 2b is assumed to be constant and equal to 4.8 meters. In Fig. 5.10 the measured and predicted distributions of depth and depth-averaged primary flow velocity are shown; the predictions are for the case M = 0. The agreement is excellent.

Table 5.4 - Sinuous Channels: Geometry

Run Number	θ_0 (rad)	$\tilde{\lambda}$ (m)	b (m)	ψ_0
Hooke (1974)				
10, 20, 35, 50	0.960	13.2	0.5	0.228
Gottlieb (1976)				
1S, 2S, 3S, 4S	0.0785	12	0.5	0.0206
Yamaoka and Hasegawa (1983)				
M1, M2	0.524	2.2	0.15	0.224
M3	0.349	2.4	0.11	0.101
Ikeda and Nishimura (1986)	0.698	3	0.15	0.219
Dietrich and Smith (1983)				
Muddy Creek	1.213	50.4	2.4	0.363

Table 5.5 - Sinuous Channels: Flow Conditions

Run Number	Q (l/s)	H (m)	U (m/s)	I	D_{50} (mm)	σ_g	R
Hooke (1974)							
10	10	0.052	0.192	0.00213	0.30	1.23	1.7
20	20	0.073	0.275	0.00207	0.30	1.23	1.7
35	35	0.095	0.368	0.00221	0.30	1.23	1.7
50	50	0.128	0.394	0.00223	0.30	1.23	1.7
Gottlieb (1976)							
1S	40	0.137	0.292	0.00109	0.55	Not given	1.65
2S	72	0.189	0.396	0.00215	0.55	''	1.65
3S	40	0.142	0.282	0.00154	1.18	''	1.65
4S	72	0.200	0.360	0.00225	1.18	''	1.65
Yamaoka and Hasegawa (1983)							
M1	0.75	0.0089	0.322	0.01410	0.43	$\cong$ 1.0	1.66
M2	1.87	0.0258	0.242	0.00333	0.43	''	1.66
M3	0.53	0.0093	0.264	0.00625	0.43	''	1.66
Ikeda and Nishimura (1986)	2.6	0.0537	0.161	0.00139	0.15	>> 1	1.65
Dietrich and Smith (1983) Muddy Creek	$1.1 \cdot 10^3$	0.40	0.573	0.00140	0.7	2.1	1.65

Table 5.6 - Sinuous Channels: Calculated Results

Run Number	F	C_f	A_s	M	A_η meas.	A_η calc. C-Prob.	A_η calc. C+F-Prob.	σ_{BL} meas.	σ_{BL} calc. C-Prob.	σ_{BL} calc. C+F-Prob
Hooke (1974)										
10	0.27	0.0295	0.81	7.40	6.9	2.95	4.85	-9	4.3	- 40.6
20	0.32	0.0196	2.34	4.64	5.6	3.86	8.11	11	8.9	9.7
35	0.38	0.0152	4.90	4.07	5.1	4.80	8.72	20	14.2	29.8
50	0.35	0.0180	7.72	3.99	4.1	4.97	8.27	12	16.5	28.1
Gottlieb (1976)										
1S	0.25	0.0172	9.21	7.56	8.5	2.84	6.91	82	20.0	25.9
2S	0.29	0.0254	12.35	4.61	6.9	3.67	6.15	70	19.4	24.2
3S	0.24	0.0270	6.58	"5.0"	8.7	2.45	4.2	85	14.0	15.0
4S	0.26	0.0341	10.24	18.03	10.9	2.53	12.73	45	15.2	- 6.8
Yamaoka and Hasegawa (1983)										
M1	1.09	0.0119	0.58	5.00	5.6	5.97	10.73	46	9.8	25.0
M2	0.48	0.0144	4.19	5.54	4.4	3.15	8.98	72	23.3	66.4
M3	0.87	0.00818	1.54	5.00	12.3	4.08	19.40	86	12.1	79.0
Ikeda and Nishimura (1986)	0.22	0.0282	9.99	7.13	3.4	2.82	6.60	54	19.8	24.2
	0.22	0.0282	9.99	"0.0"	3.4	2.82	2.31	54	19.8	29.6
Dietrich and Smith (1983) Muddy Creek	0.29	0.0167	3.48	4.31	2.26	4.23	9.22	25	14.5	38.3
	0.29	0.0167	3.48	"0.0"	2.26	4.23	2.95	25	14.5	38.6

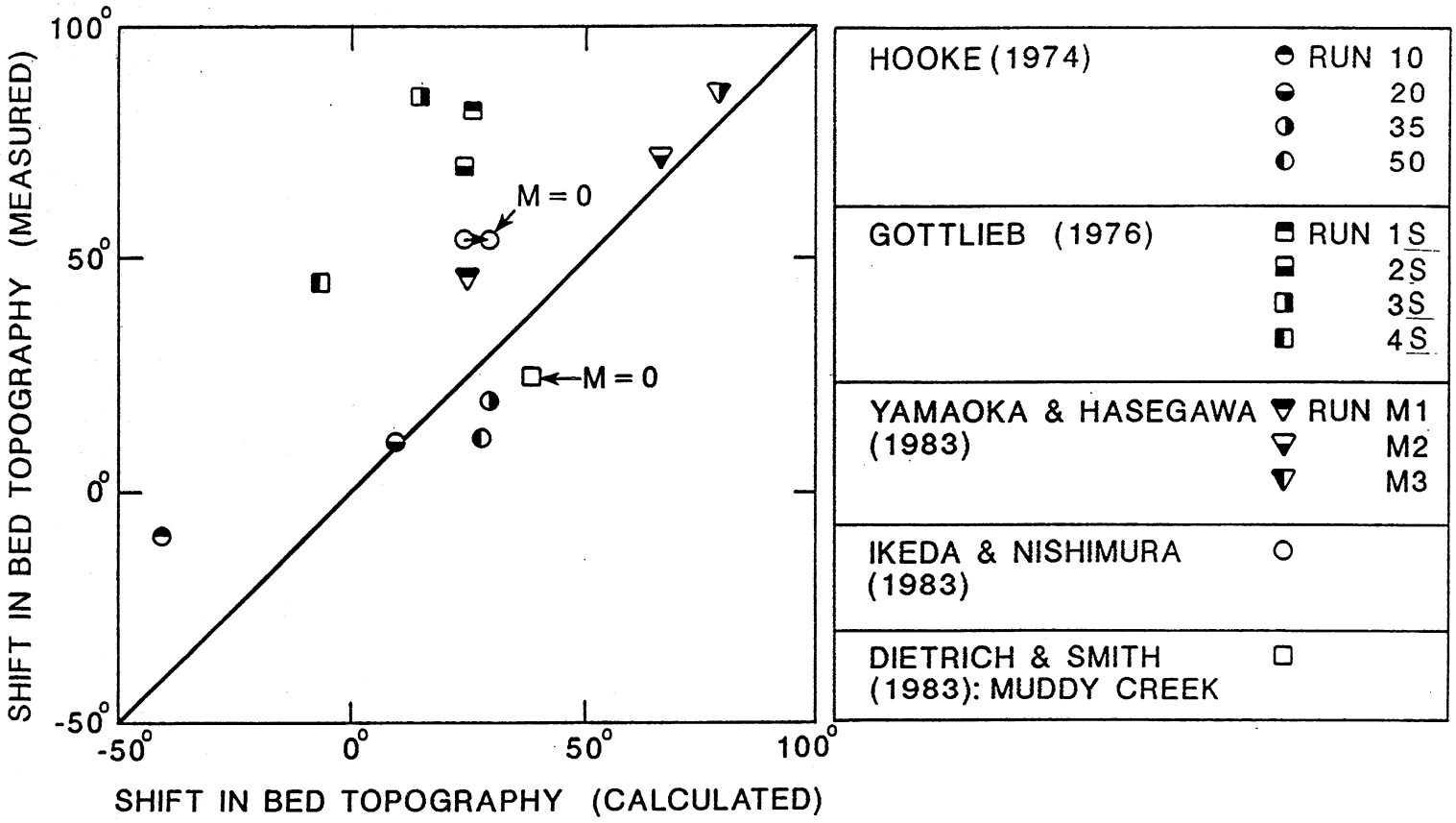

Fig. 5.6a. Shift in bed topography with respect to channel curvature as measured and predicted.

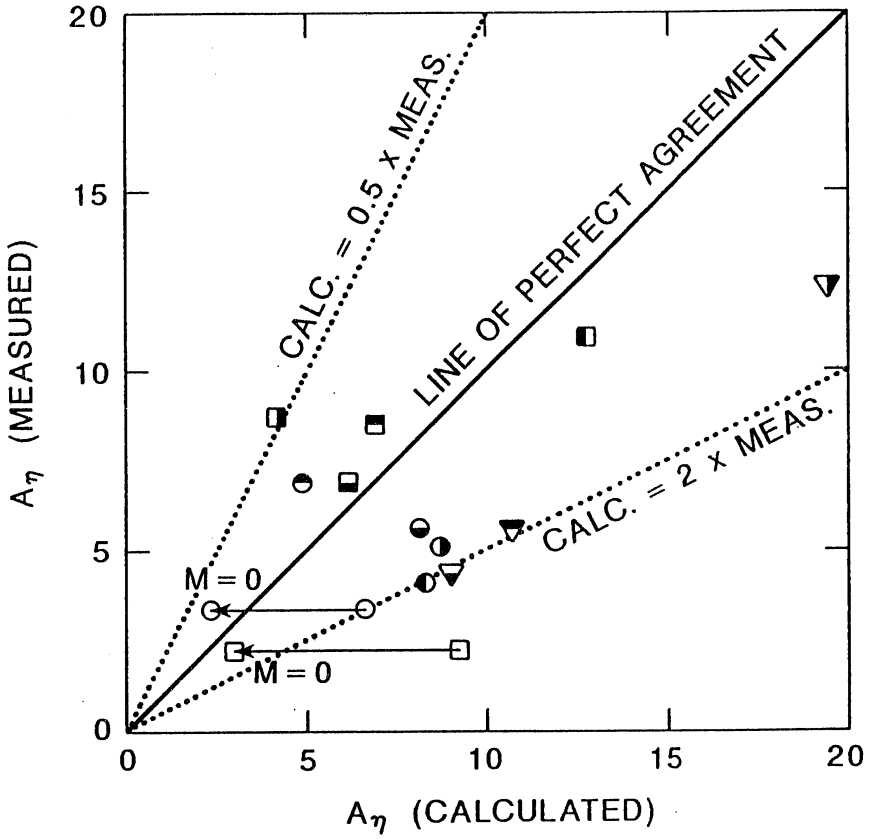

Fig. 5.6b. The amplitude, A_η, of the transverse variation in the bed topography as measured and predicted.

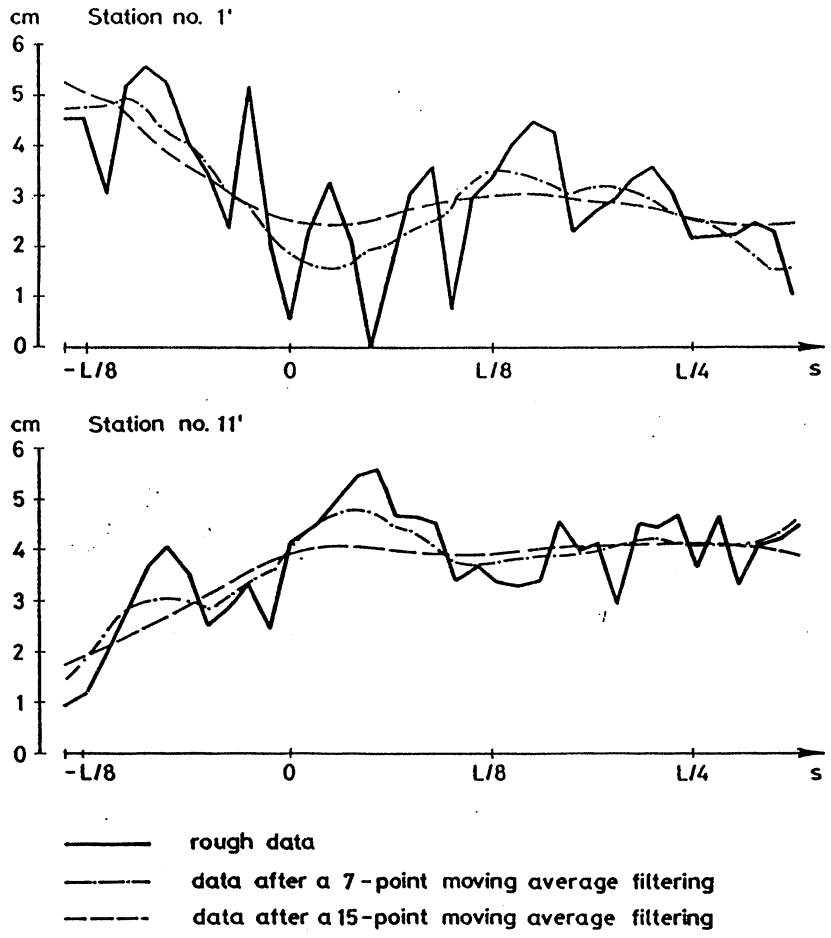

Fig. 5.7. Bed elevation measurements. Two series from Run 1S of Gottlieb (1976).

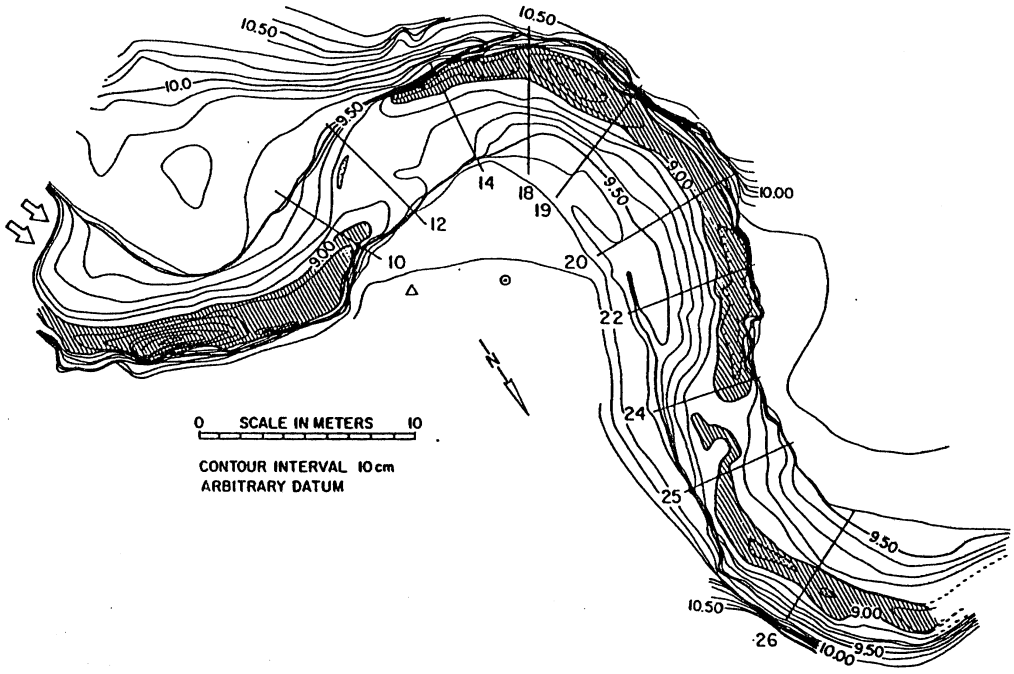

Topography of the study site. The pools have been shaded for emphasis.

Fig. 5.8. Plan view of Muddy Creek study reach.

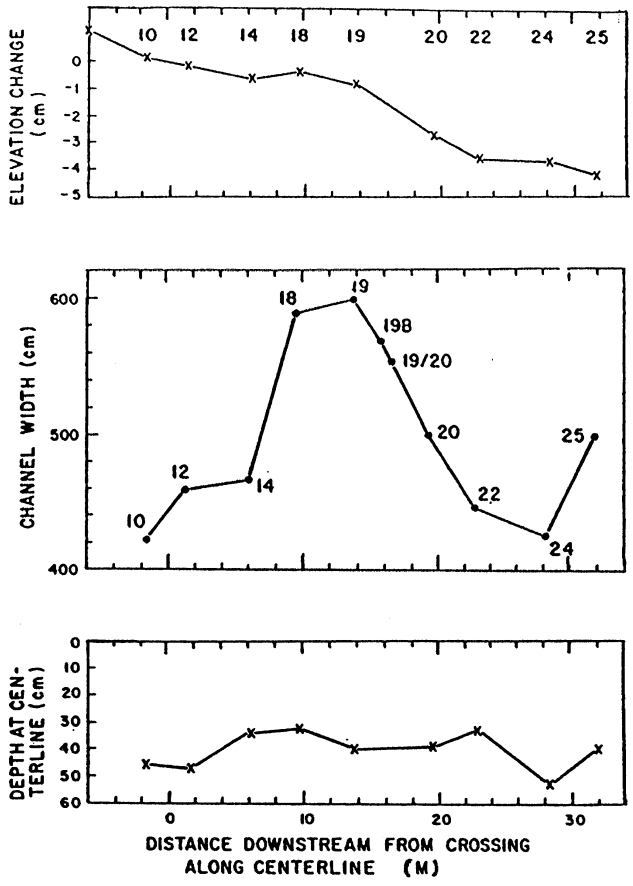

Fig. 5.9. Variation in centerline water-surface elevation, channel width, and centerline depth as a function of location along the channel centerline for a discharge of 1.1m^3/s.

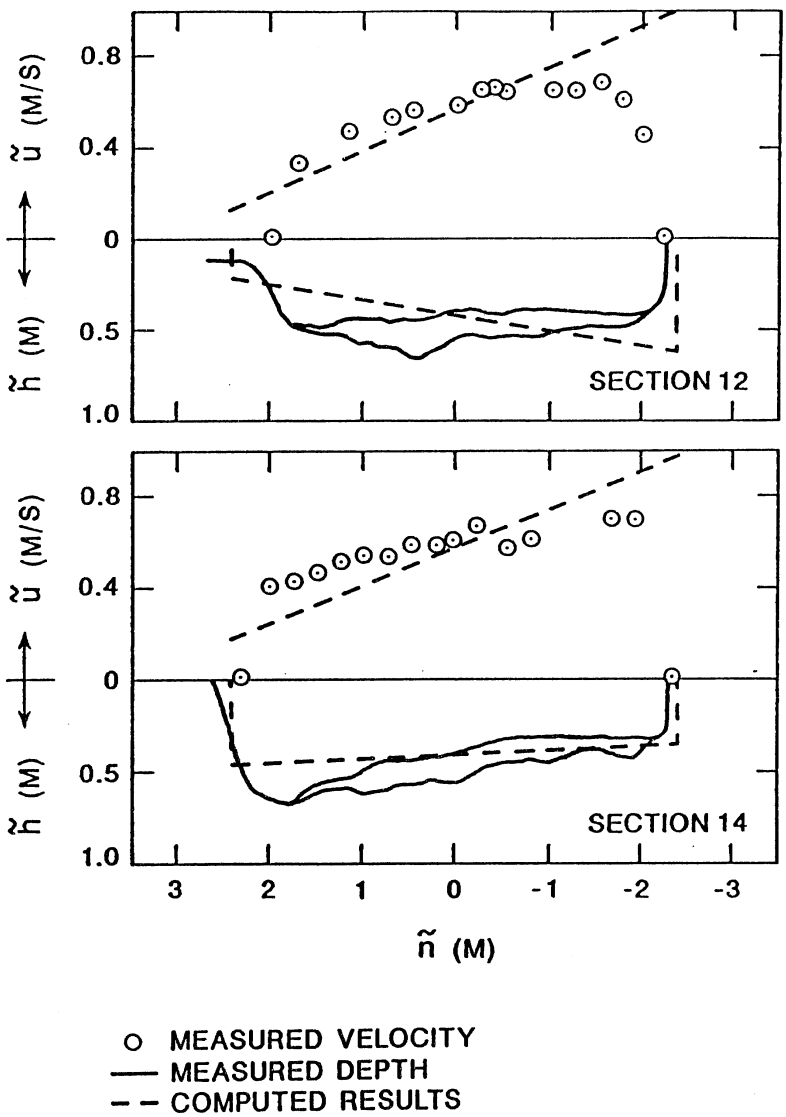

Fig. 5.10. Transverse distributions of depth and depth-averaged primary flow velocitiy as measured and predicted in the Muddy Creek study reach.

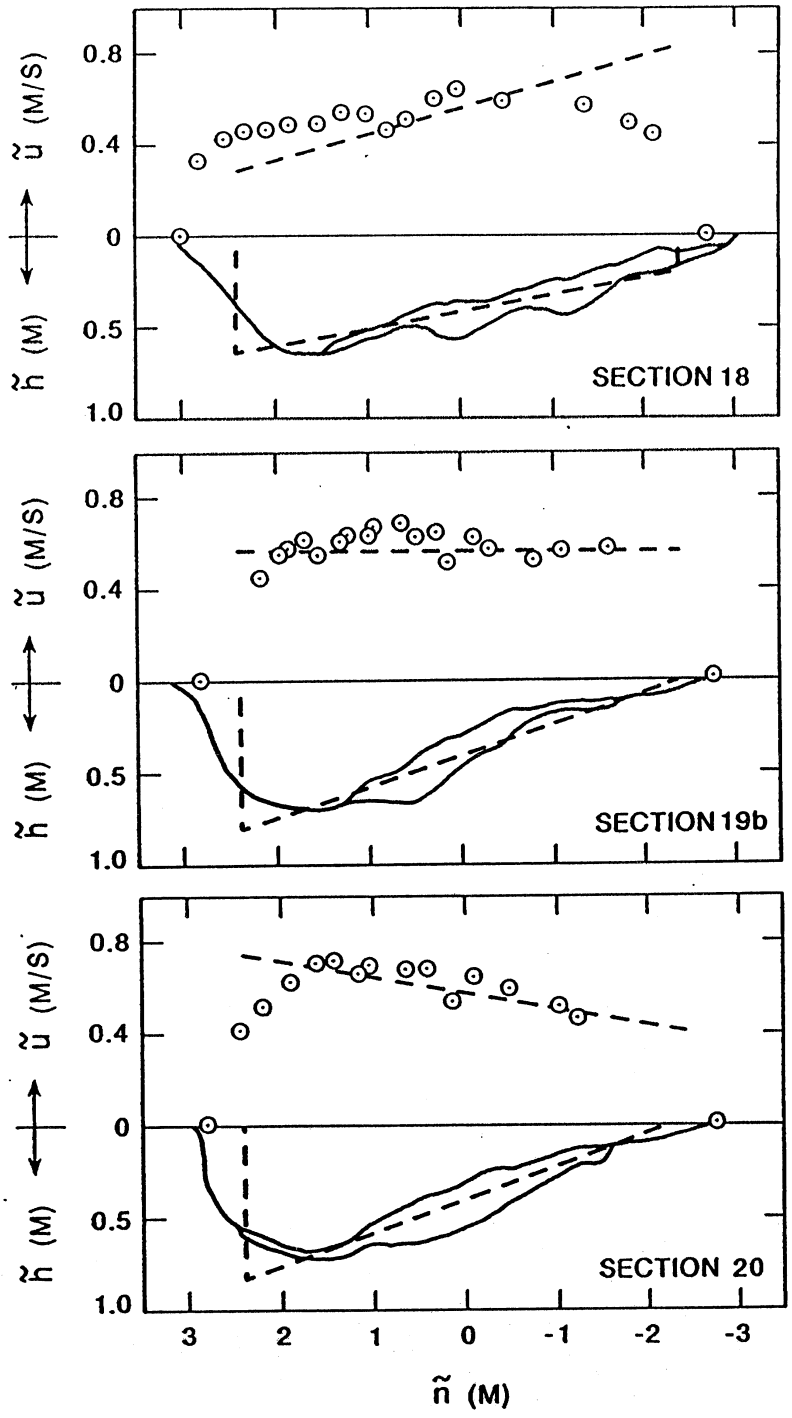

Fig. 5.10. Continued.

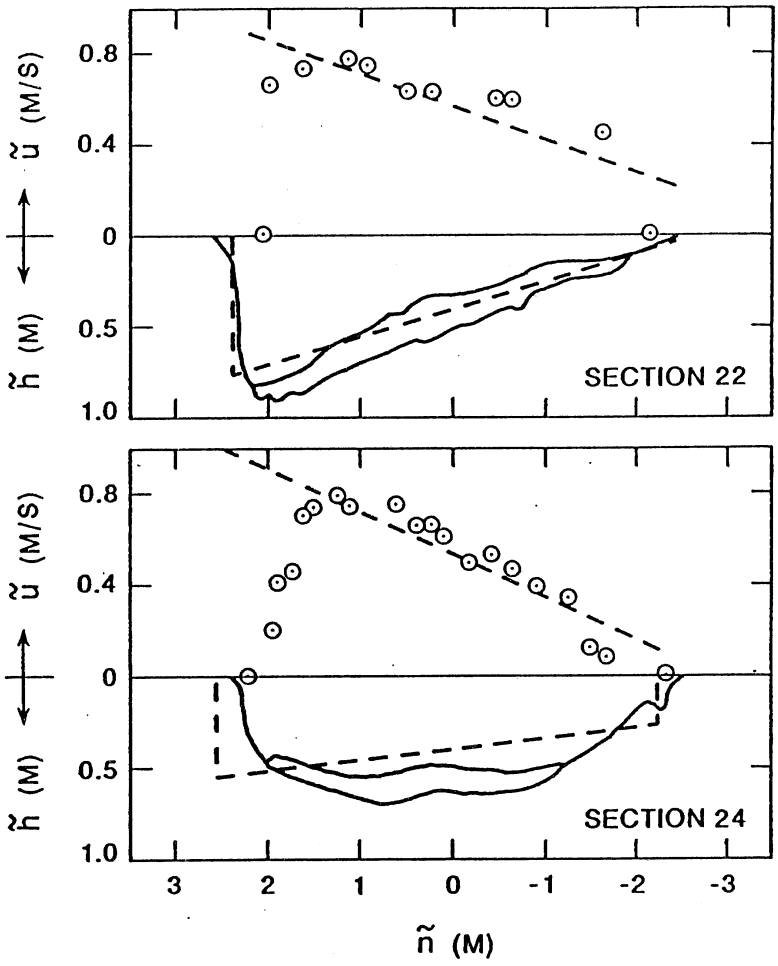

Fig. 5.10. Continued.

5.7 Conclusions

A model for calculation of flow field and bed topography in sinuous channels has been developed.

It is shown that the approach taken by Ikeda et al. (1981) according to which the bed topography in a sinuous channel is assumed to be given by the constant curvature solution is in general insufficient. The importance of the coupling between the flow field and the sediment transport in determining the bed topography is illustrated. This coupling is shown to give rise to resonant behavior for certain combinations of input variables. The theory compares well with the model of Blondeaux and Seminara (1985) which shows very similar resonant behavior. The origin of this resonance phenomena is explained in more detail in Chapter 6.

The model predicts satisfactorily the bed topography for channels with uniform sediment. For channels with highly non-uniform sediment, better results are obtained by setting $M = 0$ rather than using the value based on the mean particle grain size D_{50}. This is not totally unexpected, since the model does not take into account sorting of bedload in channel bends. By forcing M to be zero, a component of the model sensitive to sorting of the bedload is thrown out of it, which may easily be more appropriate than retaining it, for the case of non-uniform bedload: A more formal justification of this, however, would be desirable.

The model simulates satisfactorily both laboratory and field measurements.

6. RESONANCE AND ALTERNATE BARS

6.1 Introduction

Blondeaux and Seminara (1985) delineated the existence of the resonance phenomenon. Their conclusion was that for a certain combination of input variables, curvature forces a self-generated perturbation of alternate bar type. It may appear contradictory that the present model, which does not retain all of the terms of a full model of alternate bars, shows the same resonant behavior. In order to clarify this, and to further explain the origin of the phenomenon, a simple alternate bar stability analysis for a straight channel is performed using the present model.

6.2 Statement of the Problem

An expansion is introduced around the uniform flow solution, as was done in Eqs. 3.12 a through d. Herein, however, ψ_0 is no longer a measure of curvature amplitude but denotes some measure of straight-channel bed topography amplitude small enough for the linearization to be valid. The perturbations are considered to be periodic in the s - direction, with wavenumber k. The zeroth order solution is given again by Eqs. 3.13a,b,c. At $O(\psi_0)$, the governing equations are given by Eqs. 3.14a through d; therein, however, curvature σ and the secondary flow v_1 are taken to be zero, since the channel is straight. Alternate bars that change in time are to be considered. Thus the time-dependent term is added to the continuity equation of the sediment, but not to the other relations, in accordance with the quasisteady flow assumption. This gives

$$r u_1' + 2u_1 = - F^{-2} r \xi_1' + \xi_1 - \eta_1 \tag{6.1a}$$

$$F^{-2} \frac{\partial \xi_1}{\partial n} = 0 \tag{6.1b}$$

$$r u_1' + r h_1' + \frac{\partial v_1}{\partial n} = 0 \tag{6.1c}$$

$$\frac{\partial \eta_1}{\partial t} + \varepsilon Q_0 q_{s0} \left\{ r M u_1' + \frac{\partial}{\partial n} [v_1 - \Gamma \frac{\partial \eta_1}{\partial n}] \right\} = 0 \tag{6.1d}$$

The boundary conditions are, as before, given by

$$v_1 = q_{n1} = 0 \quad \text{at } n = \pm 1 \tag{6.2a,b}$$

Furthermore, it is required that the total discharge of water and the average river slope are unaffected by the perturbed quantities, to wit

$$\int_{-1}^{1}(u_1 + h_1)dn = 0 \quad ; \quad \int_{0}^{2\pi}\int_{-1}^{1}\xi_1' dn d\phi = 0 \qquad (6.3a,b)$$

6.3 Solution

In accordance with the boundary conditions (Eqs. 6.2a,b), the solution is assumed to take the following form

$$[\, u_1, \eta_1, \xi_1 \,] = [\, u_{1b}(\phi,t), \eta_{1b}(\phi,t), \xi_{1b}(\phi,t) \,] \begin{cases} \sin (m \frac{\pi}{2} n) & (m \text{ odd}) \\ \cos (m \frac{\pi}{2} n) & (m \text{ even}) \end{cases} \qquad (6.4a,b,c)$$

$$v_1 = v_m(\phi,t) \begin{cases} \cos (m \frac{\pi}{2} n) & (m \text{ odd}) \\ \sin (m \frac{\pi}{2} n) & (m \text{ even}) \end{cases} \qquad (6.4d)$$

where m = 1, 2, 3, ... determines the channel pattern (m = 1 for alternate bars, m > 1 for a braided channel), and the subscripts "b" and "m" denote "near-bank" and "middle", respectively. The assumed solution clearly satisfies the integral conditions given by Eqs. 6.3a,b.

Eq. 6.1b can be integrated to give

$$\xi_1 = \xi_1(\phi,t) \qquad (6.5)$$

which together with 6.4b reduces to

$$\xi_{1b} = 0 \qquad (6.6)$$

Substituting Eqs. 6.4a through d into Eqs. 6.1a through d and using Eq. 6.1c to eliminate v_1 , it is found that

$$r\, u_{1b}' + 2u_{1b} = -\eta_{1b} \qquad (6.7a)$$

$$\frac{\partial \eta_{1b}}{\partial t} + \varepsilon Q_0 q_{s0} [\, r (M - 1) u_{1b}' + r \eta_{1b}' + (m\frac{\pi}{2})^2 \Gamma \eta_{1b} \,] = 0 \qquad (6.7b)$$

If the unsteady term is neglected, the above result is identical to the homogeneous part of the F - Problem (Eqs. 5.52a,b).

The appropriate forms for u_{1b} and η_{1b} for a stability analysis are

$$[\, u_{1b}, \eta_{1b} \,] = [\, u_{10}, \eta_{10} \,]\, e^{\alpha t}\, [\, \sin(\phi - ct), \sin(\phi - ct - \Delta) \,] \qquad (6.8a,b)$$

Here α is the exponential growth rate, c is the wavespeed, Δ is the phase shift between the two perturbations, and u_{10} and η_{10} are O(1) coefficients. Note that instability requires that $\alpha > 0$. Direct substitution from Eqs. 6.8a,b into Eqs. 6.7a,b gives the following result for α and c:

$$\alpha = \varepsilon\, Q_0\, q_{s0}\, \frac{r^2}{r^2 + 4} [\, M - 1 - (m\tfrac{\pi}{2})^2\, \Gamma\, (1 + \frac{4}{r^2}) \,] \qquad (6.9a)$$

$$c = \varepsilon\, Q_0\, q_{s0}\, \frac{r}{r^2 + 4} [\, 6 - 2M + r^2 \,] \qquad (6.9b)$$

6.4 Discussion

It is apparent from Eq. 6.9a that m = 1 is always the most unstable mode, indicating that the simplified model can never predict braiding to be the dominant mode. In the following m will then be taken to be one, which is the appropriate choice for alternate bars.

It can be easily shown that if the resonance conditions given by Eqs. 5.55a,b are satisfied, it follows from Eqs. 6.9a,b that $\alpha = c = 0$. This confirms the conclusion of Blondeaux and Seminara (1985) that the resonance disturbances are steady and non-amplifying alternate bar perturbations forced by curvature.

It is of interest to see how far this simple bar instability analysis can be stretched. The amplification rate α (Eq. 6.9a) and the wavespeed c (Eq. 6.9b) are shown as a function of k for $\gamma = 15$ and 23.7 in Fig. 6.1a. The input variables have been selected so as to agree with those used by Colombini et al. (1987) to generate their Fig. 2 ($\tau^* = 0.3$, $D_{50}/H = 0.01$). Assuming upper regime flat bed, Eq. 2.12a gives $1/\sqrt{C_f} = 15.22$. The sediment transport formula of Meyer-Peter-Müller (Table A.3 in Appendix A) gives M = 3.56 if $\tau_c^* = 0.047$. Also note that β is taken to be 0.548 as predicted by Colombini et al. (1987) (whereas $\beta = 1.05$ if Eq. 2.14 is used). It is seen from Fig. 6.1a and from differentiation of Eq. 6.9a that $\alpha/(\varepsilon\, Q_0\, q_{s0})$ is a monotonic function in k for all γ. The model therefore cannot be used to predict the wavelengths of alternate bars. The model can, however, be used to predict whether or not alternate bars will form (Fig. 6.1b). A typical neutral curve ($\alpha = 0$) is shown in Fig. 6.1b, together with the result of Colombini et al. (1987). As seen from Fig. 6.1b, the present model gives surprisingly accurate results for low values of k and predicts accurately the critical value γ_c below which the channel is stable for all k. An expression for γ_c is obtained from Eq. 6.9a and the condition that $\alpha < 0$ for all r. This yields

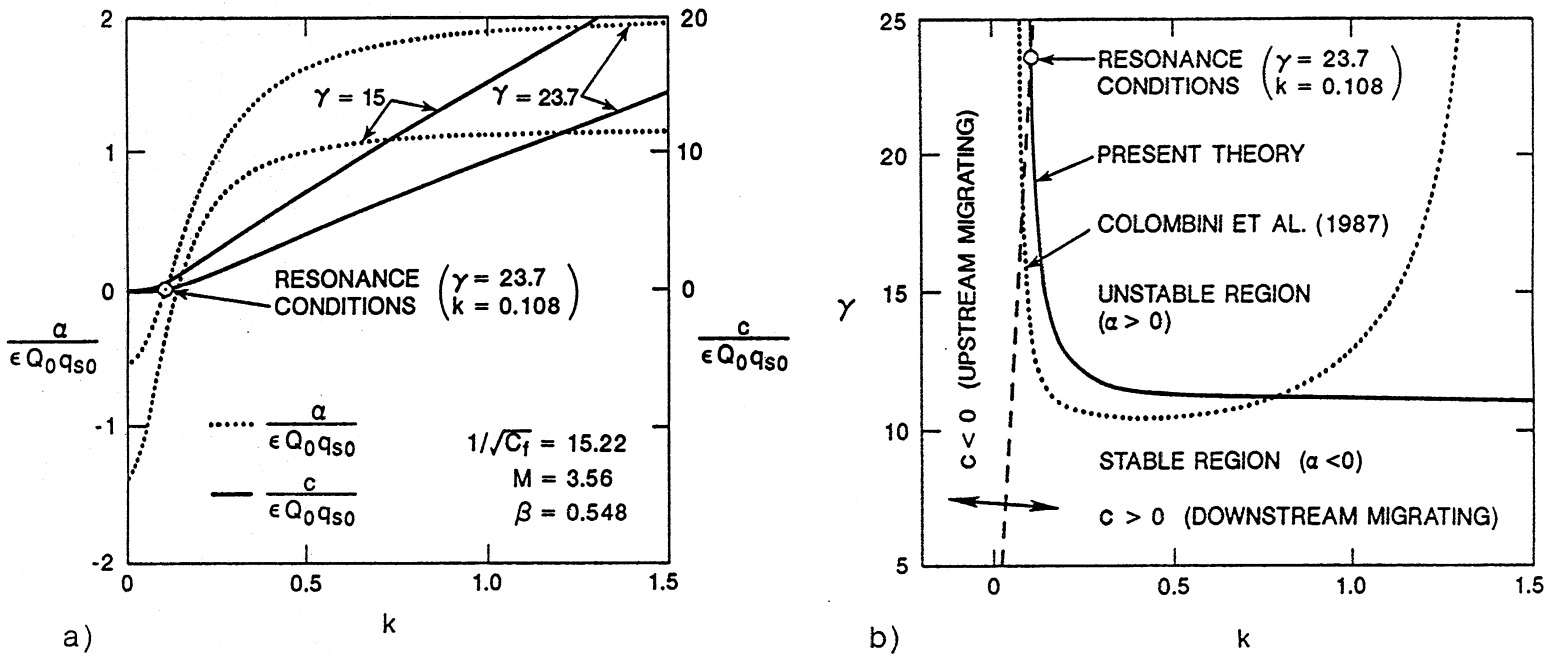

Fig. 6.1 a) Amplification rate and migration velocity as predicted by Eqs. 6.9a,b.

b) A typical neutral curve.

7. RESONANCE AND OVERDEEPENING

7.1 Introduction

Struiksma et al. (1985) observed that a significant part of the lateral bed slope in bends is often due to an "overshoot" effect induced by the redistribution of water and sediment in the upstream part of the bend. Both their experimental and theoretical findings indicate that the lateral bed slope at, or just downstream of, the entrance to a bend can be substantially higher than the slope obtained if the flow is assumed to be fully adapted to the bend curvature, as may be the case farther downstream. This phenomenon is called "overdeepening" herein. Overdeepening cannot be simulated using the model of Ikeda et al. (1981), since therein the transverse bed slope is assumed to be a function of only local channel curvature, rather than being calculated under the restriction imposed by the continuity equation of sediment transport.

Struiksma et al. (1985) explained overdeepening in terms of the wavelength and damping coefficient obtained from a linear analysis of the governing equations for the steady state case, and under the assumption of zero channel curvature. Herein, the present model is shown also to embody the elements necessary to encompass this phenomenon.

Further, it is shown that resonance (Chapters 5 and 6) and overdeepening are closely related phenomena, both arising from a bar-bend interaction reflecting the coupling between the flow field, the sediment transport, and the bed topography.

7.2 Overdeepening

Struiksma et al. (1985) explained overdeepening in terms of the wavelength and damping coefficient obtained from a linear analysis of the governing equations for the steady state case, and under the assumption of zero channel curvature. If the present model is used to carry out this analysis, the governing equations are the same as for the alternate bar analysis in Chapter 6, except that the unsteady terms are dropped. Dropping the unsteady terms in Eq. 6.7b and using Eq. 6.7a to eliminate η_{1b} from 6.7b, one gets

$$u_{1b}'' + \frac{1}{r}[3 - M + (\frac{\pi}{2})^2 \Gamma]\, u_{1b}' + 2(\frac{\pi}{2})^2 \frac{\Gamma}{r^2} u_{1b} = 0 \qquad (7.1)$$

where it has been assumed that the transverse structure of both u_1 and η_1 is proportional to $\sin(\frac{\pi}{2} n)$, as was done in the alternate bar analysis. Eq. 7.1 is seen to be identical to the homogeneous part of Eq. 5.54, which was used to explain the resonance phenomenon. The damping coefficient c_d and the wavenumber k_{res} are, as before, given by Eqs. 5.55a,b.

Defining the discriminant d of Eq. 7.1 to be

$$d = 4\,(\,c_d^2 - k_{res}^2/k^2\,) \qquad (7.2)$$

one gets the result that if $d < 0$ (negative discriminant) all solutions of Eq. 7.1 have the form

$$u_{1b} = \Lambda\, e^{-c_d \phi} \sin(\phi + \Delta) \tag{7.3}$$

where Λ and Δ are arbitrary coefficients that can be determined from boundary conditions. The wavenumber k is obtained from the condition that $(1/2)\sqrt{-d} = 1$. This, together with Eqs. 7.2 and Eq. 5.55b gives

$$\frac{k}{\varepsilon} = \frac{1}{2}\sqrt{-\left[\,3 - M + \left(\frac{\pi}{2}\right)^2 \Gamma\,\right]^2 + 8\left(\frac{\pi}{2}\right)^2 \Gamma} \tag{7.4a}$$

For the sake of completeness, the expression for the damping coefficient (Eq. 5.55a) may be written again as

$$\frac{c_d k}{\varepsilon} = \frac{1}{2}\left[3 - M + \left(\frac{\pi}{2}\right)^2 \Gamma\right] \tag{7.4b}$$

The relations for the wavenumber and the damping coefficient are shown in Fig. 7.1a,b as a function of Γ for the case M = 5. These are identical to the result obtained by Struiksma et al. (1985) for their simplified model, (Fig. 6 therein).

The similarity between the resonance phenomenon predicted by Blondeaux and Seminara (1985) and the overdeepening predicted by Struiksma et al. (1985) is now apparent. If the resonance conditions as given by Eqs. 5.55a,b are satisfied, the damping coefficient as given by Eq. 7.4b will be zero and the wavenumber as given by Eq. 7.4a will be equal to the resonant wavenumber.

7.3 Discussion and Conclusions

It is of importance to note that the overdeepening results solely from the F - Problem; if it is neglected, the predicted transverse bed slope in a constant curvature channel simply increases monotonically from zero at the bend entrance to its fully developed flow value at some distance farther downstream. The relation between overdeepening and resonance as discussed earlier can thus be easily tested with data. The measured wavelength of the overdeepening should approximately correspond to the wavelength of a steady damped disturbance, as given by Eq. 7.4a. If the damping coefficient c_d is small, the wavelength so computed should be about equal to the resonant wavelength, as given by Eq. 5.55b. Struiksma et al. (1985) estimated the wavelengths of the overdeepening for their Exp. T1, T2, and T3. The input data for these experiments is given in Table 4.2, and some calculated results are given in Table 4.3. The predicted wavelength (Eq. 7.4a) is shown to be very close to the estimated wavelength of the overdeepening (respective difference of 11%, 6%, and 3% for Exp. T1, T2, T3), as shown in Table 7.1. Furthermore, since the scaled damping coefficient squared $(2c_d k/\varepsilon)^2$ is substantially smaller than the scaled resonant wavenumber squared $(k_{res}/\varepsilon)^2 = 8(\pi/2)^2 \Gamma$ (e.g. Table 7.1) the estimated wavelength is also close to the resonant wavelength, as predicted by Eq. 5.55b (respective difference of 19%, 19%, and 9% for Exp. T1, T2, T3), as shown in Table 7.1. It should be emphasized that only for the case of zero damping does the resonant wavelength become equal to the wavelength of a steady disturbance (Eqs.

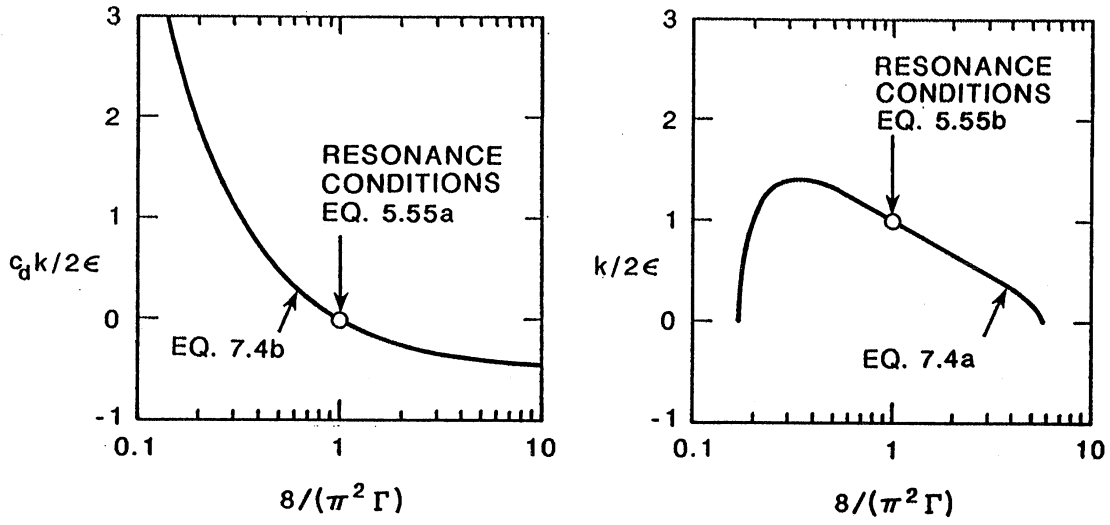

Fig. 7.1. a) Damping coefficient, and b) wavenumber of a steady perturbation of u_1 in a straight channel for the case of M = 5.

Table 7.1 - Wavelength of Overdeepening

Run Number	M Eq. 2.10a	$c_d k/\varepsilon$ Eq. 7.4b	$8(\frac{\pi}{2})^2 \Gamma$	$\tilde{\lambda}$ (m) meas.	$\tilde{\lambda}$ (m) Eq. 7.4a	$\tilde{\lambda}_{res}$ (m) Eq. 5.55b
Struiksma et al. (1985)						
T1	4.22	1.16	28.2	19.5	17.4	15.7
T2	4.23	2.17	44.5	19.5	20.6	15.7
T3	3.82	1.19	25.6	19.5	20.1	17.7

5.55b, 7.4a). Although that condition will rarely be exactly met, these calculations clearly show the close analogy between resonance and overdeepening.

8. SOLUTION FOR AN ARBITRARILY SHAPED CHANNEL

8.1 Introduction

All the components of the present model have already been developed in Chapters 4 and 5. It was illustrated in Chapters 5, 6, and 7 that the model does encompass both the resonance phenomenon of Blondeaux and Seminara (1985) and the overdeepening of Struiksma et al. (1985). What remains, then, is to generalize the results and make the model applicable to the case of a channel with arbitrary centerline curvature. Herein, this generalization is completed. The model is tested with both laboratory and field data; it gives substantially better results than the model of Ikeda et al. (1981).

8.2 Statement of the Problem

The treatment of the water-surface and the secondary flow (Eqs. 5.9, 5.11, 5.12) can be generalized to read

$$\xi_1 = F^2 \chi_{20} n \sigma(\phi) \tag{8.1}$$

and

$$\varepsilon \chi_1 v_1 = G_0(\zeta) \sigma_s(\phi) \tag{8.2a}$$

Here the function σ_s, which satisfies

$$r \frac{d\sigma_s}{d\phi} + \delta \sigma_s = \delta \sigma \tag{8.2b}$$

quantifies the strength of, and the phase shift in, the secondary flow due to changing curvature in a sinuous channel. In the above relation

$$\delta = \frac{\chi_1^2 \left(\chi + \frac{1}{4}\right)}{\frac{1}{12}\chi^2 + \frac{11}{360}\chi + \frac{1}{504}} \tag{8.2c}$$

For natural channels, the value of r/δ, and thus the phase shift between the secondary current strength and the channel curvature predicted by Eq. 8.2b,c, is typically rather modest, i.e. on the order of 10 degrees (Table 5.3). Thus σ_s does not deviate substantially from the local normalized dimensionless curvature σ in this case.

The solution for the bed profile η_1 is, as before, decomposed as

$$\eta_1 = \eta_{1C} + \eta_{1F} \tag{8.3}$$

where η_{1C} satisfies the portion of Eq. 3.14d that represents the direct effect of the secondary flow on the bed, i.e.

$$\eta_{1C} = - A\, n\, \sigma_s(\phi) \tag{8.4}$$

We likewise decompose as follows

$$u_1 = u_{1C} + u_{1F} \;\; ; \;\; h_1 = h_{1C} + h_{1F} \;\; ; \;\; v_1 = v_{1C} + v_{1F} \tag{8.5}$$

where u_{1C}, h_{1C}, and v_{1C} are terms generated directly by the bed topography, η_{1C}, and u_{1F}, h_{1F}, and v_{1F} are extra terms, needed to satisfy sediment continuity. Substituting into Eqs. 3.14a,c,d, and making use of Eqs. 8.1 and 8.2a, the problem is decomposed to:

C - Problem:

$$h_{1C} = [\, F^2 \chi_{20}\, \sigma + A\, \sigma_s(\phi)\,]\, n \tag{8.6a}$$

$$r\frac{\partial u_{1C}}{\partial \phi} + 2u_{1C} = n\,[\, - r\,\chi_{20}\frac{\partial \sigma}{\partial \phi} + \sigma\,(F^2\chi_{20} - 1)\,] + \sigma_s(\phi)\,[\, A\, n - \frac{1}{\varepsilon^2 \chi_1}\frac{\partial}{\partial n}\int_0^1 TG_0(\zeta)d\zeta\,] \tag{8.6b}$$

$$v_{1C} = - r \int_{-1}^{n} \frac{\partial}{\partial \phi}(u_{1C} + h_{1C})dn \tag{8.6c}$$

The boundary conditions on v_{1C} (Eq. 3.15a) and u_{1C} (Eq. 3.18a) are:

$$v_{1C}\,|_{n=\pm 1} = 0 \;\; ; \;\; u_{1C}\,|_{n=0} = 0 \tag{8.7a,b}$$

F - Problem:

$$r\frac{\partial u_{1F}}{\partial \phi} + 2u_{1F} = - \eta_{1F} \tag{8.8a}$$

$$\frac{\partial v_{1F}}{\partial n} = - r\,(\frac{\partial u_{1F}}{\partial \phi} + \frac{\partial h_{1F}}{\partial \phi}) \tag{8.8b}$$

$$r\,M\frac{\partial u_{1F}}{\partial \phi} + \frac{\partial v_{1F}}{\partial n} - \Gamma\frac{\partial^2 \eta_{1F}}{\partial n^2} = - r\,M\frac{\partial u_{1C}}{\partial n} - \frac{\partial v_{1C}}{\partial n} \tag{8.8c}$$

The above three equations can be reduced to

$$r\frac{\partial u_{1F}}{\partial \phi} + 2u_{1F} = -\eta_{1F} \tag{8.9a}$$

$$r(M-1)\frac{\partial u_{1F}}{\partial \phi} + \frac{\partial \eta_{1F}}{\partial \phi} - \Gamma\frac{\partial^2 \eta_{1F}}{\partial n^2} = -r(M-1)\frac{\partial u_{1C}}{\partial \phi} + r\frac{\partial h_{1C}}{\partial \phi} \tag{8.9b}$$

The boundary conditions on v_{1F} (Eq. 3.15a), η_{1F} (Eqs. 3.15b, 3.14d, and 3.18c), and u_{1F} (Eq. 3.18a) are:

$$v_{1F}\big|_{n=\pm 1} = 0 \;\; ; \;\; \frac{\partial \eta_{1F}}{\partial n}\Big|_{n=\pm 1} = 0 \tag{8.10a,b}$$

$$\eta_{1F}\big|_{n=0} = 0 \;\; ; \;\; u_{1F}\big|_{n=0} = 0 \tag{8.10c,d}$$

Once the solution to the C - Problem is obtained, the F - Problem, (Eqs. 8.9a,b together with the boundary conditions given by Eqs. 8.10a,b,c,d), becomes fully defined.

8.3 Solution of the C - Problem

Eqs. 8.1, 8.2a,b, and 8.4 give the following solution for the water-surface, secondary flow, and the bed topography

$$\xi_1 = F^2 \chi_{20}\, n\, \sigma \tag{8.11}$$

$$\varepsilon\chi_1 \upsilon_1 = G_0(\zeta)\, \sigma_s(\phi) \tag{8.12}$$

$$\eta_{1C} = -A\, n\, \sigma_s(\phi) \tag{8.13}$$

where

$$\sigma_s(\phi) = \sigma_s(0)\, e^{-(\delta/r)\phi} + \frac{\delta}{r} e^{-(\delta/r)\phi} \int_0^{\phi} e^{(\delta/r)\phi'} \sigma(\phi')\, d\phi' \tag{8.14}$$

Using again the "moment method", as done for the constant curvature case, Eq. 8.6b is reduced to

$$r\frac{\partial u_{1Cb}}{\partial \phi} + 2u_{1Cb} = -r\chi_{20}\frac{\partial \sigma}{\partial \phi} + \sigma(F^2\chi_{20} - 1) + (A + A_s)\,\sigma_s(\phi) \tag{8.15}$$

where u_{1Cb} is the value of u_{1C} at n = 1. The solution of Eq. 8.15 is

$$u_{1Cb} = [u_{1Cb}(0) + \chi_{20}\,\sigma(0)]\,e^{-2\phi/r} - \chi_{20}\,\sigma(\phi)$$

$$+\frac{1}{r}[\chi_{20}\,(F^2+2) - 1]\,e^{-2\phi/r}\int_0^{\phi}\sigma(\phi')e^{2\phi'/r}d\phi' + \frac{1}{r}(A + A_s)\,e^{-2\phi/r}\int_0^{\phi}\sigma_s(\phi')e^{2\phi'/r}d\phi' \quad (8.16)$$

8.4 Solution of the F - Problem

Using again the "moment method", as done for the F - Problem of the sine-generated channel, Eqs. 8.9a,b are reduced to

$$r\frac{\partial u_{1Fb}}{\partial\phi} + 2u_{1Fb} = -\eta_{1Fb} \quad (8.17a)$$

$$r\,(M-1)\frac{\partial u_{1Fb}}{\partial\phi} + r\frac{\partial\eta_{1Fb}}{\partial\phi} + (\frac{\pi}{2})^2\,\Gamma\,\eta_{1Fb} = -\,r\,(M-1)\frac{\partial u_{1Cb}}{\partial\phi} + r\frac{\partial h_{1Cb}}{\partial\phi} \quad (8.17b)$$

Using Eq. 8.17a to eliminate η_{1Fb} from Eq. 8.17b gives

$$\frac{\partial^2 u_{1Fb}}{\partial\phi^2} + \frac{1}{r}[\,3 - M + (\frac{\pi}{2})^2\,\Gamma\,]\frac{\partial u_{1Fb}}{\partial\phi} + 2(\frac{\pi}{2})^2\frac{\Gamma}{r^2}u_{1Fb} = \frac{1}{r}(M-1)\frac{\partial u_{1Cb}}{\partial\phi} - \frac{1}{r}\frac{\partial h_{1Cb}}{\partial\phi} \quad (8.18)$$

Defining new variables Y_1 and Y_2 to be

$$Y_1 = u_{1Fb} \;\;;\;\; Y_2 = \frac{\partial u_{1Fb}}{\partial\phi} \quad (8.19a,b)$$

a set of equations, equivalent to Eq. 8.18, can be written as

$$\frac{\partial Y_1}{\partial\phi} = Y_2 \quad (8.20a)$$

$$\frac{\partial Y_2}{\partial\phi} = -\frac{1}{r}[\,3 - M + (\frac{\pi}{2})^2\,\Gamma\,]\,Y_2 - 2(\frac{\pi}{2})^2\frac{\Gamma}{r^2}Y_1 + \frac{1}{r}(M-1)\frac{\partial u_{1Cb}}{\partial\phi} - \frac{1}{r}\frac{\partial h_{1Cb}}{\partial\phi} \quad (8.20b)$$

Eqs. 8.20a,b are solved with the IMSL subroutine DVERK, which uses the Runge Kutta - Verner fifth and sixth order methods. The boundary conditions used are

$$Y_1(0) = u_{1Fb}(0) \quad (8.21a)$$

$$Y_2(0) = \frac{\partial u_{1Fb}(0)}{\partial \phi} \tag{8.21b}$$

Note that from Eqs. 8.17a and 8.21a,b it is seen that setting $Y_1(0) = Y_2(0) = 0$ corresponds to selecting $u_{1Fb}(0) = \eta_{1Fb}(0) = 0$, which often is the appropriate choice, (e.g. if the upstream end of the study reach is at the downstream end of a straight portion of the river channel).

Having solved Eqs. 8.20a,b, for Y_1 and Y_2, u_{1Fb} and η_{1Fb} are determined as follows

$$u_{1Fb} = Y_1 \tag{8.22a}$$

$$\eta_{1Fb} = - r Y_2 - 2 Y_1 \tag{8.22b}$$

8.5 Comparison with Data

Since the model presented in this chapter is a direct generalization of the results developed in Chapters 4 and 5, it needs no further discussion. Before comparing it with data it is helpful to summarize what data the model needs as input and how the dependent variables are calculated.

Input Data:

1) U, H, I, b, $\tilde{C}(\tilde{s})$.
2) D_{50} and R if the channel has an erodible bed.
3) $u_{1Cb}(0)$, $\eta_{1Cb}(0)$, $\sigma_s(0)$, $u_{1Fb}(0)$, $\eta_{1Fb}(0)$.

Calculation Procedure:

1) C_f (Eq. 2.27a) ; F and ε (Eq. 2.28c) ; $\alpha = 0.077$; χ_1 (Eq. 2.25) ; χ (Eq. 2.21b) ; χ_{20} (Eq. 4.7) ; A_s (Eq. 4.21) ;
2) τ_C^* (Shields Diagram, Vanoni, 1977, Fig. 2.43) ; τ^* (Eq. 2.11) ; τ_G^* (Eq.2.12) ; M (Eq. 2.10) ; β (Eq. 2.14) ; A (Eq. 4.13) ;
3) ξ_1 (Eq. 8.11) ; δ (Eq. 8.2c) ; $\sigma_s(\phi)$ (Eq. 8.14) ; η_{1C} (Eq. 8.13) ; u_{1Cb} (Eq. 8.16) ; Y_1 and Y_2 (Eqs. 8.20 a,b) ; u_{1Fb} (Eq. 8.22a) ; η_{1Fb} (Eq. 8.22b).

The input data for all the experiments and the one field study simulated is summarized in Table 8.1. Some calculated results are shown in Table 8.2.

The experimental data taken by Rozovskii (1961) is ideally suited for validating the solution to the C - Problem. The F - Problem does not contribute since the channel had a

transversely horizontal (A = 0), non-erodible bed (M = 0). Rozovskii's channel (Exp. No. 1) consisted of a 180° degree bend with straight inlet and outlet reaches. The half-width of the channel was b = 0.4 meters, and the radius of the channel centerline was $\tilde{r} = 0.8$ meters for the circular reach. The assumption that $\psi_0 = b/\tilde{r}_m = 0.5$ must be considerably less than one is, therefore not very well satisfied. This experiment was successfully simulated by Leschizner and Rodi (1979) using the k-ε turbulence model.

The measured difference between the water-surface elevations at the inner and outer banks, together with the calculated results, (Eq. 8.11) are shown in Fig. 8.1a. The agreement is good, and the assumption that the transverse slope of the water-surface is mainly determined by the local channel curvature seems to hold.

The overall strength of the secondary flow is given by $\sigma_s(\phi)$. This parameter can be calculated from data using the following result, obtained from Eq. 8.2a;

$$\sigma_s(\phi) = \varepsilon\chi_1 \frac{\int_0^1 |v_1(\zeta)| d\zeta}{\int_0^1 |G_0(\zeta)| d\zeta} \tag{8.23}$$

Here $v_1(\zeta)$ is the measured velocity profile of the secondary flow at the channel centerline. The values for $\sigma_s(\phi)$ calculated from measurements are shown in Fig. 8.1b together with the predicted values obtained via Eq. 8.14. The agreement is good, although the predicted profile is shifted slightly downstream relative to the measured profile.

The measured difference between the depth-averaged primary flow velocities at the inner and the outer bank, obtained by fitting a straight line through the measurements at each cross-section, is shown in Fig. 8.2 together with the values calculated from Eq. 8.16. The agreement is seen to be very good except for the last measurement. Eq. 8.16 gives much better results than the model of Ikeda et al. (1981). The importance of the convective transport of primary flow momentum by the secondary flow is obvious, since if neglected ($A_s = 0$) the results are clearly not satisfactory. The discontinuities in the predicted velocities are of no concern. They are due to the the discontinuities in the channel curvature, and can be eliminated (Fig. 8.2) if the measured water-surface is used as an input in Eq. 8.16 rather than the predicted water-surface (Eq. 8.11).

The measured and predicted (Eq. 8.16) depth-averaged primary flow velocity profiles are shown in Fig. 8.3. Again, the agreement is very satisfactory.

The experiments of Struiksma et al. (1985), Exp. T1, T2, T3, were more complicated than Exp. 1 of Rozovskii (1961), since the bed was erodible. The channel consisted of a 140° bend, and straight inlet and outlet reaches. The half-width of the channel was b = 0.75 meters, and the radius of the channel centerline was $\tilde{r} = 12.0$ meters for the circular reach. The assumption that $\psi_0 = b/\tilde{r}_m = 0.0625$ must be considerably less than one is therefore satisfied.

The measured and predicted bed topography is compared in Fig. 8.4. The agreement is excellent considering that no calibration is performed. The computed longitudinal bed profiles are very similar to the computed results of Struiksma et al. (1985).

Their model, however, uses two calibration coefficients which took the same values for Exp. T1 and T2, but different values for Exp. T3.

It is apparent, both from the measured and the computed bed topography, Fig. 8.4, that a substantial part of the lateral bed slope in the upstream part of the bend is due to redistribution of water and sediment in the first part of the bend (the F - Problem), as concluded by Struiksma et al. (1985). The transverse bed slope cannot, therefore, be predicted solely from local conditions. In the downstream part of the bend, the flow has adjusted to the curvature, and thus approaches the solution for the constant curvature case, (Chapter 4).

In Fig. 8.4, the measured and computed depth-averaged primary flow velocities, are compared. The results are satisfactory, especially considering that any error in the bed topography simulation introduces error in the prediction of the velocity, and vice versa.

Finally, the model is used to simulate the measured results of Thorne et al. (1985) taken in two consecutive bends of the Fall River. The measurements were taken at bankfull stage, $Q = 1.73\ m^3/s$. A plan view of the Fall River study reach is shown in Fig. 8.5a. For the numerical calculation the study reach is divided, as done by Odgaard (1986b), into five reaches of constant curvature, (reach 1; $\tilde{r} = 52$ meters: reach 2, $\tilde{r} = 11$ meters: reach 3; $\tilde{r} = \infty$: reach 4; $\tilde{r} = -11$ meters: reach 5; $\tilde{r} = \infty$), as shown in Fig. 8.5b. The application of the model is not restricted to constant curvature reaches, and the simulation could as well have been carried out with smoothly varying curvature.

In Fig. 8.7, the centerline water-surface elevation, channel width, and mean depth are shown as functions of location along the channel centerline. As seen in Fig. 8.7, the water-surface slope is found to be fairly constant, as assumed in the theoretical model at first order. The channel width, however, varies from 7.2 meters at Section 2 to 13.2 meters at Section 8. The mean depth varies from 0.47 meters at Section 8 to 0.93 meters at Section 0. In the theoretical model the width and the mean depth are assumed to be constant and equal to $2b = 9.4$ meters and $H = 0.75$ meters. The assumption that $\psi_0 = b/\tilde{r}_m = 4.7/11 = 0.43$ must be considerably less than one is therefore not very well satisfied.

As, before, for data sets with highly non-uniform sediment grain size distribution, M is taken to be zero instead of the calculated value of 5.16. If the calculated value is used for M, the model will overpredict the scour for these bends. A possible reason for this is that the model does not account for sorting of the bedload, as discussed in Chapter 5.6. It is clear from Fig. 8.6 that the coarser sediment tends to be collected in the deepest ares and the bed may even be partially armored in the pool at Section No. 7.

In Fig. 8.8 the measured and predicted distributions of depth and depth-averaged primary flow velocity are shown. The agreement is good, especially considering the variation in width and mean depth, not accounted for in the model. The upstream boundary conditions were selected to be: $u_{1Cb}(0)\ \psi_0 = -0.62$, $\eta_{1Cb}(0)\ \psi_0 = -0.47$, $\sigma_s(0)\ \psi_0 = 0.14$, $u_{1Fb}(0) = 0.$, $\eta_{1Fb}(0) = 0$. This choice reproduces, as accurately as possible, the measured values of u_1 and η_1 at Section 0. The model reproduces the transverse bed slope except at the downstream end of the study reach, i.e. Sections 7 and 8, where both the width and the mean depth go through rapid changes. The transverse variation of the depth-averaged primary flow velocity is also reproduced rather well, except at Section 5, since the model predicts the crossing of the high velocity from the left bank to the right bank to be slightly upstream of the measured location.

Table 8.1 - Arbitrarily Shaped Channels: Flow Conditions

Run Number	b (m)	$\tilde{r}_m$ (m)	Q (l/s)	H (m)	U (m/s)	I	D_{50} (mm)	σ_g	R
Rozovskii (1961)									
1	0.40	0.8	12.3	0.060	0.256	Not given	Flat bed	Flat bed	Flat bed
Struiksma et al. (1985)									
T1	0.75	12	47	0.080	0.392	$2.36 \cdot 10^{-3}$	0.45	1.19	1.65
T2	''	''	61	0.100	0.407	$2.03 \cdot 10^{-3}$	''	''	''
T3	''	''	74	0.091	0.542	$4.19 \cdot 10^{-3}$	''	''	''
Thorne et al. (1985)									
Fall River	4.7	11	4000	0.75	0.57	$2.15 \cdot 10^{-3}$	1.1	2.1	1.65

Table 8.2 - Arbitrarily Shaped Channels: Calculated Results

Run Number	F	C_f	A_s	Flow Regime	A calc.	M
Rozovskii (1961)						
1	0.33	$2.72 \cdot 10^{-3}$	9.88	Flat bed	0.00	0.00
Struiksma et al. (1985)						
T1	0.44	$12.1 \cdot 10^{-3}$	1.85	lower regime dunes	4.61	4.22
T2	0.41	$12.0 \cdot 10^{-3}$	2.90	''	4.58	4.23
T3	0.57	$12.7 \cdot 10^{-3}$	2.30	''	6.21	3.82
Thorne et al. (1985)						
Fall River	0.21	$48.7 \cdot 10^{-3}$	1.05	''	3.35	5.16

* Estimated by Rozovskii (1961). (Eq. 2.27a was not used since I not given).

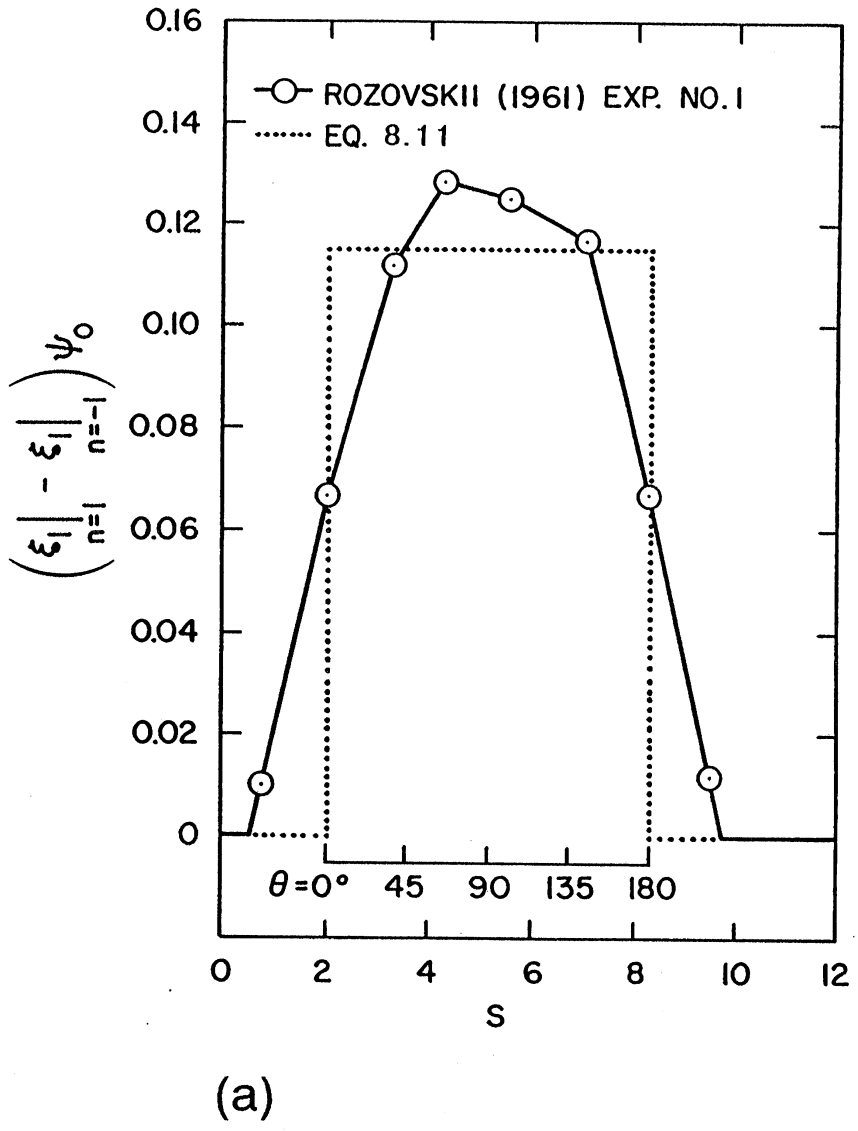

Fig. 8.1a. Difference between the water-surface elevations at the outer and the inner bank.

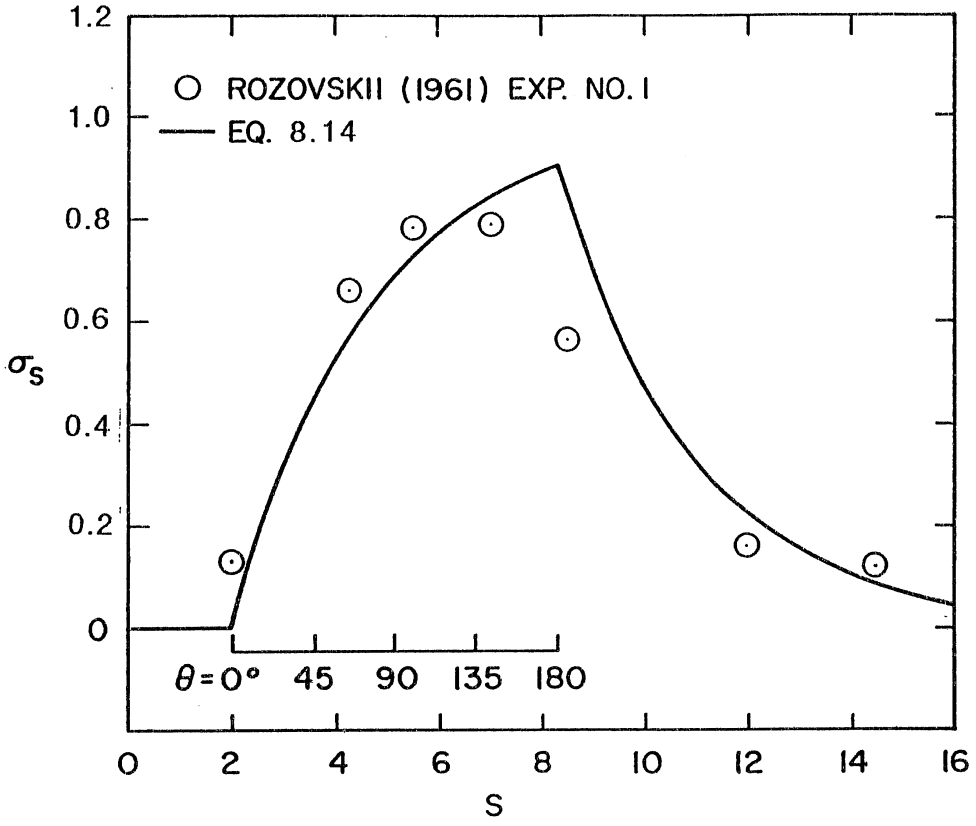

(b)

Fig. 8.1b. Strength of the secondary flow, $\sigma_s(s)$.

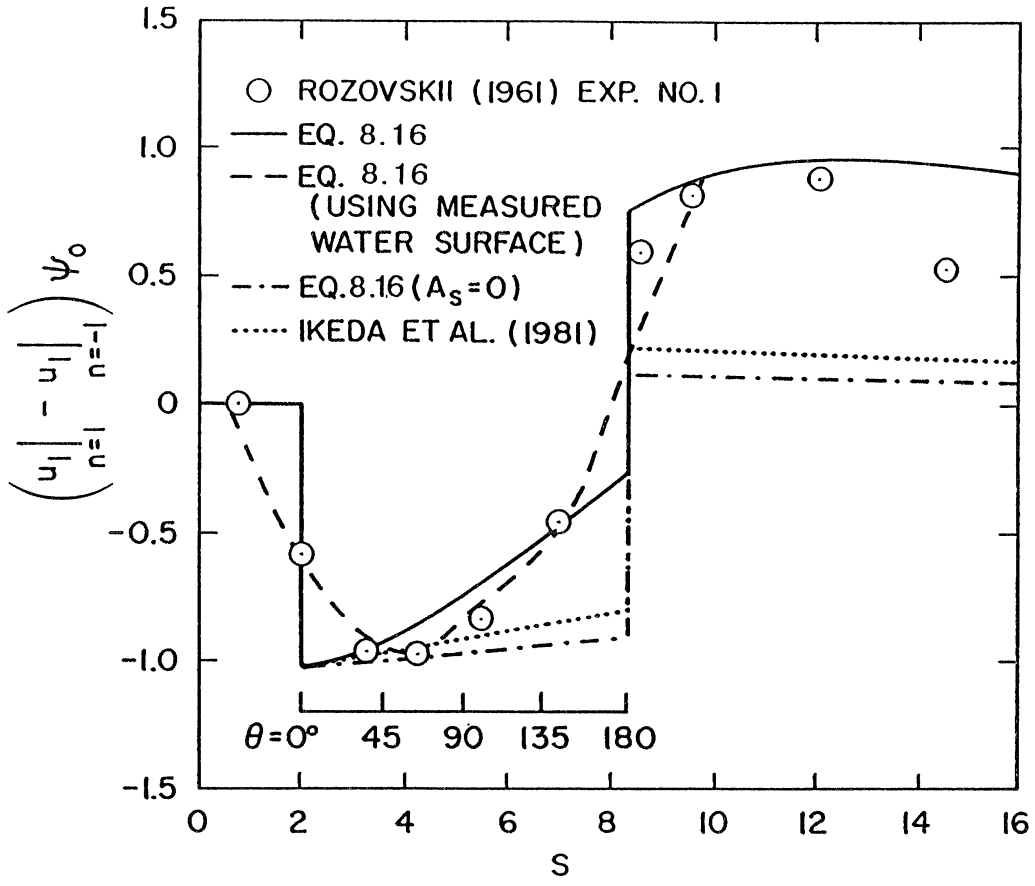

Fig. 8.2. Difference between the depth-averaged primary flow velocities at the outer and the inner bank as measured by Rozovskii (1961) and predicted by various theories.

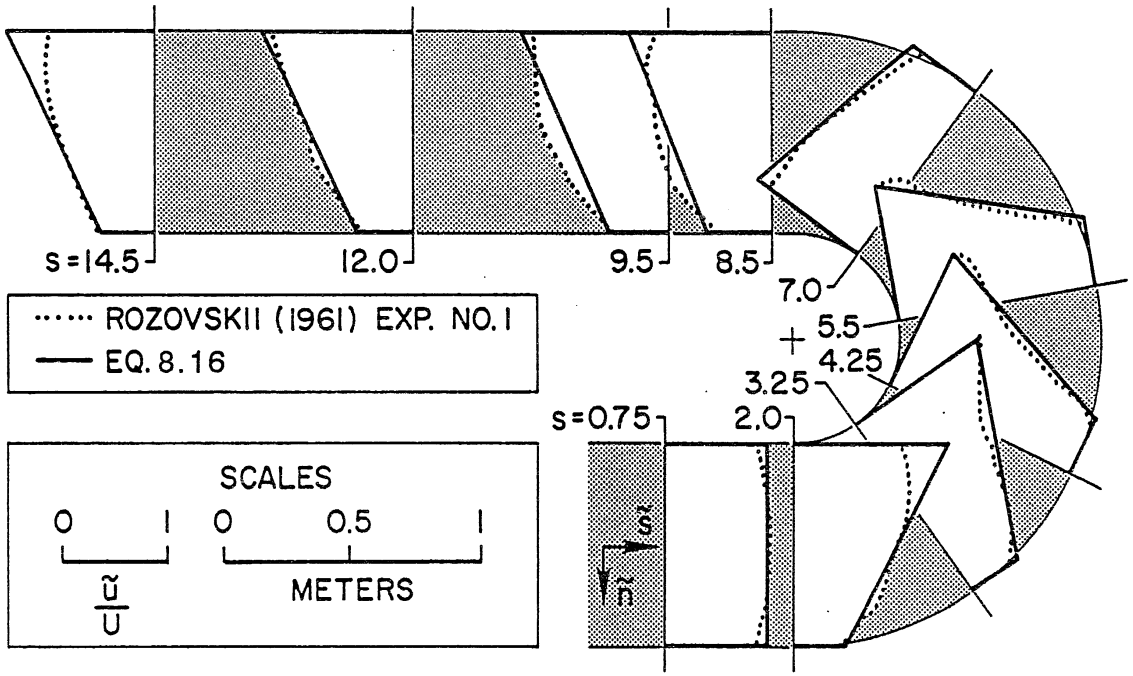

Fig. 8.3. Profiles of depth-averaged primary flow velocity.

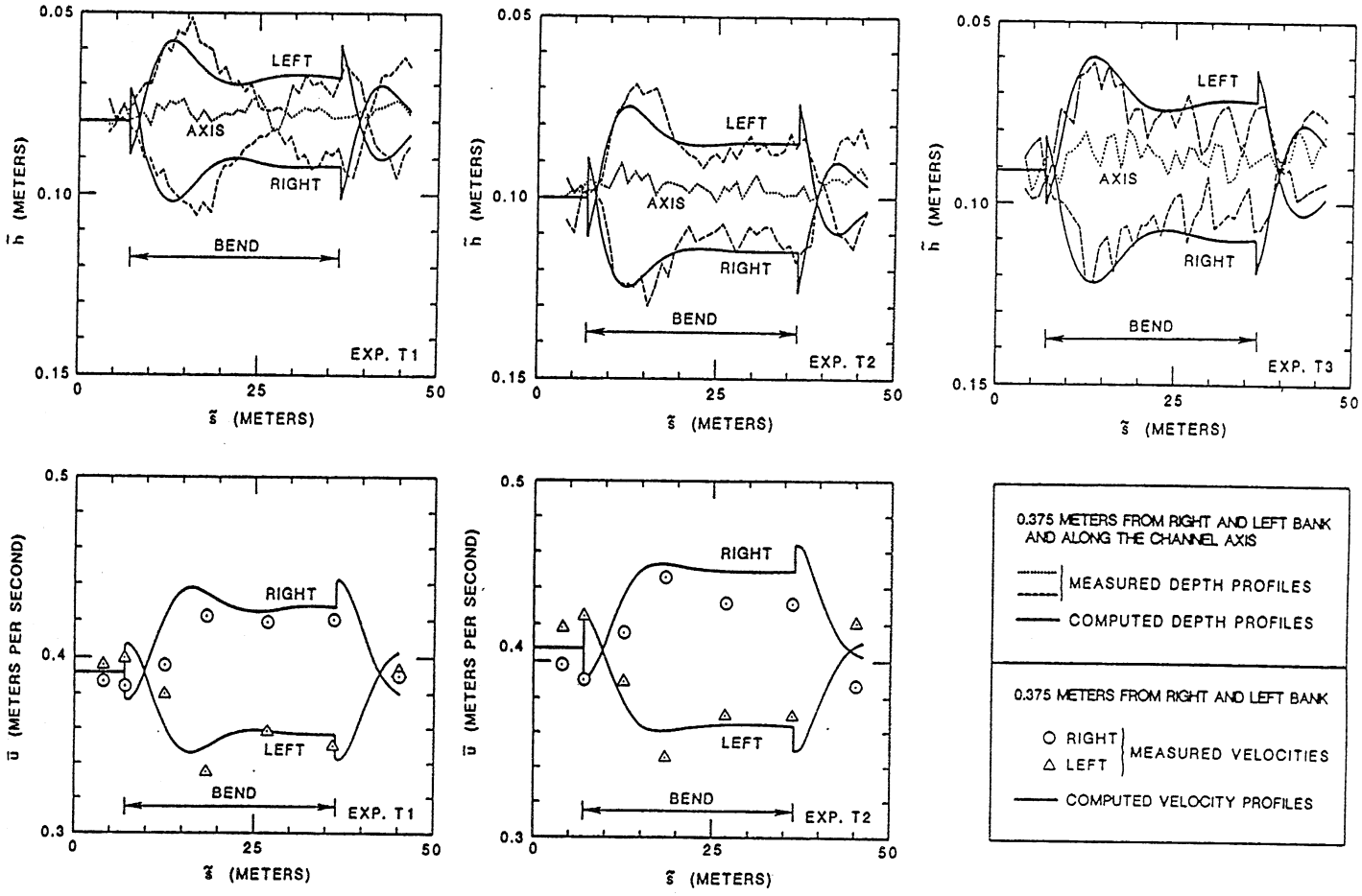

Fig. 8.4. Longitudinal variation in depth, $\tilde{h}$, and depth-averaged primary flow velocity, $\tilde{u}$, as measured by Struiksma et al. (1981) and predicted by the proposed model.

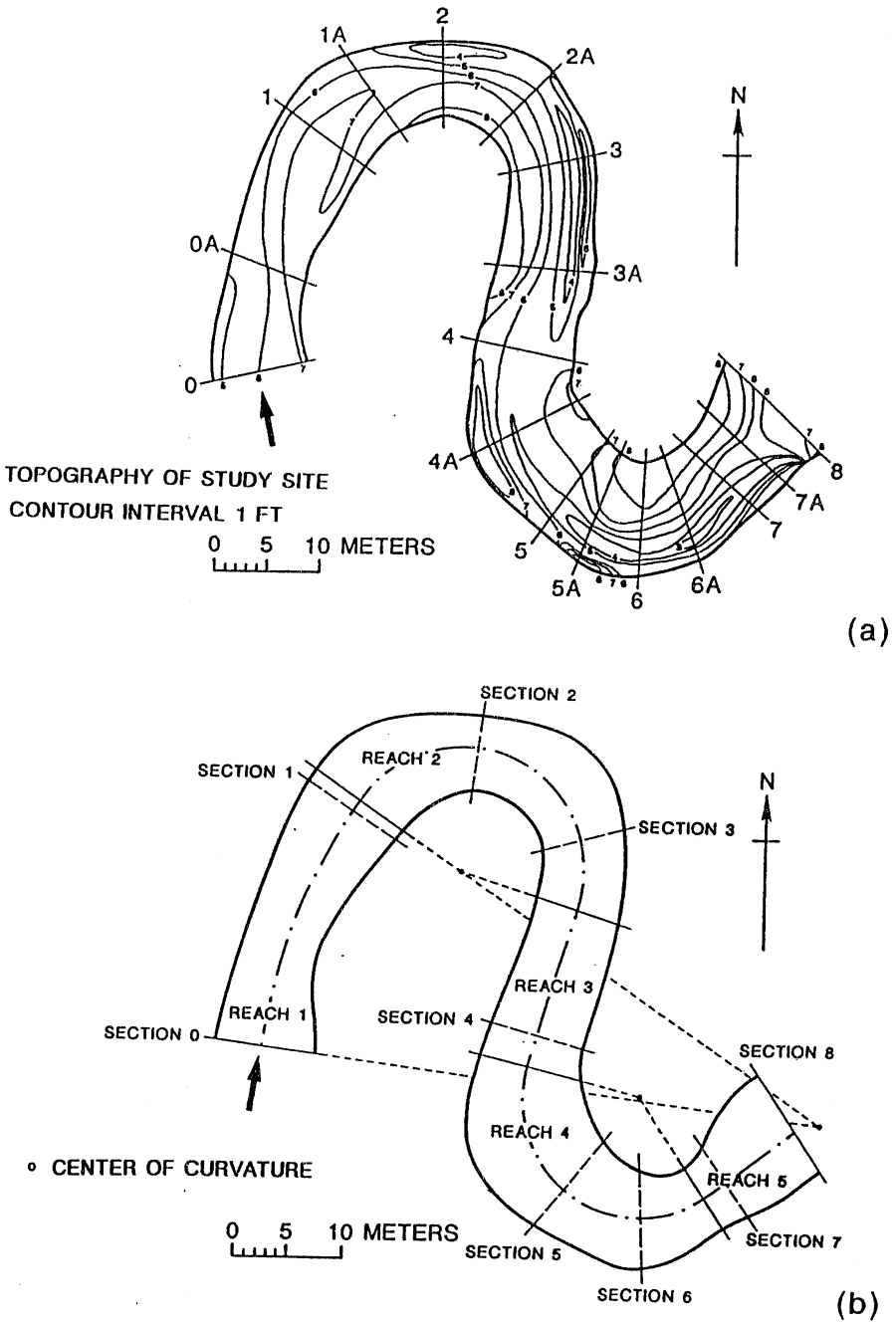

Fig. 8.5. a) Plan view of the Fall River study reach.

b) Discretization of the study reach into reaches of constant curvature (from Odgaard (1986b)).

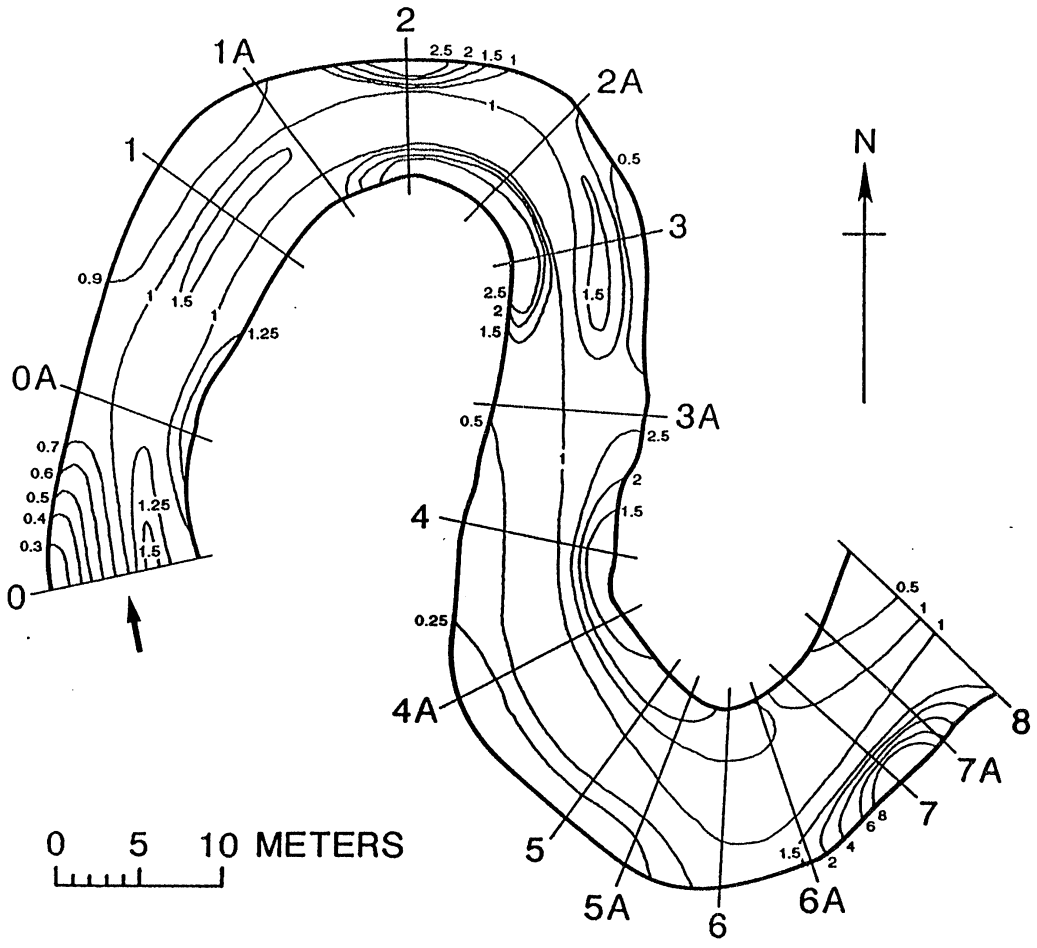

Fig. 8.6. Distribution of median bed material size (mm) in the Fall River study reach.

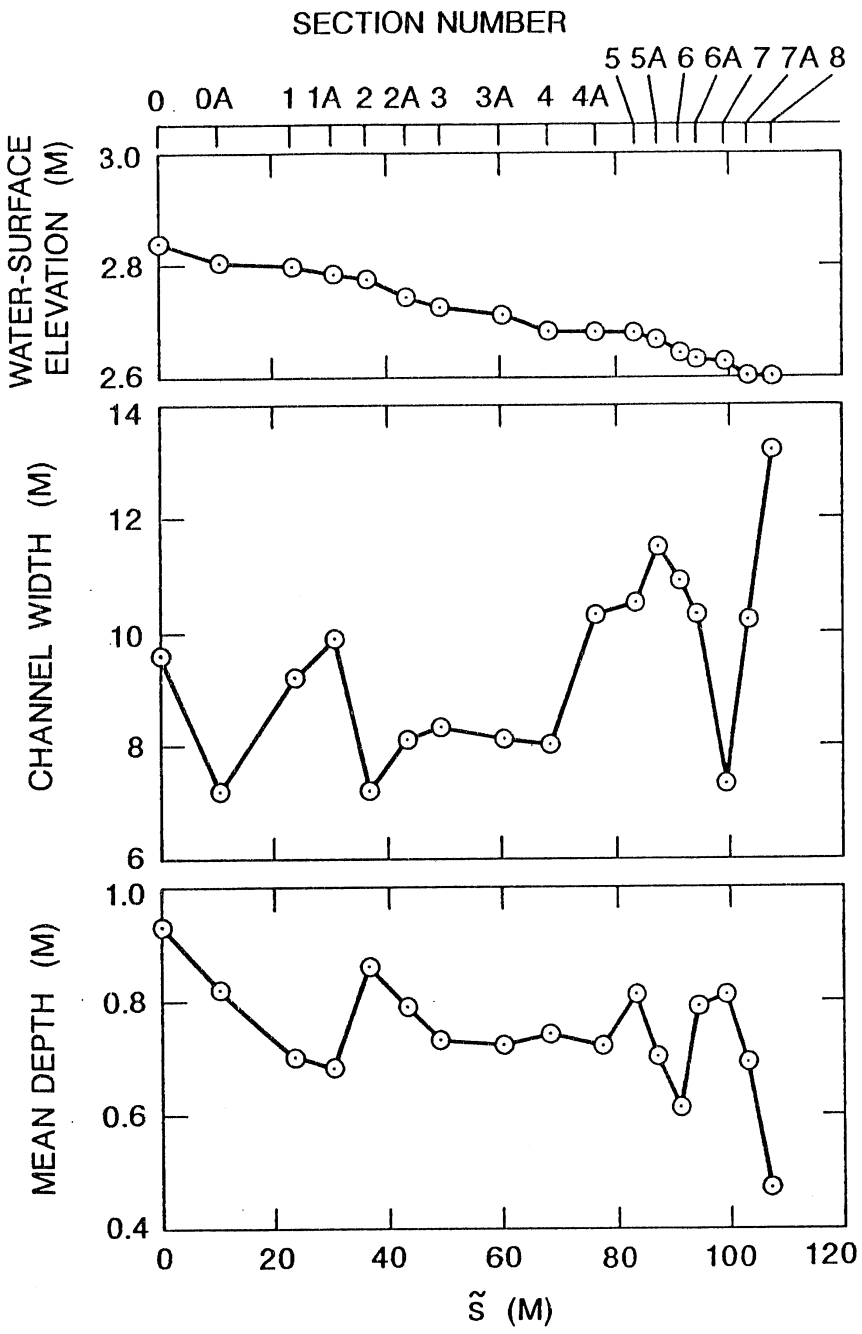

Fig. 8.7. Variation in centerline water-surface elevation, channel width, and mean depth as a function of location along the channel centerline for a discharge of 4.0 m^3/sec.

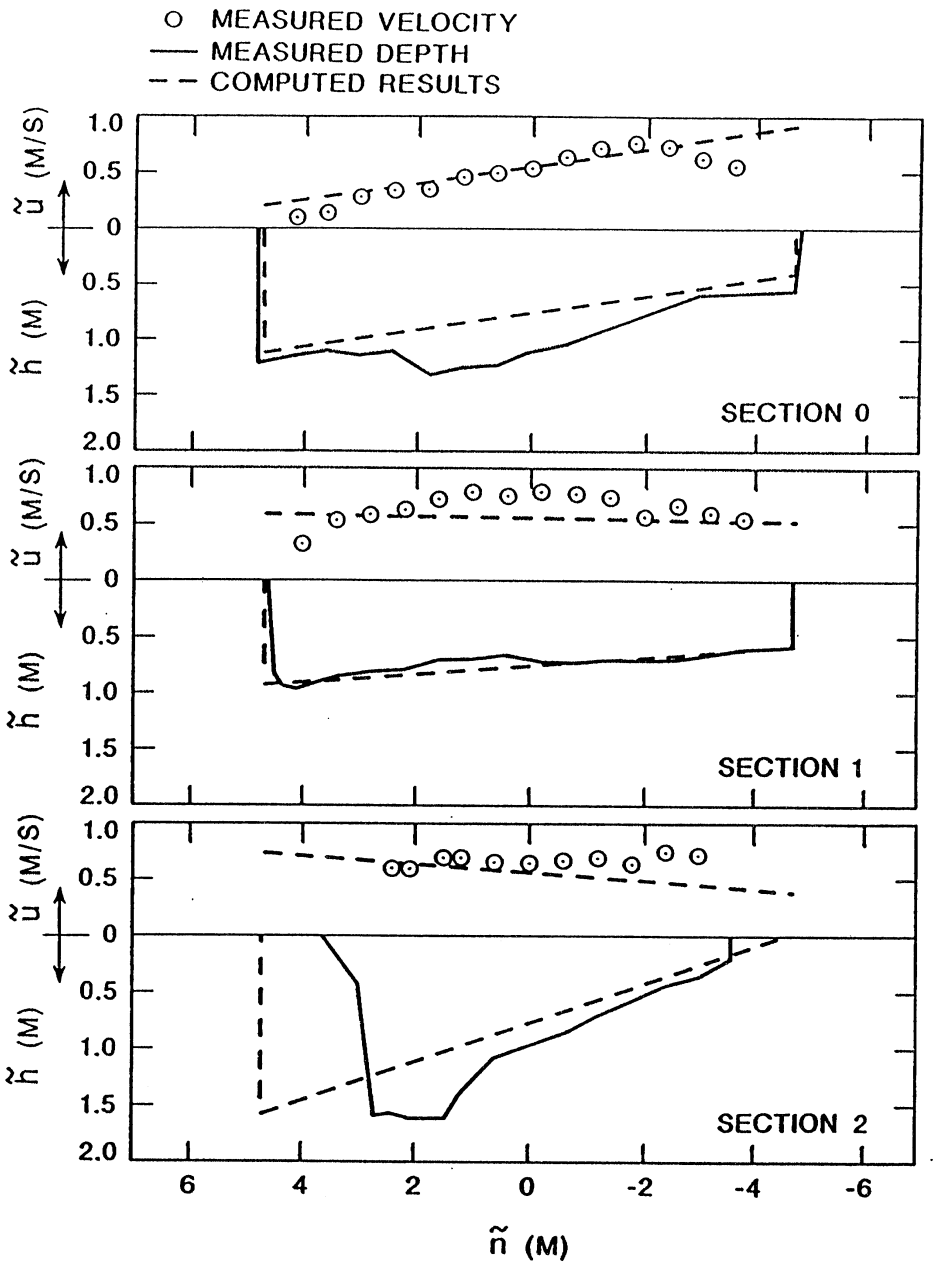

Fig. 8.8. Transverse distribution of depth and depth-averaged primary flow velocity as measured and predicted in the Fall River study reach.

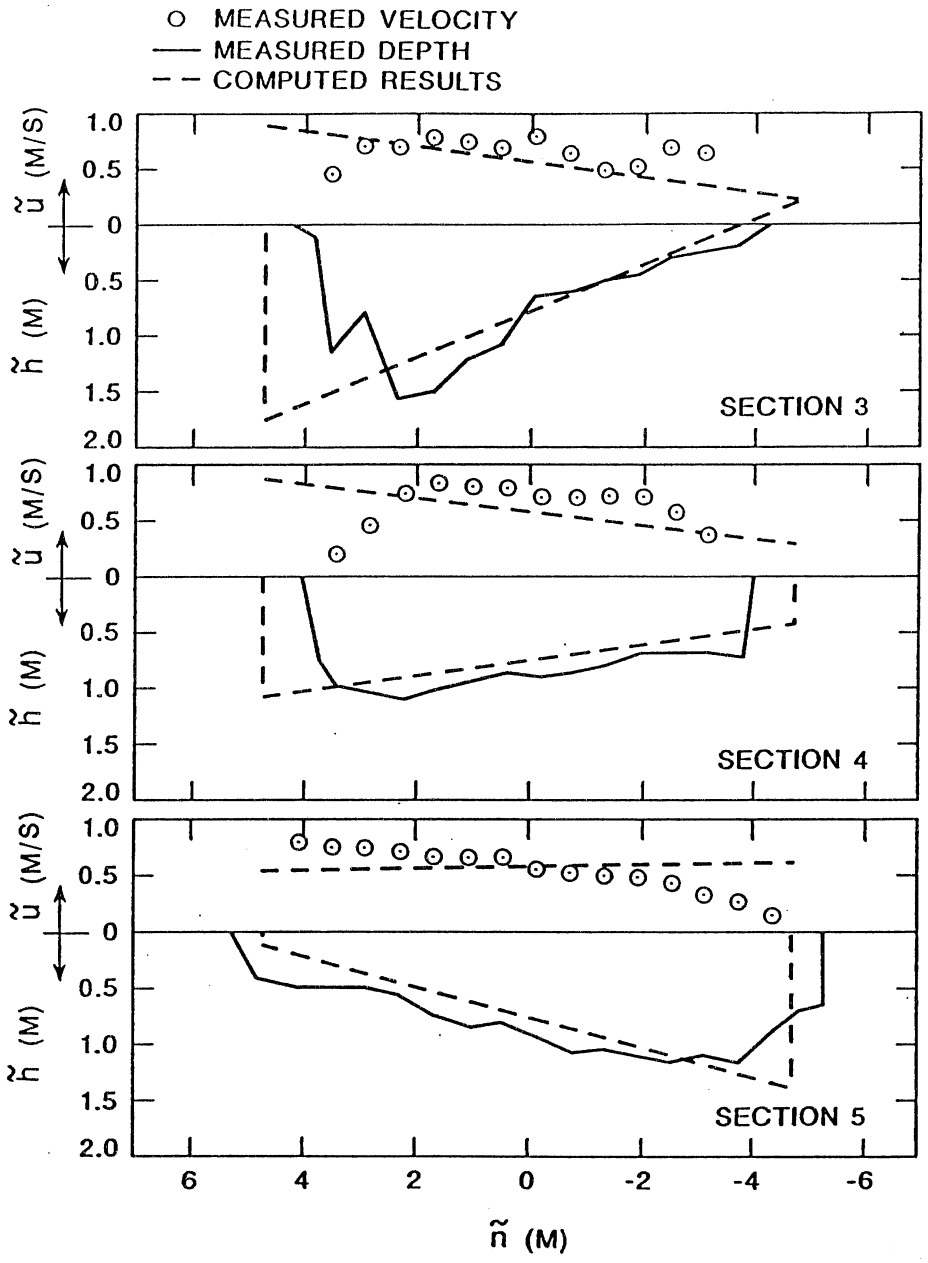

Fig. 8.8. Continued.

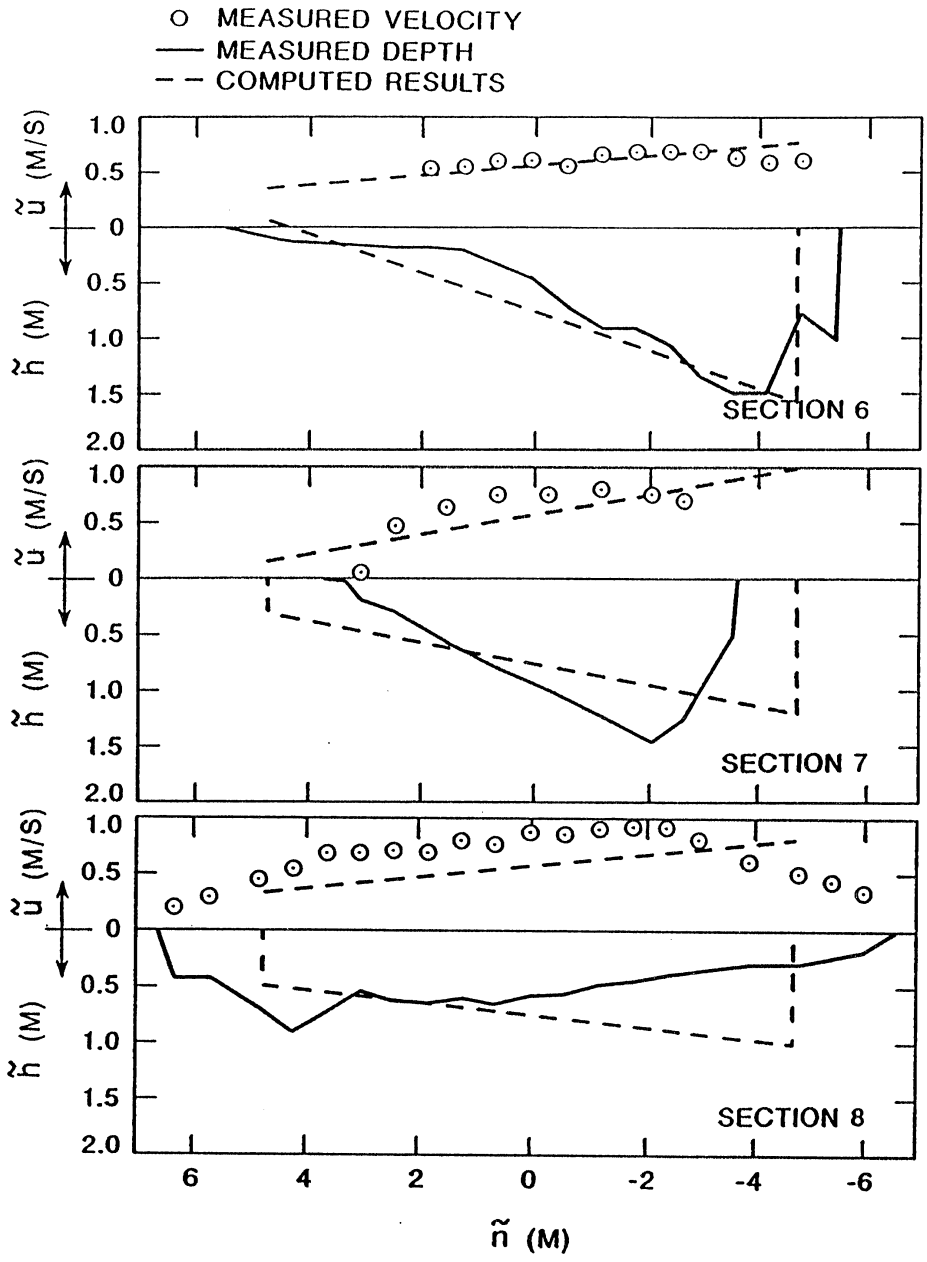

Fig.8.8. Continued.

8.6 Discussion and Conclusions

A model for calculation of the flow field and bed topography in arbitrarily shaped channels has been developed. The comparison with Rozovskii's data clearly shows that if the bed topography is given as input for the model, as is the case for channels with a non-erodible flat bed, the predicted flow field compares very well with data. This indicates that the flow field component of the model is performing satisfactorily.

As for the sine-generated channel, the model predicts rather well the bed topography for channels with uniform sediment. For channels with highly non-uniform sediment, better results are obtained by setting M = 0, rather than using the value based on the mean particle grain size, D_{50}; see Chapter 5.6 for a possible reason. Again, the conclusion can be tentatively reached that the flow field component of the model is gives good results. Once M has been taken to be zero for the case of non-uniform sediment (e.g. the Fall River), the predicted bed topography approximately matches the measured values and the predicted flow field agrees very well with the measured velocities.

It is apparent, both from the measured and the computed bed topography for Exp. T1, T2, and T3, that a substantial part of the lateral bed slope in the upstream part of the bend in those experiments is due to redistribution of water and sediment in the first part of the bend, (F - Problem), as concluded by Struiksma et al. (1985). This phenomenon, called overdeepening herein, is explained in Chapter 7. An analytical expression (Eq. 7.4a) is derived for the wavelength of the overdeepening in Chapter 7. The predicted wavelength (Eq. 7.4a) agrees very well with the measured values (Table 7.1). The excellent agreement between the measured and predicted bed topography in Fig. 8.4 is therefore not totally unexpected.

Having illustrated the close relation between the overdeepening and the resonance (Chapter 7) and demonstrated that the theoretical predictions match very accurately the experimental data of Struiksma et al. (1985) the following question arises: Has either overdeepening or resonance been observed in the field? Fig. 8.9 shows the damage to the Los Angeles River channel in the aftermath of the flood of 1938. As seen from Fig. 8.9, the river, which before the flood was bound by levees on both sides, flows through a very sharp bend. Upstream and downstream of the bend the channel was straight. The channel geometry was therefore somewhat similar to the experimental setup of Struiksma et al. (1985). From Fig. 8.9 it is seen that the sudden change in channel curvature caused the river to break through the levees during the flood. The oscillatory pattern in which the river broke through the levees certainly looks very much as if it could be caused by what herein has been called overdeepening (Fig. 8.4).

Fig. 8.9. Upstream view of damage to the Los Angeles River channel in the flood of 1938 (Maximum discharge 1700 m^3/sec; maximum velocity about 6 m/sec). (Photo obtained from Gildea, 1963).

9. BANK EROSION AND BEND INSTABILITY

9.1 Introduction

A detailed overview of the available bank erosion models is given in Chapter 1.3. As mentioned, therein, the bank erosion model of Ikeda et al. (1981) has, over the last few years, gradually become accepted as a very reasonable choice. It has been extensively used by the river mechanics group at the St. Anthony Falls Hydraulic Laboratory (Parker, 1982; Beck et al. 1983a,b; Johannesson, 1985) and more recently at the University of Genova, Italy (Blondeaux and Seminara, 1985), at the Iowa Institute of Hydraulic Research (Odgaard, 1987), and at the Delft Hydraulics Laboratory, Netherlands (Crosato, 1987) (Table 1.2).

Herein, the bank erosion model of Ikeda et al. (1981) is described. It is used together with the rederived flow field and bed topography model to predict the wavelength of river meanders. The results are compared with both laboratory and field data and are shown to significantly improve upon those of Ikeda et al. (1981).

9.2 Equation Describing the Bank Erosion

Ikeda et al. (1981) assumed that the normal bank erosion rate, $\tilde{\zeta}$, of the "left" bank of Fig. 9.1b is a function of the tangential flow velocity near that bank. This functional relationship is estimated as

$$\tilde{\zeta} = \tilde{\zeta}(U) + \frac{d\tilde{\zeta}}{d\tilde{u}}\Big|_U U\, u_{1b}\, \Psi_0 \tag{9.1}$$

Defining the dimensionless erosion rate as $\zeta = \tilde{\zeta}/U$, Eq. 9.1 can be written in dimensionless form as

$$\zeta = \zeta(U) + \frac{d\zeta}{du}\Big|_{u=1} u_{1b}\, \Psi_0 \tag{9.2}$$

Note, that ζ, as defined in Eq. 9.2, is not to be confused with the dimensionless distance above the bed, $\zeta = \tilde{z}/\tilde{h}$, defined in earlier chapters.

Assuming the river to have constant width in time, $\zeta(U)$ vanishes. Defining a positive coefficient of bank erosion $E(U) = [d\zeta / du]\,|_{u=1}$, Eq. 9.2 becomes

$$\zeta = E(U)\, u_{1b}\, \Psi_0 \tag{9.3}$$

As discussed by Ikeda et al. (1981) the dependance of E(U) on U may be neglected at the linear level, in which case E(U) can be taken to be constant and equal to E_0. The following result is then obtained for the erosion rate, ζ,

$$\zeta = E_0\, u_{1b}\, \Psi_0 \tag{9.4}$$

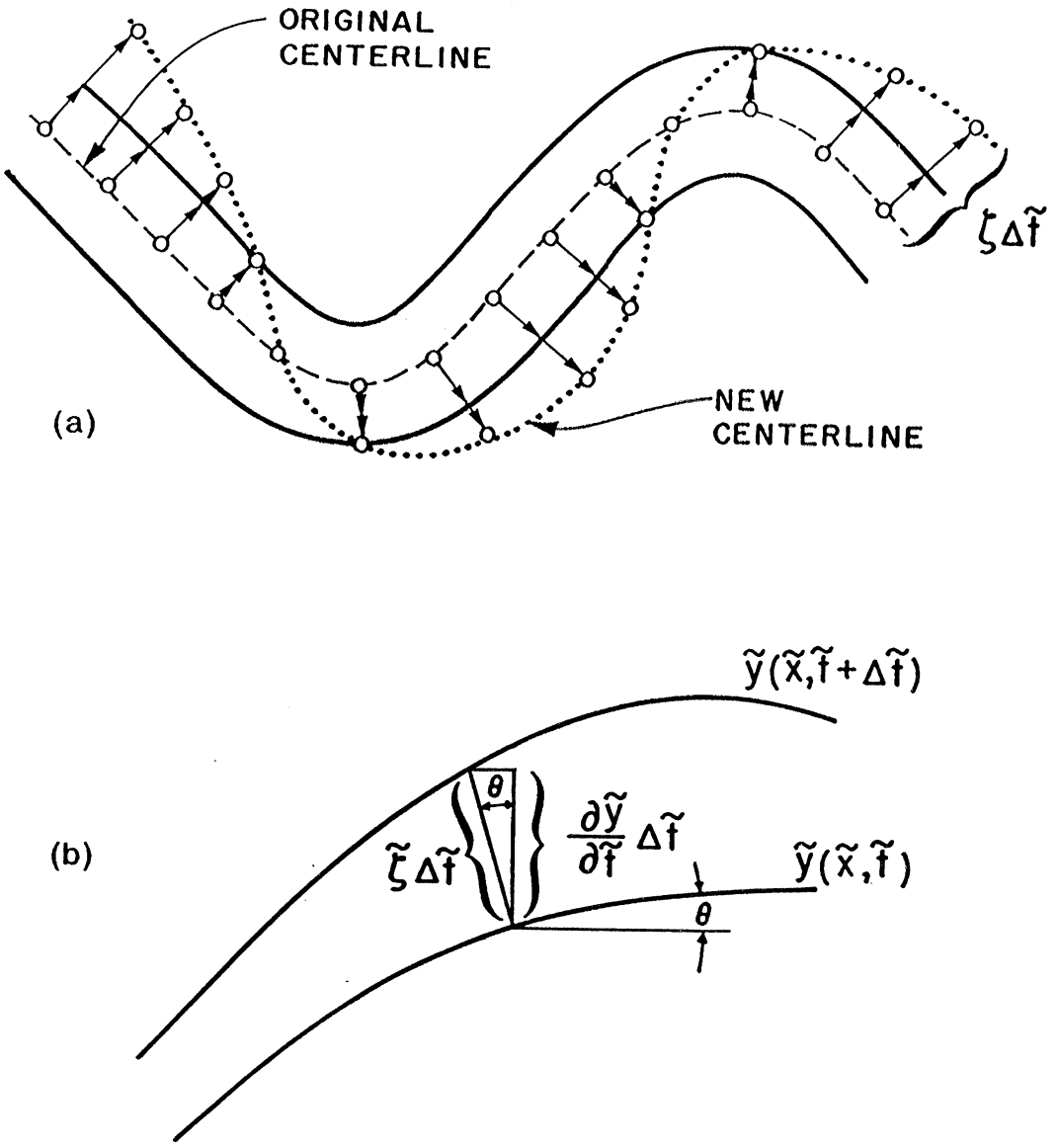

Fig. 9.1. Definition diagram for the bank erosion model.

a) Illustration of the use of the orthogonal Hickin mapping.

b) Diagram for the derivation of Eqs. 9.5a,b.

where the erosion coefficient, E_0, is a measure of the erodibility of the bank material.

A channel migration can be modeled using Eq. 9.4, together with what Parker (1983) called a "Hickin mapping", in honor of the work of Hickin (1974). As seen in Fig. 9.1a, the channel migration is accomplished by shifting each point on the channel centerline some distance normal to the downstream direction. The distance is determined by Eq. 9.4. Referring in Fig. 9.1b to a point on the channel centerline that is located at Cartesian coordinates $\tilde{x}_0$ and $\tilde{y}_0$ at time $\tilde{t}_0$, its coordinates a short time $\Delta\tilde{t}$ later are given by

$$\tilde{x} = \tilde{x}_0 - \tilde{\zeta}\,\Delta\tilde{t}\,\sin(\theta) \tag{9.5a}$$

$$\tilde{y} = \tilde{y}_0 + \tilde{\zeta}\,\Delta\tilde{t}\,\cos(\theta) \tag{9.5b}$$

The condition of constant width assures that the right bank, left bank, and the channel centerline all move in the same way, so that the erosion model is complete.

9.3 Bend Instability

Let us consider the stability of an initially straight river to an arbitrary fluctuation of the channel centerline around the $\tilde{x}$ - axis

$$y = y_0\, e^{\alpha_0 t} \sin(\phi - \omega_0 t) \tag{9.6}$$

where y has been nondimensionalized with the channel half-width b, α_0 is the dimensionless exponential bend growth rate, and ω_0 is a dimensionless circular frequency, such that ω_0/k is a dimensionless bend migration speed. The channel curvature is then found to be

$$C = -k^2 \frac{\partial^2 y}{\partial \phi^2} = k^2\, y_0\, e^{\alpha_0 t} \sin(\phi - \omega_0 t) = \psi_0\, \sigma \tag{9.7}$$

where $\psi_0 = k^2\, y_0\, e^{\alpha_0 t}$ and $\sigma = \sin(\phi - \omega_0 t)$.

From Fig. 9.1b and Eq. 9.5b the following geometrical result is obtained

$$\zeta \cos(\theta) = \frac{\partial y}{\partial t} \tag{9.8}$$

In the limit of a small amplitude bend, $\cos\theta \approx 1$ and Eq. 9.8, together with Eq. 9.4, reduces to

$$\frac{\partial y}{\partial t} = E_0\, u_{1b}\, \psi_0 \tag{9.9}$$

In Chapter 5 a solution for u_{1b} for the case of a sine-generated curve is derived. Direct substitution of that result into Eq. 9.9 yields

$$\frac{\partial y}{\partial t} = E_0 \left[(\tilde{a}_C + \tilde{a}_F) \cos(\phi - \omega_0 t) + (\tilde{b}_C + \tilde{b}_F) \sin(\phi - \omega_0 t) \right] \psi_0 \qquad (9.10)$$

where $\tilde{a}_C$, $\tilde{b}_C$, $\tilde{a}_F$, and $\tilde{b}_F$ are given by Eqs. 5.45c,d and 5.53c,d, respectively. Differentiating Eq. 9.6 once with respect to time gives

$$\frac{\partial y}{\partial t} = \left[-\frac{\omega_0}{k^2} \cos(\phi - \omega_0 t) + \frac{\alpha_0}{k^2} \sin(\phi - \omega_0 t) \right] \psi_0 \qquad (9.11)$$

Direct comparison of Eqs. 9.10 and 9.11 yields the following expressions for α_0 and ω_0

$$\alpha_0 = E_0 k^2 (\tilde{b}_C + \tilde{b}_F) \quad ; \quad \omega_0 = -E_0 k^2 (\tilde{a}_C + \tilde{a}_F) \qquad (9.12a,b)$$

The wavenumber k which maximizes instability i.e. α_0, is found using the IMSL subroutine ZXGSN, which uses the golden section search method. The results are compared with data (75 field cases and 89 experiments) in Fig. 9.2. All the input data needed for the generation of Fig. 9.2 are summarized in Appendix B. These are the same data used by Ikeda et al. (1981) for the generation of their Fig 5, except that experiments in channels with non-erodible banks are excluded. Insofar as the available information usually did not allow for calculation of these parameters, and in order to make the calculation procedure uniform, the transverse bed slope parameter, A, and the power, M in the streamwise bedload transport relation are taken to be 2.89 (same as the value used by Ikeda et al. (1981)) and 5 (typical value for M e.g. Struiksma et al. (1985)), respectively, for all of the data. As seen from Fig. 9.2, the present theory predicts the right orders of magnitude of meander wavelengths both for the laboratory and the field data. The scatter is substantial, but indeed considerably less than that obtained by Ikeda et al. (1981). Even more important than the reduced scatter is the fact that the model can explain the scatter as being partly due to the sensitivity of the predicted wavelength values to the value of M. On the other hand, a change in A does not modify the results much.

9.4 Discussion and Conclusions

The rederived flow field and bed topography model, together with the bank erosion relation of Ikeda et al. (1981), predicts wavelengths of river meanders that are in general agreement with both laboratory and field data. The agreement is indeed better than if the full theory of Ikeda et al. (1981) is used. More importantly, the present theory can explain the large scatter in Fig. 9.2 as being partly due to the sensitive nature of the results to the value of the power, M, in the streamwise bedload transport relation.

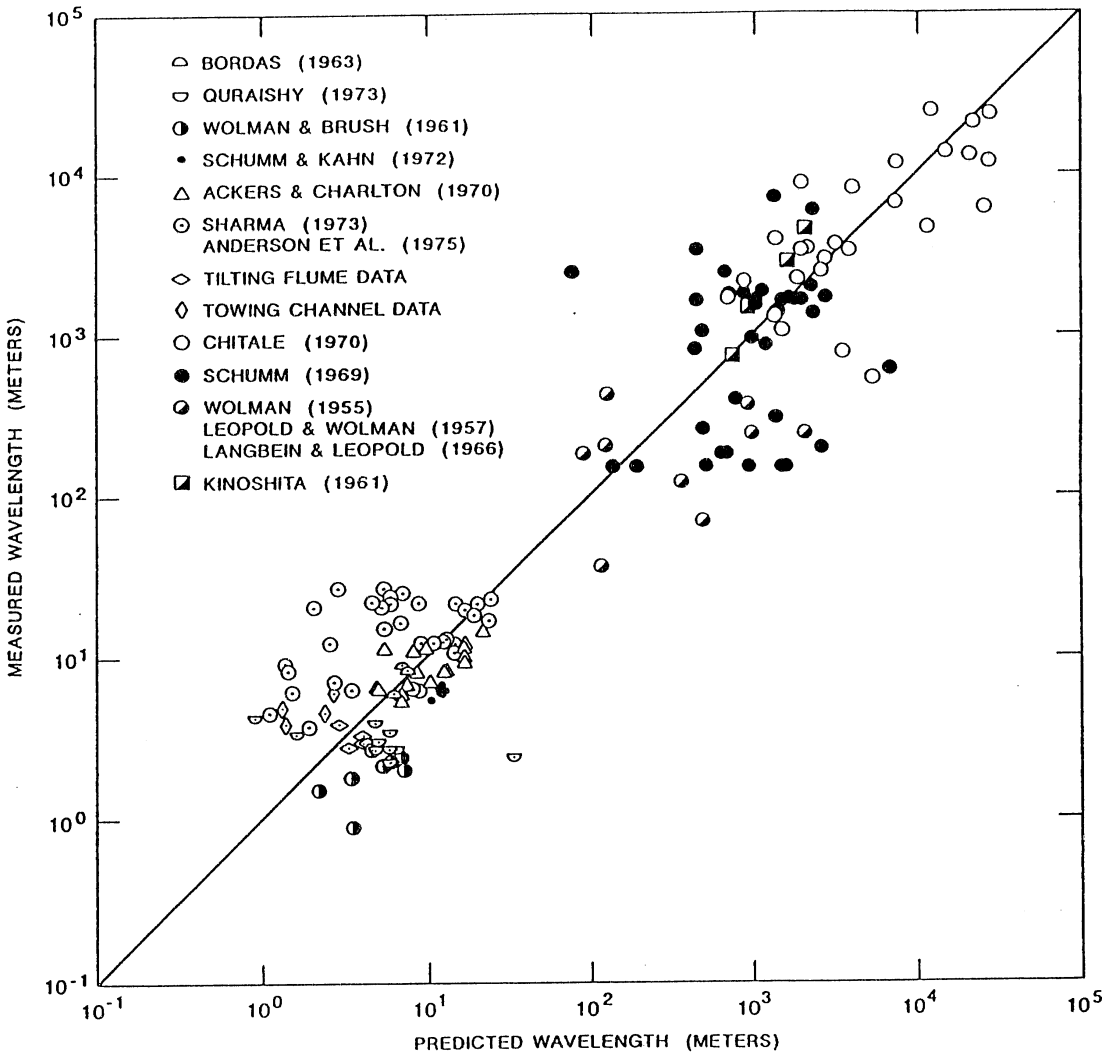

Fig. 9.2. Wavelengths of river meanders as measured and predicted.

10. SUMMARY AND CONCLUSIONS

A mathematical model for calculating the flow field and bed topography in curved channels with an erodible bed is presented. The results can be viewed as a complete rederivation of the flow and bed topography model of Ikeda et al. (1981). A small perturbation approach is used to linearize the governing equations, which retain the full coupling between the flow field, the bedload transport, and the bed topography. It is demonstrated by comparison with data, that the new model constitutes a considerable improvement to the analysis of Ikeda et al. (1981) both as regards the flow field and the bed topography. It accounts for the following physical processes absent in their model:

1) The metric coefficients that arise in a curvilinear coordinate system; this introduces the term - $n\sigma$ in Eq. 3.14a (e.g. Tamai and Ikeuchi, 1984; Johannesson, 1985; Blondeaux and Seminara, 1985). As shown in Chapter 4, this term becomes important in the limiting case of a flat bed channel with large aspect ratio, ($\gamma = b/H \rightarrow \infty$).

2) The convective transport of primary flow momentum by the secondary flow (the last term on the right hand side of Eq. 3.14a). This term can be of considerable importance when calculating the lateral distribution of the depth averaged primary flow velocity, as shown in Chapters 4 and 8. The approximate manner (the "moment method") in which this influence of the secondary flow is accounted for seems to yield very satisfactorily results.

3) The downstream convective acceleration of the secondary flow (the first term on the left hand side of Eq. 3.14b). Ikeda et al. (1981) used the depth-averaged form of the transverse momentum equation, which does not allow for the calculation of the secondary flow. They then determined the secondary flow using an expression derived for fully developed bend flow in circular channels. Equation 3.14b, on the other hand, can allow for a more accurate calculation of the secondary flow. Most importantly, it allows for calculation of the phase lag between the channel curvature and the secondary flow strength. This lag tends to be rather small for natural channels, but is quite large for many commonly quoted experiments, (Chapter 5).

4) The continuity equation of sediment transport. Ikeda et al. (1981) assumed the bed topography to be solely driven by the secondary flow. This corresponds to setting $M = 0$ and neglecting v_1 in Eq. 3.14d. As shown in Chapters 5 to 8, this is the reason the model of Ikeda et al. (1981) cannot predict the resonance phenomenon detected by Blondeaux and Seminara (1985) nor the overdeepening observed and predicted by Struiksma et al. (1985).

The coupling between the flow field, the bedload transport, and the bed topography, missing from the model of Ikeda et al. (1981), is shown to be responsible for the overdeepening observed and predicted theoretically by Struiksma et al. (1985), and the resonance detected by Blondeaux and Seminara (1985). The overdeepening and the resonance are further shown to be a manifestation of the same phenomenon, (Chapter 7).

The present theory is in general agreement with the work carried out at the Delft Hydraulics Laboratory (Struiksma et al., 1985) and at the University of Genova (Blondeaux and Seminara, 1985). All of the above theories are, however, quite different

from the theory of Odgaard (1986a), from which the continuity equation of sediment is absent and in which the overdeepening is explained as being due to an inertial term $\bar{u}\,(\partial\bar{v}/\partial\tilde{s})$ in the relation for transverse momentum balance.

The model, using the bank erosion relation of Ikeda et al. (1981), predicts wavelengths of river meanders that are in general agreement with both laboratory and field data. The agreement is indeed better than if the full theory of Ikeda et al. (1981) is used. More importantly, the present theory can explain the large scatter in Fig. 9.2 as being partly due to the sensitive nature of the results to the value of the exponent M in the streamwise bedload transport relation. The results indicate that the new flow field and bed topography model, together with the bank erosion model of Ikeda et al. (1981), may eliminate at least some of the calibration needed when the full model of Ikeda et al. (1981) is used to simulate river migration, (e.g. Parker, 1982; Beck 1983a,b; Johannesson, 1985). All these river migration studies should be repeated, using the new flow field and bed topography model, to verify this.

Although the predicted flow field and bed topography compares well with laboratory data, care should be taken when using it to simulate field cases. All the laboratory data used for comparison herein, except the data set of Ikeda and Nishimura (1986), was obtained using fairly uniform sediment ($\sigma_g \leq 1.6$). This is the appropriate data to use for testing the theory, in which only the mean particle grain size D_{50} is used to characterize the sediment. The results from simulations of data sets where the sediment grain size distributions were highly non-uniform ($\sigma_g \geq 1.6$) (Ikeda and Nishimura, 1986, Chapter 5; Muddy Creek, Chapter 5; Fall River, Chapter 8), indicate that the model may overpredict scour in the field where the sediment grain size distribution is typically not uniform. It was found that better results were obtained for these cases by setting M (the power in the sediment transport relation) equal to zero rater than using the value based on the mean particle grain size, D_{50}. This is not totally unexpected, since the model does not take into account sorting of bedload in channel bends. By forcing M to be zero, a component of the model that is very sensitive to sorting of the bedload is thrown out of the model, which may easily be more appropriate than retaining it, for the case of non-uniform bedload. The apparent lack of formal justification for doing this illustrates the need to expand the theory to encompass sediment sorting and armoring; this hopefully will improve the predicted bed topography for field rivers.

In addition to generalizing the model to account for sediment sorting and armoring, relaxing the constraint of constant width will significantly enhance the value of the model. It is also important to compare the results obtained from some of the non-linear numerical models (Smith and McLean, 1985; Struiksma et al., 1985) to the results of the linear models. This would allow for a determination of a upper limit on, for example, the dimensionless curvature, $b/\tilde{r}$, beyond which the linear analysis fails.

Finally, it should be emphasized that the present model is the first vertically integrated model capable of describing the dispersive effect of the secondary flow on streamwise momentum. It is, however, of importance to note that although the model seems to yield very satisfactorily results using the "moment method" to account for the convective transport of primary flow momentum by the secondary flow, the result will surely break down in the limiting case of a channel with large aspect ratio, $\gamma = b/H \rightarrow \infty$, as discussed in Chapter 4. This phenomenon is essentially a side wall effect, and cannot be expected to penetrate the flow to the centerline in the limit of very large width ($\gamma \rightarrow \infty$). In this limit, then, the linear transverse profile assumed herein to describe the depth-averaged streamwise flow velocity breaks down. Additional research is needed to further clarify this.

11. REFERENCES

Adachi, S. (1967). "A theory of stability of streams," Proc. 12th Congr. IAHR, Vol. 1, 338-343.

Ackers, P., and Charlton, F. G. (1970). "The slope and resistance of small meandering channels," The Institution of Civil Engineers, Proceedings Supplement XV, Paper 7362S, 349-370.

Anderson, A. G., Parker, G., and Wood, A. (1975). "The flow and stability characteristics of alluvial river channels," Project Report No. 161, St. Anthony Falls Hydraulic Laboratory, Univ. of Minnesota, U.S.A., 1-116.

Aris, R. (1956). "On the dispersion of a solute in a fluid flowing through a tube," Proc. R. Soc. London, Ser. A 235, 67-77.

Beck, S. M. (1983). "Mathematical modeling of meander interaction," Proceedings, River Meandering, Rivers '83 Conference, ASCE, New Orleans, 932-941.

Beck, S. M. (1985). "Self-stabilization of stalled meander bends," 7th Canadian Hydrotechnical Conference Proceedings, CSCE, 1A, May 27-31, Saskatoon, Saskatchewan, Canada, 149-167.

Beck, S. M. (1988). "Computer-simulated deformation of meandering river patterns," Ph.D. thesis, Univ. of Minnesota, U.S.A., 1-207.

Beck, S. M., Harrington, R. A., and Andres, D. D. (1983a). "Lateral channel stability of the Pembina River near Rossington, Alberta," unpublished report, Research Council of Alberta, Edmonton, Alberta, Canada.

Beck, S. M., Melfi, D. A., and Yalamanchili, K. (1983b). "Lateral migration of the Genesee River, New York," Proceedings, River Meandering, Rivers '83 Conference, ASCE, New Orleans, 510-517.

Blondeaux, P., and Seminara, G. (1983). "Bed topography and instabilities in sinuous channels," Proceedings, River Meandering, Rivers '83 Conference, ASCE, New Orleans, 747-758.

Blondeaux, P., and Seminara, G. (1985). "A unified bar-bend theory of river meanders," Journal of Fluid Mechanics, 112, 363-377.

Bordas, M. (1963). "Contribution a l'etude des relations entre le debit generateur et les meandres d'une riviere," Grafica da Universidade do Rio Grande do Sul, Porto Alegre, Brasil, 1-78.

Brownlie, W. R. (1983). "Flow depth in sand-bed channels," Journal of Hydraulic Engineering, 109(7), 959-990.

Callander, R. A. (1969). "Instability and river channels," Journal of Fluid Mechanics, 36, 465-480.

Callander, R. A. (1978). "River meandering," Annual review of Fluid Mechanics, 129-158.

Chitale, S. V. (1970). "River channel patterns," Journal of the Hydraulics Division, ASCE, 96(1), 201-221.

Colombini, M., Seminara, G., and Tubino, M. (1987). "Finite-amplitude alternate bars," Journal of Fluid Mechanics, 181, 213-232.

Crosato, A. (1987). "Simulation model of meandering processes of rivers," Extended Abstracts, Euromech 215 Conference, Sept. 15-19, Genova, Italy, 158-1613.

De Vriend, H. J. (1981). "Velocity redistribution in curved rectangular channels," Journal of Fluid Mechanics, 107, 423-439.

De Vriend, H. J., and Geldof, H. J. (1983). "Main flow velocity in short river bends," Journal of Hydraulic Engineering, ASCE, 109(7), 991-1011.

Dietrich, W. E., and Smith, J. D. (1983). "Influence of the point bar on flow through curved channels," Water Resources Research, 19(5), 1173-1192.

Dietrich, W. E., and Smith, J. D. (1984). "Bed load transport in river meander," Water Resources Research, 20(10), 1355-1380.

Engelund, F. (1974). "Flow and bed topography in channel bends," Journal of the Hydraulics Division, ASCE, 100(11), 1631-1648.

Engelund, F. (1975). "Instability of flow in a curved alluvial channel," Journal of Fluid Mechanics," 72(1), 145-160.

Engelund, F., and Hansen, E. (1967). "A monograph on sediment transport in alluvial streams," Danish Technical Press, Copenhagen.

Engelund, F., and Skovgaard, O. (1973). "On the origin of meandering and braiding in alluvial streams," Journal of Fluid Mechanics, 57, 289-302.

Falcon, M. (1979). "Analysis of flow in alluvial channel bends," Ph.D. thesis, Univ. of Iowa, U.S.A., 1-224.

Falcon, M., and Kennedy, J. F. (1983). "Flow in alluvial-river curves," Journal of Fluid Mechanics, 133, 1-16.

Fredsoe, J. (1978). "Meandering and braiding of rivers," Journal of Fluid Mechanics, 84, 607-624.

Gildea, A. P. (1963). "Design practice for levee revetment on west coast intermittent streams," Proceedings, Federal Inter-Agency Sedimentation Conf., Paper No. 57, Miscellaneous Publication No. 970, Agricultural Research Service, U.S. Department of Agriculture, 492-507.

Gottlieb, L. (1976). "Three-dimensional flow pattern and bed topography in meandering channels," Series paper 11, Institute of Hydrodynamics and Hydraulic Engineering, Technical University of Denmark, 1-79.

Hansen, E. (1967). "The formation of meanders as a stability problem," Hydraulic Laboratory, Technical Univ. of Denmark, Basic Res. Prog. Rep., No. 13.

Hasegawa, K., and Yamaoka, I. (1983). "Phase shifts of pools and their depths in meander bends," Proceedings, River Meandering, Rivers '83 Conference, ASCE, New Orleans, 885-895.

Hayashi, T. (1970). "The formation of meanders in rivers," Proc. Japan Soc. Civ. Eng., No. 180 (in Japanese).

Hayashi, T., and Ozaki, Y. (1976). "On the meander wavelength from the view point of bar instability theory," Proc. 20th Annual Meeting, Hydraul., Japan Soc. Civ. Eng., 89-96 (in Japanese).

Hickin, E. J. (1974). "The development of meanders in natural river channels," American Journal of Science, 274, 414-442.

Hickin, E. J. (1978). "Mean flow structure in meanders of the Squamish River, British Columbia," Canadian Journal of Earth Sciences, 15, 1833-1849.

Hickin, E. J., and Nanson, G. C. (1975). "The character of channel migration of the Beatton River, Northeast British Columbia, Canada," Geological Society of America Bulletin, 86, 487-494.

Hickin, E. J., and Nanson, G. C. (1984). "Lateral migration rates of river bends," Journal of Hydraulic Engineering, ASCE, 110(11), 1557-1567.

Hooke, R. L. (1974). "Shear-stress and sediment distribution in a meander bend," Ungi Rep. No. 30, Univ. of Uppsala, Sweden, 1-58.

Hooke, R. L. (1975). "Distribution of sediment transport and shear stress in a meander bend," Journal of Geology, 83, 543-565.

Ikeda, S. (1982). "Lateral bed load transport on side slopes," Journal of the Hydraulics Division, ASCE, 108(11), 1369-1373.

Ikeda, S., and Nishimura, T. (1985). "Bed topography in bends of sand-silt rivers," Journal of Hydraulic Engineering, ASCE, 111(11), 1397-1411.

Ikeda, S., and Nishimura, T. (1986). "Flow and bed profile in meandering sand-silt rivers," Journal of Hydraulic Engineering, ASCE, 112(7), 562-579.

Ikeda, S., Parker, G., and Sawai, K. (1981). "Bend theory of river meanders. Part 1. Linear development," Journal of Fluid Mechanics, 112, 363-377.

Ikeda, S., Tanaka, M., and Chiyoda, M. (1985). "Turbulent flow in a sinuous air duct," Proceedings, International Symposium on Refined Flow Modeling and Turbulence Measurements, The Univ. of Iowa, Iowa City, IAHR, I-24, 7-10.

Johannesson, H. (1985). "Computer simulated migration of meandering rivers," M.S. thesis, University of Minnesota, U.S.A., 1-115.

Johannesson, H., and Parker, G. (1985). "Computer simulated migration of meandering rivers in Minnesota," Project Report No. 242, St. Anthony Falls Hydraulic Laboratory, Univ. of Minnesota, 1-82.

Johannesson, H., and Parker, G. (1988a). "Theory of river meanders," Proceedings, Hydraulic Engineering, National Conference, ASCE, Aug. 8-12, Colorado Springs, U.S.A., 684-689.

Johannesson, H., and Parker, G. (1988b). "Inertial effects on secondary and primary flow in curved channels," External Memorandum No. 208, St. Anthony Falls Hydraulic Laboratory, Univ. of Minnesota.

Johannesson, H., and Parker, G. (1989a). "Secondary flow in a mildly sinuous channel," Journal of Hydraulic Engineering, ASCE, in press.

Johannesson, H., and Parker, G. (1989b). "Velocity redistribution in meandering rivers," submitted to Journal of Hydraulic Engineering, ASCE.

Johannesson, H., and Parker, G. (1989c). "Linear theory of river meanders," River Meandering, Geophysical Monograph Series, AGU, Chapter 7.

Kalkwijk, J. P. Th., and De Vriend, H. J. (1980). "Computation of the flow in shallow river bends," Journal of Hydraulic Research, 18(4), 327-342.

Kalkwijk, J. P. Th., and Booij, R., (1986). "Adaptation of secondary flow in nearly-horizontal flow," Journal of Hydraulic Research, 24(1), 17-37.

Kikkawa, H., Ikeda, S., and Kitagawa, A. (1976). "Flow and bed topography in curved open channels," Journal of the Hydraulics Division, ASCE, 102(9), 1327-1342.

Kinoshita, R. (1976). "Investigation of channel deformation in Ishikari River," Report of Bureau of Resources, Department of Science and Technology, Japan, 1-174 (in Japanese).

Kitanidis, P. K., and Kennedy, J. F. (1984). "Secondary current and river-meander formation," Journal of Fluid Mechanics, 144, 217-229.

Langbein, W. B., and Leopold, L. B. (1966). "River meanders - theory of minimum variance," USGS Professional Paper 422H, 1-15.

Lapointe, M. F., and Carson, M. A. (1986). "Migration patterns of an asymmetric meandering river: The Rouge River, Quebec," Water Resources Research, 22(5), 731-743.

Leopold, L. B., and Wolman, M. G. (1957). "River channel patterns: Braided, meandering and straight," USGS Professional Paper 282B, 1-85.

Leschziner, M. A., and Rodi, W. (1979). "Calculation of strongly curved open channels," Journal of the Hydraulics Division, ASCE, 105(10), 1297-1314.

Nanson, G. C., and Hickin, E. J. (1983). "Channel migration and incision on the Beatton River," Journal of the Hydraulics Division," 109(3), 327-337.

Nelson, J. M. (1988). "Mechanics of flow and sediment transport over nonuniform erodible beds," Ph.D. thesis, Univ. of Washington, 1-227.

Odgaard, A. J. (1981). "Transverse bed slope in alluvial river bends," Journal of the Hydraulics Division, ASCE, 107(12), 1677-1694.

Odgaard, A. J. (1986a). "Meander flow model. I: Development," Journal of Hydraulic Engineering, ASCE, 112(12), 1117-1136.

Odgaard, A. J. (1986b) "Meander flow model. II: Applications," Journal of Hydraulic Engineering, ASCE, 112(12), 1137-1150.

Odgaard, A. J. (1987). "Streambank erosion along two rivers in Iowa," Water Resources Research, 23(7), 1225-1236.

Parker, G. (1975). "Meandering of supraglacial melt streams," Water Resources Research, 11, 551-552.

Parker, G. (1976). "On the cause and characteristic scales of meandering and braiding in rivers," Journal of Fluid Mechanics, 76, 457-480.

Parker, G. (1982). "Stability of the channel of the Minnesota River near State Bridge No. 93, Minnesota," Project Report No. 205, St. Anthony Falls Hydraulic Laboratory, University of Minnesota, U.S.A., 1-33.

Parker, G. (1983). "Theory of meander bend deformation," Proceedings, River Meandering, Rivers '83 Conference, ASCE, Oct. 24-26, New Orleans, U.S.A., 722-732.

Parker, G. (1984). "Discussion of," Lateral bed load transport on side slopes, by S. Ikeda, Journal of Hydraulic Engineering, ASCE, 110(2), 197-199.

Parker, G., and Andrews, E. D. (1985). "Sorting of bed load sediment by flow in meander bends," Water Resources Research, 21(9), 1361-1373.

Parker, G., and Andrews, E. D. (1986). "On the time development of meander bends," Journal of Fluid Mechanics, 162, 139-156.

Parker, G., Diplas, P., and Akiyama, J. (1983). "Meander bends of high amplitude," Journal of the Hydraulics Division, ASCE, 109(10), 1323-1337.

Parker, G., and Johannesson, H. (1989). "Observations on several recent theories of resonance and overdeepening in meandering channels," River Meandering, Geophysical Monograph Series, AGU, Chapter 12.

Parker, G., Sawai, K., and Ikeda, S. (1982). "Bend theory of river meanders. Part 2. Nonlinear deformation of finite amplitude bends," Journal of Fluid Mechanics, 115, 303-314.

Ponce, V. M., and Mahmood, K. (1976). "Meandering thalwegs in straight alluvial channels," Proc. ASCE Rivers Conf., Fort Collins, Colorado, U.S.A.

Quraishy, M. S. (1973). "The meandering of alluvial rivers," Sind University Research Journal, (Science Series) VII(1), 95-152.

Roher, W. L. M. (1983). "Effects of flow and bank material on meander migration in alluvial rivers," Proceedings, River Meandering, Rivers '83 Conference, ASCE, Oct. 24-26, New Orleans, U.S.A., 770-782.

Rozovskii, I. L. (1961). "Flow of water in bends of open channels," Israel Program for Scientific Translations, Jerusalem, Israel, 1-233.

Schumm, S. A. (1969). "River metamorphosis," Journal of the Hydraulics Division, ASCE, 95(1), 255-273.

Schumm, S. A., and Khan, H. R. (1972). "Experimental study of channel patterns," Bulletin of Geological Society of America, 88, 1755-1770.

Sharma, H. D. (1973). "Extract of the work done at U.P. Irrigation Research Institute, Roerkee, on meandering, braiding, and avulsion of rivers and their prevention," U.P.I.R.I. Report, Roorke, Uttar Pradesh, India.

Smith, J. D., and McLean, S. R. (1984). "A model for flow in meandering streams," Water Resources Research, 20(9), 1301-1315.

Struiksma, N. (1985). "Prediction of 2-D bed topography in rivers," Journal of Hydraulic Engineering, 111(8), 1169-1182.

Struiksma, N., Olesen, K. W., Flokstra, C., and De Vriend, H. J. (1985). "Bed deformation in curved alluvial Channels, Journal of Hydraulic Research, 23(1), 57-59.

Suga, K. (1963). "On local scour at river bends," Tech. Memo Public Works Res. Inst., Min. of Const. Japan, Vol. 5, No. 4 (in Japanese).

Sukegawa, N. (1970). "Conditions for the occurrence of river meanders," Journal of the Faculty of Engineering, Univ. of Tokyo, 30, 289-306.

Tamai, N., and Ikeuchi, K. (1984). "Longitudinal and Transverse Variations of the depth-averaged flow fields in a meandering channel," Journal of Hydroscience and Hydraulic Engineering, 2(2), 11-33.

Thorne, C. R., Zevenbergen, L. W., Bradley, J. B., and Pitlick, J. C. (1985). "Measurements of bend flow hydraulics on the Fall River at Bankfull stage," WRD Project Report No. 85-3, National Park Service, Colorado State Univ., Fort Collins, Colorado, 1-70.

Van Dyke, M. D. (1964). "Perturbation methods in fluid mechanics," Academic Press Inc., New York and London, 1-229.

Vanoni, V. A. (1977). "Sedimentation Engineering," ASCE Manual and Reports on Engineering Practice - No. 54, 1-745.

Wiberg, P. L., and Smith, J. D. (1985). "A theoretical model for saltating grains in water," Journal of Geophysical Research, 90(C4), 7341-7354.

Wolman, M. G. (1955). "The natural channel of Brandywine Creek Pennsylvania," USGS Professional Paper 271, 1-56.

Wolman, M. G., and Brush, L. M. (1961). "Factors controlling the size and shape of stream channels in coarse noncohesive sands," USGS Professional Paper 282G, 183-210.

Yamaoka, I., and Hasegawa, K. (1983). "Effects of bends and alternating bars on meander evolution," Proceedings, River Meandering, Rivers '83 Conference, ASCE, Oct. 24-26, New Orleans, U.S.A., 770-782.

Yen, B. C. (1965). "Characteristics of subcritical flow in a meandering channel," Ph.D. thesis, Univ. of Iowa, U.S.A., 1-149.

Zimmermann, C., and Kennedy, J. F. (1978). "Transverse bed slopes in curved alluvial channels," Journal of the Hydraulics Division, ASCE, 104(1), 33-48.

APPENDIX A

Derivation of an Expression for the Power M in the Streamwise Bedload Transport Relation

APPENDIX A

Herein, the derivation of the expression for M as given by Eqs. 2.10a,b is discussed. Parker (1976), Blondeaux and Seminara (1985), and Parker and Johannesson (1989) did not assume a simplified streamwise bedload transport relation corresponding to Eq. 2.9. Therein, formulas are given for linearization of arbitrary bedload transport relations which include the expansion of the friction factor. However, in the present analysis, the friction factor C_f is taken to be constant as done by Ikeda et al. (1981) and Struiksma et al. (1985).

Parker and Anderson (1977) have shown that when relating $\tilde{q}_s$ and C_f to flow parameters they are a function of up to two independent hydraulic variables. Parker (1976) expressed $\tilde{q}_s$ and C_f as functions of u and energy slope. The complete equivalent formulation of Blondeaux and Seminara (1985), according to which

$$q_s = q_s(\tau_s, h) \quad ; \quad C_f = C_f(\tau_s, h) \tag{A.1a,b}$$

is used, herein, to investigate the error introduced by the power law assumed for the bedload transport (Eq. 2.9) and the assumption of constant friction factor.

Using equations A.1a,b, the linearized form of the governing equations (Eqs. 2.30, 2.31, 2.32, 2.33, and 2.35) becomes (e.g. Parker and Johannesson (1989));

$$r\, u_1' + 2Pu_1 = -F^{-2} r\, \xi_1' - n\sigma + P_1(\xi_1 - \eta_1) - \frac{1}{\varepsilon}\frac{\partial}{\partial n}\int_0^1 T\upsilon_1 d\zeta \tag{A.2a}$$

$$\varepsilon Tr\,(\underline{\varepsilon v}_1 \underline{T} + \upsilon_1)' - T^2\sigma = -F^{-2}\frac{\partial \xi_1}{\partial n} - \underline{\varepsilon}^2 \underline{v}_1 + \varepsilon\chi_1 \ddot{\upsilon}_1 \tag{A.2b}$$

$$r\, u_1' + r\, h_1' + \frac{\partial v_1}{\partial n} = 0 \tag{A.2c}$$

$$r\, M\, u_1' - rM_1(\xi_1 - \eta_1) + \frac{\partial}{\partial n}\left[v_1 + \frac{\chi_1 \dot{\upsilon}_1(0)}{\varepsilon} - \Gamma\frac{\partial \eta_1}{\partial n}\right] = 0 \tag{A.2d}$$

where the unsteady term has been dropped from the continuity equation of sediment transport since the flow and the bed topography is assumed to be fully adapted in time to the channel curvature.

The coefficients P, P_1, M, and M_1 in the above relations result from linearizing Eqs. A.1a,b;

$$P = \frac{1}{1 - \dfrac{\partial C_f}{\partial \tau_s}} \quad ; \quad P_1 = 1 - \frac{1}{C_{f0}}\frac{\partial C_f}{\partial h} P \tag{A.3a,b}$$

$$M = 2P\frac{\tau_{s0}}{q_{s0}}\frac{\partial q_s}{\partial \tau_s} \quad ; \quad M_1 = (P_1 - 1)\frac{\tau_{s0}}{q_{s0}}\frac{\partial q_s}{\partial \tau_s} - \frac{1}{q_{s0}}\frac{\partial q_s}{\partial h} \qquad \text{(A.3c,d)}$$

where τ_{s0}, C_{f0}, and q_{s0} are the values of τ_s, C_f, and q_s associated with the zeroth order flow (Eqs. 2.27a,b,c).

The coefficients P, P_1, M, and M_1 are evaluated using the Engelund-Hansen (1967) sediment transport relation for both lower regime dune-covered bed and upper regime flat bed. The results are summarized in Tables A.1 and A.2. The coefficients are also evaluated using the Meyer-Peter-Müller sediment transport relation assuming a flat bed. The result is summarized in Table A.3.

In Tables A.1, A.2, and A.3 simplified expressions for P, P_1, M, and M_1 are also given assuming a constant friction factor. From Eqs. A.3a,b it is seen that this gives $P = P_1 = 1$. Noting that for natural streams $10 \le 1/\sqrt{C_f} \le 30$ or $0.1 \ge \sqrt{C_f} \ge 0.033$ the simplified expressions for M and M_1 are obtained by further assuming $\sqrt{C_f} << 1$. This gives for example that M_1 which is $O(C_f)$ can be neglected compared to M in Eq. A.2d. M_1 is therefore taken to be zero in the simplified model.

The theory can easily be generalized to include the full expressions for P, P_1, M, and M_1. This has been done by Parker and Johannesson (1989). There is, however, considerable advantage of using the simplified expressions in the present model, especially considering that there is no general agreement on which is the most appropriate bedload transport relation to use. Further, it is important to realize that the error introduced by the above simplifications may often be much less than the variation obtained by using several different bedload transport relations.

Table A.1 - Engelund-Hansen (1967) Bedload Relation

(lower regime dune-covered bed)

Exact	Simplified
$P = \dfrac{1}{(1 + 5\sqrt{C_{fG}})\, 2\, (1 - \tau^*_C/\tau^*_G) - 5\sqrt{C_{fG}}}$	$P = 1$
$P_1 = \dfrac{(1 + 5\sqrt{C_{fG}})\, 2\, (1 - \tau^*_C/\tau^*_G)}{(1 + 5\sqrt{C_{fG}})\, 2\, (1 - \tau^*_C/\tau^*_G) - 5\sqrt{C_{fG}}}$	$P_1 = 1$
$M = 2 + \dfrac{3}{2}\dfrac{2}{(1 + 5\sqrt{C_{fG}})\, 2\, (1 - \tau^*_C/\tau^*_G) - 5\sqrt{C_{fG}}}$	$M = 2 + \dfrac{3}{2}\dfrac{1}{1 - \tau^*_C/\tau^*_G}$
$M_1 = \dfrac{3}{2}\dfrac{5\sqrt{C_{fG}}}{(1 + 5\sqrt{C_{fG}})\, 2\, (1 - \tau^*_C/\tau^*_G) - 5\sqrt{C_{fG}}}$	$M_1 = 0$

The Engelund-Hansen (1967) sediment transport relation and friction law used to generate the above result can be summarized as

$$C_f\, q^* = 0.05\, (\tau^*)^{5/2} \quad ; \quad \tau^*_G = \tau^*_C + 0.4\, \tau^{*2} \quad ; \quad 1/\sqrt{C_{fG}} = 6 + 2.5 \ln \left(\frac{1}{2.5} \frac{\tilde{h}_G}{D_{50}} \right)$$

where $\tilde{h}_G/\tilde{h} = C_{fG}/C_f = \tau^*_G/\tau^*$.

Table A.2 - Engelund-Hansen (1967) Bedload Relation

(upper regime flat bed)

Exact	Simplified
$P = 1$	$P = 1$
$P_1 = 1 + 5\sqrt{C_f}$	$P_1 = 1$
$M = 5$	$M = 5$
$M_1 = \frac{15}{2}\sqrt{C_f}$	$M_1 = 0$

The Engelund-Hansen (1967) sediment transport relation and friction law used to generate the above result can be summarized as

$$C_f q^* = 0.05 (\tau^*)^{5/2} \quad ; \quad 1/\sqrt{C_f} = 6 + 2.5 \ln \left(\frac{\tilde{h}}{2.5 D_{50}} \right)$$

Table A.3 - Meyer-Peter-Müller Bedload Relation (flat bed)

Exact	Simplified
$P = 1$	$P = 1$
$P_1 = 1 + 5\sqrt{C_f}$	$P_1 = 1$
$M = 3\dfrac{1}{1 - \tau_c^*/\tau^*}$	$M = 3\dfrac{1}{1 - \tau_c^*/\tau^*}$
$M_1 = \dfrac{15}{2}\dfrac{1}{1 - \tau_c^*/\tau^*}\sqrt{C_f}$	$M_1 = 0$

The Meyer-Peter-Müller sediment transport relation and friction law used to generate the above result can be summarized as

$$q^* = 8\,(\tau^* - \tau_c^*)^{3/2} \quad ; \quad 1/\sqrt{C_f} = 6 + 2.5 \ln\left(\frac{\tilde{h}}{2.5\,D_{50}}\right)$$

APPENDIX B

Data for Natural and Experimental Meanders

APPENDIX B. Table B.1 - River Meanders: Field Data

River Name	River Location	Specific Gravity	D_{50} (mm)	σ_g	Q m^3/sec	I $\cdot 10^3$	2b (m)	H (m)	$\tilde{\lambda}_c$ (m)
			Wolman (1955)						
Brandywine Cr.	near Cornog, PA	2.65	97	----	22.1	3.4	16.2	0.74	122
	at Seven Springs, PA	"	71	----	39.6	2.8	24.1	1.83	183
	at South Downington, PA	"	104	----	45.3	0.66	21.9	1.52	366
	Embreeville, PA	"	23	----	62.3	0.69	28.0	1.60	244
	Wawaset, PA	"	41	----	70.8	0.62	22.6	1.50	244
			Leopold & Wolman (1957) and Langbein & Leopold (1966)						
Watts Branch	near Rockville, MD	2.65	25	----	6.97	3.1	6.71	1.01	36.6
Baldwin Cr.	near Lander, WY	"	----	----	5.10	0.93	7.62	0.549	70.1
Popo Agie	near Hudson, WY	"	----	----	48.1	1.84	30.5	1.98	427
Pole Cr.	near Pinedale, WY	"	----	----	9.91	2.05	18.1	0.661	204
			Schumm (1969)						
Nowood Cr.	near Tensleep, WY	2.65	----	----	43.6	0.45	18.0	1.52	152
Tongue R.	near Miles City, MT	"	----	----	125	1.9	60.4	1.52	1040
M. F. Powder R.	near Kaycee, WY	"	----	----	41.1	1.6	11.3	1.22	305
Powder R.	near Locate, MT	"	----	----	311	1.1	99.1	1.86	1830
Little Missouri R.	near Alzada, MT	"	----	----	77.9	0.9	14.0	1.74	198
Lance Cr.	near Spencer, WY	"	----	----	76.5	1.2	32.0	1.49	396
Cheyenne R.	near Spencer, WY	"	----	----	90.6	1.4	78.6	1.22	792

Table B.1 - Continued

River Name	River Location	Specific Gravity	D_{50} (mm)	σ_g	Q m^3/sec	I $\cdot 10^3$	2b (m)	H (m)	$\tilde{\lambda}_c$ (m)
Cheyenne R.	at Edgemont, SD	"	----	----	122	1.4	85.3	1.16	1770
White R.	near Whitney, NE	"	----	----	25.5	1.2	8.2	1.74	183
S. F. White R.	at White River, NE	"	----	----	65.1	2.0	29.9	0.76	1370
Niobrara R.	near Hay Springs, NE	"	----	----	31.1	1.8	20.1	0.73	1770
S. Loup R.	at St. Michael, NE	"	----	----	122	0.9	37.5	1.22	1680
N. Loup R.	at Taylor, NE	"	----	----	42.5	1.3	46.6	0.88	1620
Calamus	near Burwell, NE	"	----	----	16.4	1.1	46.0	1.13	2440
N. Loup	at Scotia, NE	"	----	----	181	1.2	125	1.68	3350
N. Loup	near St. Paul, NE	"	----	----	246	1.2	131	1.74	2440
Elkhorn R.	at Norfolk, NE	"	----	----	147	0.8	58.5	1.31	1680
Republican R.	at Benkelman, NE	"	----	----	125	2.0	31.7	1.16	1620
S. Republican R.	near Benkelman, NE	"	----	----	142	2.2	63.1	0.91	1620
Frenchman Cr.	at Palisade, NE	"	----	----	29.2	1.6	9.1	1.65	183
Frenchman Cr.	at Culbertson, NE	"	----	----	41.1	1.3	22.6	1.37	259
Republican R.	at McCook, NE	"	----	----	99.1	1.5	35.1	1.37	1520
Red Willow Cr.	near Red Willow, NE	"	----	----	63.7	0.77	13.7	2.16	152
Republican R.	at Cambridge, NE	"	----	----	221	1.2	97.5	1.07	1620
Republican R.	near Orleans, NE	"	----	----	187	0.83	44.5	1.83	1980
Beaver Cr.	near Beaver City, NE	"	----	----	29.7	1.0	16.8	3.05	152
Beaver Cr.	at Ludell, KS	"	----	----	18.0	1.2	8.5	2.44	152
Sappa Cr.	near Stamford, NE	"	----	----	59.5	0.7	18.3	3.05	152
Praire Dog Cr.	at Norton, KS	"	----	----	90.6	1.1	15.2	3.05	152
Republican	at Concordia, KS	"	----	----	263	0.6	76.5	2.16	1620
Solomon R.	at Niles, KS	"	----	----	227	0.26	38.4	2.32	610

Table B.1 - Continued

River Name	River Location	Specific Gravity	D_{50} (mm)	σ_g	Q m^3/sec	I $\cdot 10^3$	2b (m)	H (m)	$\tilde{\lambda}_c$ (m)
Kansas R.	at Wamego, KS	"	----	----	1100	0.8	194	3.05	5850
Kansas R.	at Topeke, KS	"	----	----	1360	0.5	244	5.49	7070
Murrumbidgee R.	at Wagga Wagga	"	----	----	736	0.17	83.2	8.23	1340
Murrumbidgee R.	at Narrandera	"	----	----	425	0.21	75.0	7.62	945
Murrumbidgee R.	at Darlington Point	"	----	----	311	0.13	67.1	7.01	853
		Chitale (1970)							
Vatrak	at Kaira, Gujrath State	2.65	0.15	----	2100	0.328	206	6.40	2930
Yamuna	at Delhi	"	0.32	----	2000	0.310	366	3.96	8000
Indus	at Hajipur, Pakistan	"	0.18	----	7100	0.100	983	4.88	13520
Ramganga	in U.P. State	"	0.19	----	6600	0.1065	344	7.32	6040
Sutlej	in Samasatta, Pakistan	"	0.17	----	2800	0.182	1181	3.35	8650
Khipra	at Ujjain in M.P. State	"	5.00	----	1700	0.230	274	5.01	3600
Tapi	at Nanavarachha, Gujrth State	"	0.25	----	21200	0.470	605	11.89	11570
Ganga	at Mokameh, Bihar State	"	0.43	----	52300	0.160	4020	5.18	23160
Purna	in Surat dist., Gujrth State	"	4.00	----	2000	0.90	160	7.92	2140
Vatrak	at Mehmadabad, Gujrth State	"	0.15	----	1400	0.342	178	5.43	3380
Mohor	at Kapadganj, Gujrth	"	0.043	----	1100	0.460	152	3.96	2440
Yamuna	at Hamirpur, U.P. State	"	0.18	----	30600	0.159	975	10.97	12870
Bhagirathi	in West Bengal State	"	0.18	----	1700	0.058	218	5.94	4560
Tapi	at Ukai, Gujrth State	"	1.60	----	17000	0.191	274	15.24	11670
Jhelum	at Shrinagar, J. and K. State	"	0.041	----	396	0.137	102	5.18	1050
Jhelum Out Fall Channel	J. and K. State	"	0.67	----	481	0.085	152	4.57	3310

Table B.1 - Continued

River Name	River Location	Specific Gravity	D_{50} (mm)	σ_g	Q m^3/sec	I $\cdot 10^3$	2b (m)	H (m)	$\tilde{\lambda}_c$ (m)
Salandi	at Bidhyadharpur, Orissa State	"	0.96	----	850	0.67	152	3.05	2190
Burhi Gandak	at Muzaffarpur, Bihar	"	0.10	----	1400	0.190	213	4.57	3260
Mutha	at Poona, Maharashtra State	"	1.50	----	850	0.670	152	6.10	1690
Saraswati	at Sidhpur, Gujrth State	"	0.30	----	1300	1.25	320	2.59	3860
Bennihalla	Gadag, Hubliline	"	0.04	----	453	0.227	137	1.83	530
Redihall	Gadag, Hubliline	"	0.04	----	340	0.227	146	1.52	770
Savannah	in Georgia, U.S.A	"	0.80	----	850	0.110	107	5.18	6520
Beaver	Alberta, Canada	"	0.50	----	142	0.240	55	2.74	1280
Mississippi	Vicksburg to Angola, U.S.A	"	0.50	----	42500	0.0473	1380	20.12	20570
Mississippi	Cairo to Memphis, U.S.A.	"	0.30	----	42500	0.0815	2140	16.76	24470
		Kinshita (1961)							
Uryu R.		2.65	----	----	169	1.45	70	1.50	720
Ishikari R.	Fukagwa	"	----	----	151	1.12	90	1.28	1450
Ishikari R.	Fushiko	"	----	----	324	0.500	140	1.96	2800
Ishikari R.	Naie	"	----	----	837	0.345	170	3.49	4500

Table B.2 - River Meanders: Experimental Data

Reference	Run No.	Specific Gravity	D_{50} (mm)	σ_g	Q l/sec	I $\cdot 10^3$	2b (m)	H (cm)	$\tilde{\lambda}_c$ (m)	Flume Type	Q_s gm/sec
Bordas (1963)	1	2.65	0.45	1.77	3.4	2.40	0.75	2.00	9	R-E	----
	2	''	''	''	1.7	2.75	0.71	1.35	6	''	----
	3	''	''	''	2.5	2.00	0.71	1.65	8.4	''	----
Quraishy (1973)	1	2.65	0.70	----	0.36	3.3	0.15	0.92	2.75	S-E	0.27
	2	''	''	----	0.36	5.0	0.15	0.79	2.75	''	0.27
	3	''	''	----	0.36	5.0	0.15	0.79	3.49	''	0.50
	4	''	''	----	0.59	3.3	0.15	1.73	2.75	''	1.00
	5	''	''	----	0.59	3.3	0.23	1.17	3.05	''	0.72
	6	''	''	----	0.36	3.3	0.30	1.70	4.27	''	1.50
	7	''	''	----	1.13	3.3	0.23	2.26	3.97	''	1.37
	8	''	''	----	1.13	5.0	0.15	0.84	2.44	''	0.50
	9	''	''	----	0.38	5.0	0.23	0.56	2.29	''	1.50
	10	''	''	----	0.36	5.0	0.30	0.98	3.36	''	1.50
Wolman and and Brush (1961)	3	2.65	0.67	1.30	0.57	3.9	0.20	1.0	2.44	S-E	0.21
	4	''	''	''	1.08	3.9	0.29	1.3	2.04	''	1.04
	6	''	''	''	0.31	6.9	0.21	0.55	1.83	''	----
	7	''	''	''	0.54	6.4	0.26	1.0	1.52	''	2.62
	8a	''	''	''	1.13	6.8	0.51	0.94	2.80	''	3.49
	11	''	''	''	0.71	6.3	0.44	0.83	0.91	''	----
	12	''	''	''	0.54	6.7	0.39	0.53	2.19	''	----
	32	''	''	''	0.68	5.1	0.23	0.99	2.32	''	----

Table B.2 - Continued

Reference	Run No.	Specific Gravity	D_{50} (mm)	σ_g	Q l/sec	I $\cdot 10^3$	2b (m)	H (cm)	$\tilde{\lambda}_c$ (m)	Flume Type	Q_s gm/sec
Schumm and Kahn (1972)		2.65	0.70	----	4.25	2.6	0.94	1.8	5.5	R-E	3.17
		''	''	----	4.25	4.3	1.16	1.3	5.9	''	4.00
		''	''	----	4.25	5.9	1.22	1.1	6.0	''	5.88
		''	''	----	4.25	6.4	1.25	0.99	6.2	''	6.47
		''	''	----	4.25	7.5	1.37	0.85	6.3	''	6.92
		''	''	----	4.25	8.5	1.43	0.80	6.4	''	7.17
		''	''	----	4.25	10.0	1.43	0.72	6.8	''	8.53
		''	''	----	4.25	13.0	1.49	0.61	6.9	''	9.38
Ackers and Charlton (1970)	4M	2.65	0.15	----	10.6	2.07	1.1	3.8	7.22	S-E	----
	5M	''	''	----	9.3	2.02	1.5	4.0	6.95	''	----
	5D	''	''	----	8.5	1.91	2.4	2.6	5.55	''	----
	6M	''	''	----	18.5	1.41	2.3	4.1	10.33	''	----
	6D	''	''	----	17.6	1.96	2.2	6.7	11.55	''	----
	7M	''	''	----	17.8	1.46	2.1	4.1	9.57	''	----
	8M	''	''	----	32.0	1.13	2.7	6.5	12.43	''	----
	9M	''	''	----	54.8	1.55	3.1	7.2	14.84	''	----
	10M	''	''	----	30.9	1.75	3.2	6.3	11.61	''	----
	11D	''	''	----	28.2	1.79	3.9	5.2	11.21	''	----
	12M	''	''	----	30.2	2.36	2.4	4.9	11.83	''	----

Table B.2 - Continued

Reference	Run No.	Specific Gravity	D_{50} (mm)	σ_g	Q l/sec	I $\cdot 10^3$	2b (m)	H (cm)	$\tilde{\lambda}_C$ (m)	Flume Type	Q_s gm/sec
	13D	''	''	----	14.0	1.92	2.1	4.3	8.29	''	----
	14M	''	''	----	16.1	1.97	2.2	3.8	8.35	''	----
	19M	''	''	----	10.0	2.29	2.3	3.5	6.55	''	----
	19D	''	''	----	6.9	1.93	2.3	2.2	6.13	''	----
	20/ID	''	''	----	17.3	1.74	2.7	3.5	8.47	''	----
	21M	''	''	----	8.6	1.99	2.7	2.8	6.74	''	----
Sharma (1973)		2.65	0.40	----	27.1	2.7	3.9	2.9	10.7	S-E	----
		''	''	----	29.1	3.0	3.7	3.1	12.2	''	----
		''	''	----	28.2	3.5	3.2	3.5	12.5	''	----
		''	''	----	27.6	4.0	3.8	2.9	12.2	''	----
		''	''	----	57.4	2.2	4.1	5.0	16.8	''	----
		''	''	----	55.7	2.7	2.5	6.7	18.3	''	----
		''	''	----	55.2	3.0	5.5	3.7	19.8	''	----
		''	''	----	110.7	3.0	5.9	5.7	22.9	''	----
		''	''	----	27.7	3.0	5.49	2.1	13.0	''	----
		''	''	----	29.5	3.25	4.51	2.7	12.3	''	----
		''	''	----	29.3	3.6	4.50	3.0	12.2	''	----
		''	''	----	55.0	3.6	9.37	2.8	21.9	''	----
		''	''	----	57.0	4.0	8.69	1.9	21.3	''	----
		''	''	----	56.4	4.3	6.40	2.9	21.6	''	----

Table B.2 - Continued

Reference	Run No.	Specific Gravity	D_{50} (mm)	σ_g	Q l/sec	I $\cdot 10^3$	2b (m)	H (cm)	$\tilde{\lambda}_C$ (m)	Flume Type	Q_s gm/sec
		''	''	----	45.8	3.2	8.38	4.1	21.9	''	----
		''	''	----	51.7	3.3	6.71	5.0	23.8	''	----
		''	''	----	49.4	3.0	6.25	4.8	25.0	''	----
		''	''	----	38.2	3.4	13.1	2.7	26.8	''	----
		''	''	----	70.0	3.6	7.62	6.2	26.8	''	----
		''	''	----	6.55	3.9	1.34	6.6	6.1	''	----
		''	''	----	7.21	4.0	1.40	7.5	9.14	''	----
		''	''	----	7.1	3.3	1.30	2.5	6.28	''	----
		''	''	----	7.1	4.7	2.41	2.0	6.34	''	2.6
		''	''	----	7.1	4.0	1.82	1.8	6.40	''	5.2
		''	''	----	7.1	5.6	2.33	2.2	7.11	''	10.5
		''	''	----	1.7	4.0	2.00	1.2	4.57	''	----
		''	''	----	1.7	6.0	1.44	0.95	3.76	''	----
		''	''	----	28.3	3.7	5.75	3.09	20.3	''	2.3
		''	''	----	28.3	6.4	5.73	2.15	21.7	''	2.3
		''	''	----	1.7	8.7	2.49	0.52	8.23	''	----
		''	''	----	14.2	5.0	3.48	2.10	15.2	''	1.3
		''	''	----	14.2	6.7	5.94	1.6	12.2	''	1.3
		''	''	----	14.2	8.1	7.88	1.23	20.3	''	1.3
		''	''	----	28.3	7.7	7.68	1.34	16.3	''	2.3

Table B.2 - Continued

Reference	Run No.	Specific Gravity	D_{50} (mm)	σ_g	Q l/sec	I $\cdot 10^3$	2b (m)	H (cm)	$\tilde{\lambda}_c$ (m)	Flume Type	Q_s gm/sec
Anderson et al. (1975) Tilting Flume Exp.	117	2.65	0.62	1.39	0.7	8.05	0.44	0.77	2.8	R-E	1.40
	118	''	''	''	0.8	7.43	0.43	0.79	3.0	''	2.50
	119	''	''	''	0.9	7.10	0.49	0.81	3.0	''	1.44
	121	''	''	''	0.5	6.28	0.40	0.60	3.3	''	0.83
	126	''	''	''	0.7	5.95	0.42	0.96	3.9	''	0.57
Anderson et al. (1975) Towing Channel Exp.	M-1-2	2.65	0.22	1.44	1.41	5.05	1.07	1.50	4.91	R-E	----
	M-1-3	''	''	''	2.83	4.46	1.36	1.77	4.59	''	----
	M-1-4	''	''	''	2.83	5.62	1.57	1.96	3.89	''	----
	M-1-5	''	''	''	2.83	4.76	1.23	1.75	6.07	''	----

Flume Type: Feed: S = New sediment supplied; R = sediment recirculated.
Banks: E = erodible.

APPENDIX C

Equations Used to Calculate the Coefficients a_1, a_2, a_3, a_4, χ_1, and χ_2 for the General Solution of Secondary Flow in a Sine–Generated Channel

APPENDIX C

The unknown coefficients a_1, a_2, a_3, a_4, χ_2, and χ_3 in Eqs. 5.14 and 5.17a,b are found by requiring that the solution for υ_1 satisfies the boundary conditions given by Eqs. 5.5a,b,c. Note that $G(\zeta)$ and $H(\zeta)$ must independently satisfy the boundary conditions since the solution for υ_1, as given by Eq. 5.13, has to be valid for all ϕ.

Applying condition 5.5b to $G(\zeta)$ and $H(\zeta)$ gives $\dot{G}(1) = \dot{H}(1) = 0$, or

$$e^a (\cos a - \sin a)\, a_1 + e^a (\cos a + \sin a)\, a_2 - e^{-a} (\cos a + \sin a)\, a_3 + e^{-a} (\cos a - \sin a)\, a_4 = 0 \tag{C.1}$$

$$e^a (\cos a + \sin a)\, a_1 - e^a (\cos a - \sin a)\, a_2 - e^{-a} (\cos a - \sin a)\, a_3 - e^{-a} (\cos a + \sin a)\, a_4 = 0 \tag{C.2}$$

Applying condition 5.5a to $G(\zeta)$ and $H(\zeta)$ gives $G(0) = \chi \dot{G}(0)$ and $H(0) = \chi \dot{H}(0)$, or

$$(1 - \chi a)\, a_1 - \chi a\, a_2 + (1 + \chi a)\, a_3 - \chi a\, a_4 - \frac{\chi_1}{r}\chi_3 = \frac{2}{r^2}(2\chi + 1) \tag{C.3}$$

$$-\chi a\, a_1 - (1 - \chi a)\, a_2 + \chi a\, a_3 + (1 + \chi a)\, a_4 + \frac{\chi_1}{r}\chi_2 = -\frac{\chi_1}{r}\left[\left(\frac{\chi}{\chi_1}\right)^2 + \frac{6}{r^2}\right] \tag{C.4}$$

Applying condition 5.5c to $G(\zeta)$ and $H(\zeta)$ gives $\int_0^1 G(\zeta)d\zeta = \int_0^1 H(\zeta)d\zeta = 0$, or

$$\frac{a_1}{2a}\left[e^a (\cos a + \sin a) - 1\right] + \frac{a_2}{2a}\left[e^a (\sin a - \cos a) + 1\right] + \frac{a_3}{2a}\left[e^{-a} (\sin a - \cos a) + 1\right]$$

$$+ \frac{a_4}{2a}\left[-e^{-a} (\sin a + \cos a) + 1\right] - \frac{\chi_1}{r}\chi_3 = -\frac{\chi_1}{r}\left[\frac{6}{r} - \frac{2}{r\,\chi_1}(2\chi + 1)\right] \tag{C.5}$$

$$\frac{a_1}{2a}\left[e^a (\sin a - \cos a) + 1\right] - \frac{a_2}{2a}\left[e^a (\cos a + \sin a) - 1\right] + \frac{a_3}{2a}\left[e^{-a} (\sin a + \cos a) - 1\right]$$

$$+ \frac{a_4}{2a}\left[e^{-a} (\sin a - \cos a) + 1\right] + \frac{\chi_1}{r}\chi_2 = \frac{\chi_1}{r}\left[\frac{1}{\chi_1^2}\left(\chi^2 + \frac{2}{3}\chi + \frac{2}{15}\right) - \frac{6}{r^2}\right] \tag{C.6}$$

The above 6 equations have to be solved together to obtain values for a_1, a_2, a_3, a_4, χ_2, and χ_3. This was done using the IMSL subroutine LEQT2F. It is also possible to derive direct expressions for a_1, a_2, a_3, a_4, χ_2, and χ_3 from Eqs. C.1 to C.6. These expressions can be found in Johannesson and Parker (1989a) and are not included herein.